DOI: 10.1002/ejoc.201000409

Experimental and Theoretical Investigation of the Enantiomerization of Lithium α-*tert*-Butylsulfonyl Carbanion Salts and the Determination of Their Structures in Solution and in the Crystal

Roland Scholz,[a][‡] Gunther Hellmann,[a][‡‡] Susanne Rohs,[a][‡‡‡] Gerhard Raabe,[a] Jan Runsink,[a] Diana Özdemir,[a][‡‡‡‡] Olaf Luche,[a][‡‡‡‡‡] Thomas Heß,[a][‡‡‡‡‡‡] Alexander W. Giesen,[a][‡‡‡‡‡‡‡] Juliana Atodiresei,[a] Hans J. Lindner,[b] and Hans-Joachim Gais*[a]

Keywords: Carbanions / Chirality / Enantiomerization / Ab initio calculations / Cryoscopy

Dynamic NMR (DNMR) spectroscopy of $[R^1C(R^2)SO_2R^3]Li$ (R^1, R^2 = alkyl, phenyl; R^3 = Ph, *t*Bu, adamantyl, CEt_3) in $[D_8]$THF has shown that the *S*-*t*Bu, *S*-adamantyl, and *S*-CEt_3 derivatives have a significantly higher enantiomerization barrier than their *S*-Ph analogues. C_α–S bond rotation is most likely the rate-determining step of the enantiomerization of the salts bearing a bulky group at the S atom and two substituents at the C_α atom. Ab initio calculations on $[Me(Ph)SO_2tBu]^-$ gave information about the two C_α–S rotational barriers, which are dominated by steric effects. Cryoscopy of $[R^1C(R^2)SO_2tBu]Li$ in THF at –108 °C revealed the existence of monomers and dimers. X-ray crystal structure analysis of the monomers and dimers of $[R^1C(R^2)SO_2tBu]Li{\cdot}L_n$ (R^1 = Me, Et, $tBuCH_2$, $PhCH_2$, *t*Bu; R^2 = Ph, L = THF, 12-crown-4, PMDTA) and $[R^1C(R^2)SO_2Ph]Li{\cdot}2$diglyme [$R^1$ = R^2 = Me, Et; R^1–R^2 = $(CH_2)_5$] showed them to be O–Li contact ion pairs (CIPs). The monomers and dimers have a C_α–S conformation in which the lone-pair orbital at the C_α atom bisects the O–S–O angle and a significantly shortened C_α–S bond. The C_α atom of $[R^1C(R^2)SO_2R^3]Li{\cdot}L_n$ (R^1 = Ph; R^3 = Ph, *t*Bu) is planar, whereas the C_α atom of $[R^1C(R^2)SO_2R^3]Li{\cdot}L_n$ (R^1 = R^2 = alkyl) is strongly pyramidalized in the case of R^3 = Ph and most likely planar for R^3 = *t*Bu. Ab initio calculations on $[MeC(Me)SO_2R]^-$ gave a pyramidalized C_α atom for R = Me and a nearly planar one for R = CF_3 and *t*Bu. The $[R^1C(R^2)SO_2tBu]Li$ salts were characterized by ^1H, ^{13}C, and ^6Li NMR spectroscopy. $^1H\{^1H\}$ and $^6Li\{^1H\}$ NOE experiments are in accordance with the existence of O–Li CIPs. ^1H and ^{13}C NMR spectroscopy of $[R^1C(R^2)SO_2tBu]Li$ in $[D_8]$THF at low temperatures showed equilibrium mixtures of up to five different species being most likely monomeric and dimeric O–Li CIPs with different configurations. According to ^7Li NMR spectroscopy, the addition of HMPA to $[MeC(Ph)SO_2tBu]Li$ in $[D_8]$THF at low temperatures causes the formation of the separated ion pair $[MeC(Ph)SO_2tBu]Li(HMPA)_4$.

Introduction

Lithium α-sulfonyl carbanion salts **I** and **II** (Figure 1) have found wide-spread application in organic synthesis.[1,2] It is therefore not surprising that their structure and reactivity have been continuously studied both by experimental[3–5] and theoretical[3k,3q,6] methods. One of the most captivating structural features of salts **I** (planar C_α atom) and **II** (pyramidalized C_α atom) bearing two different substituents ($R^1 \neq R^2$) at the C_α atom is the chirality of the carbanion. Whereas the carbanion of salt **I** has a stereogenic axis, that of **II** has both a stereogenic axis and a stereogenic center. A decisive factor for the stereogenicity of **I** and **II** is the

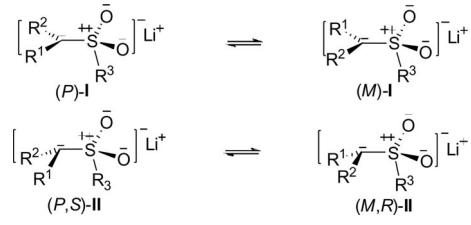

Figure 1. Chiral lithium α-sulfonyl carbanion salts (priority: $S > R^1 > R^2$).

[a] Institute of Organic Chemistry, RWTH Aachen University, Landoltweg 1, 52056 Aachen, Germany
Fax: +49-241-8092665
E-mail: gais@rwth-aachen.de
[b] Clemens-Schöpf-Institut, TU Darmstadt, Petersenstrasse 22, 64287 Darmstadt, Germany
[‡] Current address: Kelheim Fibres, Regensburger Strasse 109, 93309 Kelheim, Germany
[‡‡] Current address: DSM Nutritional Products Ltd., Wurmisweg 576, 4002 Kaiseraugst, Switzerland
[‡‡‡] Current address: ICG-1: Stratosphäre, Forschungszentrum Jülich, 52425 Jülich, Germany
[‡‡‡‡] Current address: Lummus Novolen Technology GmbH, Gottlieb-Daimler-Strasse 8, 68165 Mannheim, Germany
[‡‡‡‡‡] Current address: Lisi Automotive (Beijing) Co Ltd., 28 Linhe Street, Linhe Industrial Development Zone Shunyi District, Beijing, PRC 101300, P. R. China
[‡‡‡‡‡‡] Current address: Jaspertstrasse 5 H, 60435 Frankfurt, Germany
[‡‡‡‡‡‡‡] Current address: Merianstrasse 16, 41749 Viersen, Germany

Supporting information for this article is available on the WWW under http://dx.doi.org/10.1002/ejoc.201000409.

C_α–S conformation of the carbanions in which the lone-pair orbital at the C_α atom bisects the O–S–O angle. This conformation is generally preferred for steric reasons and stabilization by negative hyperconjugation (n_C–σ^*_{SR3}).[3k,3q,6] The chirality of α-sulfonyl carbanions was first inferred from base-mediated H/D-exchange experiments of optically active sulfones, which proceeded with a high degree of retention of configuration.[7] Final proof of the chirality of **I** and **II** was provided by X-ray crystal structure analysis.[3] Previous attempts towards an enantioselective synthesis of *S*-phenyl-substituted derivatives of **I** and **II** have been uniformly unsuccessful,[1j,8] presumably because of fast racemization even at low temperatures (see below). A few enantioselective reactions of magnesium and lithium α-sulfonyl carbanion salts have been achieved by treatment with electrophiles in the presence of chiral ligands on the metal atom.[6r,9,10] These interesting reactions presumably follow dynamic kinetic[9] and dynamic thermodynamic[6r] resolution pathways. In the course of our structural studies of α-sulfonyl carbanions and their salts[3b–3i,3k,3m,6h,6j] we became interested in the design and enantioselective synthesis of derivatives of **I** and **II** that are configurationally stable on the timescale of their synthesis, reaction with electrophiles, and structural investigation. The availability of such lithium α-sulfonyl carbanion salts would not only allow a study of their dynamics and reactivity, but could perhaps also lead to interesting applications in stereoselective synthesis. A prerequisite to an enantioselective synthesis and study of **I** and **II** is a sufficiently high configurational stability at low temperatures. The enantiomerization of (*P*)- and (*M*)-**I** has to include, besides perhaps other steps, a C_α–S bond rotation, and the enantiomerization of (*P*,*S*)- and (*M*,*R*)-**II** both a C_α–S bond rotation and an inversion of the C_α atom (not shown in Figure 1). Ab initio calculations on counterion-free *S*-methylsulfonyl carbanions have revealed a small barrier towards inversion and a much higher barrier towards C_α–S rotation, the latter being determined by both steric effects and the n_C–σ^*_{SR3} interaction.[6a,6b,6h,6j] Based on the results of our ab initio calculations on fluorine-substituted α-sulfonyl carbanions,[6h,6j] we speculated that salts **I** and **II** carrying the strongly electronegative and sterically demanding trifluoromethyl group[11] at the S atom should have a significantly higher configurational stability than their *S*-phenyl derivatives. Indeed, the *S*-trifluoromethyl-substituted salts (*P*)-**Ia** (R^1 = Ph, R^2 = CH_2Ph, R^3 = CF_3) and (*M*)-**IIa** (R^1 = CH_2Ph, R^2 = Me, R^3 = CF_3) exhibited such a configurational stability at low temperatures, which allowed their enantioselective synthesis and structural study.[3f,3g] Unfortunately, the strong n_C–σ^*_{SCF3} interactions in (*P*)-**Ia** and (*M*)-**IIa** bestows the salts not only with a relatively high configurational stability, but also with a low reactivity towards electrophiles at low temperatures.[3f,3g,6r,10,12] Therefore derivatives of **I** and **II** were sought that would combine both a relatively high configurational stability and a high reactivity at low temperatures. To meet these requirements we envisioned the introduction of a group at the S atom of **I** and **II** that is sterically more demanding[11] but much less electronegative than the CF_3 group. Derivatives of **I** and **II** that carry a bulky alkyl group at the S atom should be much more reactive towards electrophiles than their *S*-trifluoromethyl-substituted analogues because of the reduced stabilization by negative hyperconjugation and electrostatic interaction. Although the decreased hyperconjugation provided by the bulky *S*-alkyl group is expected to lower the C_α–S rotational barrier,[6h,6j] this effect should be outweighed, at least in part, by a higher torsional effect.

In this paper we describe the results of an investigation into the enantiomerization of lithium α-*tert*-butylsulfonyl carbanion salts. It is shown that lithium α-sulfonyl carbanion salts have a barrier that should allow the attainment of derivatives that are configurationally stable at low temperatures on the timescale of the synthesis. Therefore the structures of lithium *S*-*tert*-butylsulfonyl carbanion salts both in solution and in the crystal form were determined.[13] This work was undertaken to provide the basis for a study of their enantioselective synthesis, configurational stability, and reactivity, the results of which will be described in a separate paper.[14]

Results and Discussion

Enantiomerization Barriers of α-Sulfonyl Carbanions

Enantiomerization and Topomerization of Nuclei

To gain general information about the influence of the substituents at the S and C_α atoms of salts **I** and **II** upon their configurational stability, the enantiomerization of the racemic salts *rac*-**1**–**10** (Figure 2) was investigated by ^1H and ^{13}C dynamic NMR (DNMR) spectroscopy.

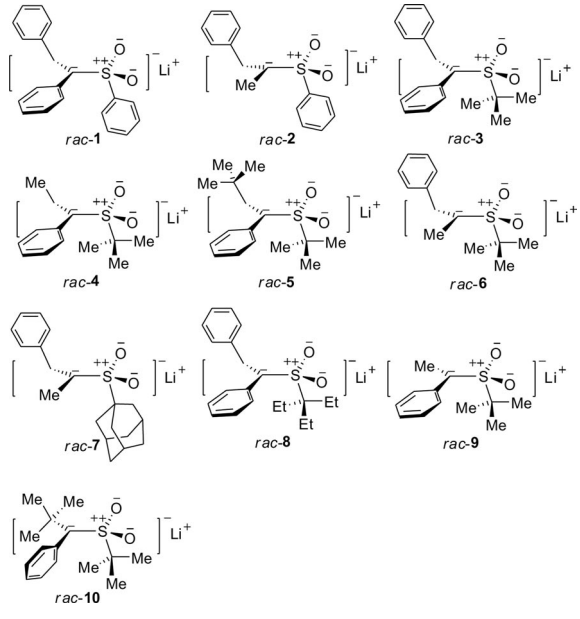

Figure 2. Lithium salts of chiral *S*-phenyl-, *S*-*tert*-butyl-, *S*-adamantyl-, and *S*-triethylmethyl-substituted α-sulfonyl carbanions.

The anions of *rac*-**1**–**10** carry a Ph, *t*Bu, adamantyl, or Et_3C group at the S atom. These substituents were selected on the basis of their increasing steric size according to the Taft parameters [E_s (Ph) = –1.01/–3.82, E_s (CMe_3) = –2.78, E_s (adamantyl) = –4.0, and E_s (CEt_3) = –5.04].[11] Whereas the salts *rac*-**1**, *rac*-**3**–**5**, and *rac*-**8**–**10** are also benzylic carbanions, the salts *rac*-**2**, *rac*-**6**, and *rac*-**7** carry only alkyl groups at the C_α atom. The different substituents at the C_α atom were chosen to study the influence of the coordination geometry of the anionic C atom and the benzylic conjugation upon the configurational stability of the salts. The enantiomerization of salts *rac*-**1**–**10** has to involve a C_α–S bond rotation and that of *rac*-**2**, in addition, a C_α inversion (not shown in Figure 3) because its C_α atom is most likely pyramidalized. Although the configurations of the C_α atoms of the *S*-*tert*-butyl- and *S*-adamantyl-substituted salts *rac*-**6** and *rac*-**7** have not been experimentally determined, there is evidence to suggest that they are planar or nearly planar (see below). Furthermore, the salts *rac*-**1**–**8** undergo C_α–CH_2 bond rotation during enantiomerization. Because the anions of *rac*-**1**–**8** each have a CH_2R group (R = Ph, Me, *t*Bu) at the C_α atom, their enantiomerization is accompanied by topomerization of the diastereotopic methylene protons H_a and H_b, as highlighted for *rac*-**3** and *rac*-**6** in Figure 3. This should provide a means of studying the enantiomerization of the salts *rac*-**1**–**8** by temperature-dependent NMR spectroscopy. In addition, the *tert*-butyl-substituted salt *rac*-**10** was investigated. Whereas the salts *rac*-**1**, *rac*-**3**, and *rac*-**4** have and *rac*-**8** and *rac*-**9** are expected to have a C_α–Ph conformation as depicted, the phenyl ring of the salt *rac*-**10** is orthogonal to the C_i–C_α–S plane (see below). Therefore enantiomerization of *rac*-**10** is accompanied by topomerization of the nuclei at the *ortho* and *meta* positions of the phenyl ring. This process should be accessible by DNMR spectroscopy provided the barrier to C_α–Ph rotation is higher than that to C_α–S rotation. Finally, it was of interest to determine the C_α–Ph rotational barriers for the salts *rac*-**1**–**9** as a probe for the benzylic conjugation and its influence on the configurational stability. Rotation around the C_α–Ph bond leads to topomerization of the nuclei of the phenyl ring in the *ortho* and *meta* positions, as depicted for *rac*-**3**, which can, in principle, also be monitored by DNMR spectroscopy.

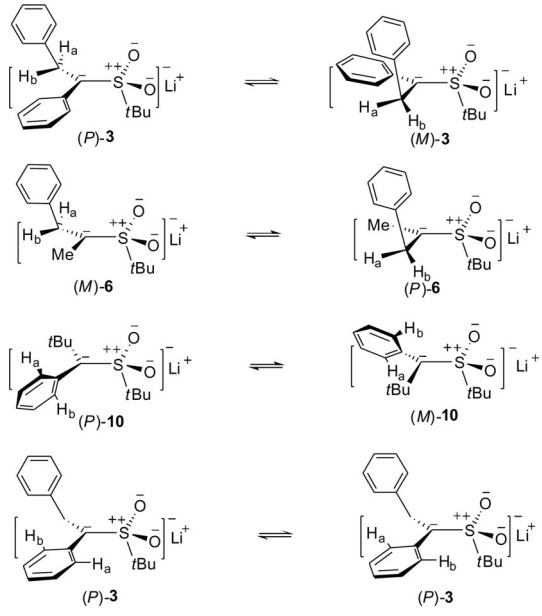

Figure 3. Topomerization of nuclei in the enantiomerization and C_α–Ph rotation of α-sulfonyl carbanions.

Synthesis of Racemic Sulfones

The racemic *S*-*tert*-butyl sulfones *rac*-**17** and *rac*-**18** were prepared starting from the corresponding sulfides **11**[15a] and **12**[15b] (Scheme 1). Oxidation of sulfides **11** and **12** gave the corresponding sulfones **13**[15c] and **14**[15d] in 79 and 81% yields, respectively. Deprotonation of sulfones **13** and **14** with *n*BuLi in THF afforded the corresponding racemic salts *rac*-**15** and *rac*-**16**. Treatment of these salts with $PhCH_2Br$ and MeI, respectively, furnished the corresponding sulfones *rac*-**17** and *rac*-**18** in 86 and 93% yields, respectively. A substitution approach was followed for the synthesis of the racemic *S*-*tert*-butyl sulfones *rac*-**27**–**30**. This approach was chosen because of its proposed use in the synthesis of the corresponding enantiomerically pure sulfones. Treatment of the racemic bromide *rac*-**19** and chlorides *rac*-**20**,[16a] *rac*-**21**,[16b] and *rac*-**22**[16b] with sodium *tert*-butylthiolate in dimethylformamide (DMF) gave the corresponding racemic sulfides *rac*-**23**,[15b,17a] *rac*-**24**, *rac*-**25**, and *rac*-

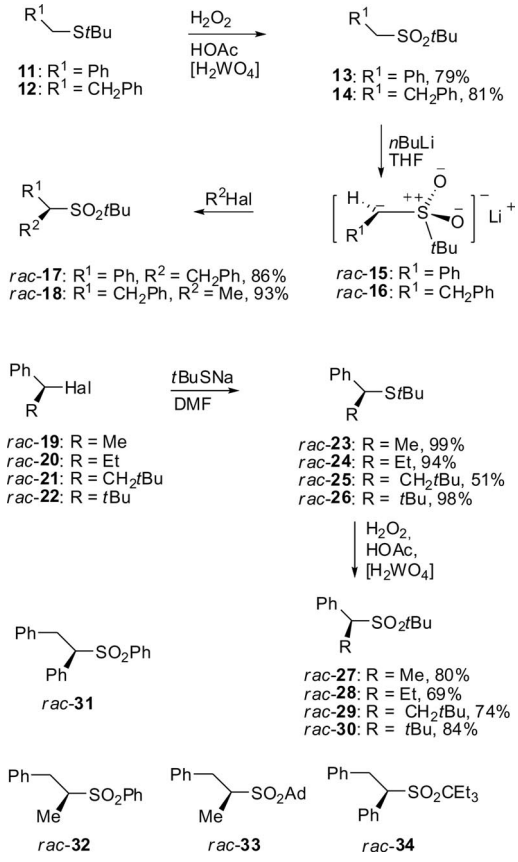

Scheme 1. Synthesis of sulfones *rac*-**17**, *rac*-**18**, *rac*-**27**–**30**, and *rac*-**31**–**34**.

26[17b] in 99, 94, 51, and 98% yields, respectively. Finally, oxidation of the sulfides furnished the corresponding sulfones *rac*-**27**,[18] *rac*-**28**, *rac*-**29**, and *rac*-**30** in 80, 69, 74, and 84% yields, respectively. The racemic sulfones *rac*-**31**,[19a] *rac*-**32**,[19b] *rac*-**33**, and *rac*-**34** were prepared following similar routes (see the Supporting Information).

DNMR Spectroscopy

The ^{1}H NMR spectra of the salts *rac*-**1**–**8**, which were prepared from the corresponding sulfones *rac*-**31**, *rac*-**32**, *rac*-**17**, *rac*-**28**, *rac*-**29**, *rac*-**18**, *rac*-**33**, and *rac*-**34** with *n*BuLi and *n*PrLi in [D$_8$]THF and [D$_{14}$]diglyme, showed in all cases a temperature-dependent reversible coalescence phenomenon for the signals of the diastereotopic protons of the methylene group. The activation free energies for the enantiomerization of *rac*-**1**–**8** at the coalescence temperature were estimated[20] based on the assumption that the process follows first-order kinetics (see below). DNMR spectroscopy of the benzylic *S*-phenyl-substituted salt *rac*-**1** in [D$_8$]THF at a concentration of c = 0.32 mol L^{-1} gave an estimated enantiomerization barrier $\Delta G^{\ddagger}_{enant}$ of 9.5 kcal mol^{-1} at the coalescence temperature of 210 K (Table 1, entry 1). This translates into an estimated half-life of enantiomerization ($\tau_{½}$) for *rac*-**1** of only 1.12×10^{-3} s at 210 K. Lowering the concentration of *rac*-**1** to c = 0.20 mol L^{-1} and finally to 0.06 mol L^{-1} had no influence on the height of the estimated enantiomerization barrier. Next the influence of HMPA upon the enantiomerization barrier of *rac*-**1** was probed. In the presence of 2 equiv. of [D$_{18}$]-HMPA, the barrier of *rac*-**1** increased to $\Delta G^{\ddagger}_{enant}$ = 9.9 kcal mol^{-1} at the coalescence temperature of 218 K (entry 2). Whereas the anionic C atom of the benzylic salt *rac*-**1** should be planar, that of the non-benzylic *S*-phenyl-substituted salt *rac*-**2** is expected to be strongly pyramidalized[3d] (see below). DNMR spectroscopy of *rac*-**2** in [D$_8$]THF at a concentration of c = 0.28 mol L^{-1} gave an estimated activation barrier of $\Delta G^{\ddagger}_{enant}$ = 9.6 kcal mol^{-1} at the coalescence temperature of 213 K (entry 3). Thus, the planar and pyramidalized lithium salts *rac*-**1** and *rac*-**2**, respectively, have similar barriers to enantiomerization.

Next the benzylic *S*-*tert*-butyl-substituted salts *rac*-**3** and *rac*-**4** were studied by DNMR spectroscopy. The *tert*-butyl group has a higher Taft parameter than the phenyl group [E_s(CMe$_3$) = –2.78 and E_s(Ph) = –1.01/–3.82].[11] The benzylic *S*-*tert*-butyl-substituted salt *rac*-**3** in [D$_8$]THF has, at a concentration of c = 0.28 mol L^{-1}, an estimated activation free energy of enantiomerization $\Delta G^{\ddagger}_{enant}$ of 13.5 kcal mol^{-1} at the coalescence temperature of 283 K (entry 4). This translates into an estimated half-life of enantiomerization for *rac*-**1** of $\tau_{½} = 3.22 \times 10^{-3}$ s at 283 K. The estimated barrier for the C_α-ethyl-substituted derivative *rac*-**4** is 14.2 kcal mol^{-1} at 295 K (entry 5). Thus, the barriers to the enantiomerization of the *S*-*tert*-butyl-substituted salts *rac*-**3** and *rac*-**4** are, as envisioned, significantly higher than those of the *S*-phenyl-substituted derivatives *rac*-**1** and *rac*-**2**. A change in solvent from [D$_8$]THF to [D$_{14}$]diglyme had no significant effect on the enantiomerization barrier of *rac*-**4** (entry 6). The enantiomerization barrier for the C_α-neopentyl- and *S*-*tert*-butyl-substituted salt *rac*-**5** in [D$_8$]THF could not be determined because of the relatively low boiling point of the solvent. However, because of a coalescence temperature of ≥333 K, the activation free energy $\Delta G^{\ddagger}_{enant}$ of *rac*-**5** was estimated to be ≥15.7 kcal mol^{-1} (entry 7). DNMR spectroscopy of *rac*-**5** in [D$_{14}$]diglyme at a concentration of c = 0.10 mol L^{-1} gave an estimated activation free energy $\Delta G^{\ddagger}_{enant}$ of 16.2 kcal mol^{-1} at the coalescence temperature of 343 K (entry 8). DNMR spectroscopy of the *S*-*tert*-butyl-substituted salt *rac*-**6**, the C$_\alpha$ atom of which carries a methyl and a benzyl group, revealed an activation free energy of enantiomerization $\Delta G^{\ddagger}_{enant}$ of 13.6 kcal mol^{-1} at the coalescence temperature of 288 K (entry 9). Thus, the benzylic salt *rac*-**5**, the C$_\alpha$ atom of which is planar, and the non-benzylic salt *rac*-**6**, the C$_\alpha$ atom of which is most likely also planar (see below), have similar enantiomerization barriers. Finally, the two salts *rac*-**7** and *rac*-**8**, which carry a sterically demanding adamantyl and triethylmethyl group at the S atom, respectively, and a C$_\alpha$ atom that is most likely planar, were studied. Their enantiomerization barriers $\Delta G^{\ddagger}_{enant}$ were estimated by DNMR spectroscopy to be 13.9 kcal mol^{-1} at 297 K and 15.1 kcal mol^{-1} at 325 K (entries 10 and 11).

The activation parameter for the enantiomerization of the *tert*-butyl-substituted salt *rac*-**10** was not accessible by DNMR spectroscopy because of the lack of different chemical shifts for the diastereotopic nuclei in the *ortho* and *meta* positions of the phenyl group (see below). Neither could

Table 1. Estimation of the enantiomerization barriers of the salts *rac*-**1**–**8** by DNMR spectroscopy.

Entry	Salt	Solvent	c [mol L^{-1}]	$\Delta\nu$ [Hz]	J_{AB} [Hz]	k_{enant} [s^{-1}]	T_c [K]	$\Delta G^{\ddagger}_{enant}$ [kcal mol^{-1}]
1	*rac*-**1**	[D$_8$]THF	0.32, 0.20, 0.06	225	14.5	506	210 ± 5	9.5 ± 0.2
2	*rac*-**1**	[D$_8$]THF[a]	0.16	246	16.2	553	218 ± 5	9.9 ± 0.3
3	*rac*-**2**	[D$_8$]THF	0.28	225	14.5	550	213	9.6 ± 0.2
4	*rac*-**3**	[D$_8$]THF	0.28	86	17.9	214	283 ± 5	13.5 ± 0.2
5	*rac*-**4**	[D$_8$]THF	0.10	70[b]	15	176	295 ± 5	14.2 ± 0.3
6	*rac*-**4**	[D$_{14}$]Diglyme	0.10	98[b]	14	231	295 ± 5	14.1 ± 0.3
7	*rac*-**5**	[D$_8$]THF	0.10	148	15	339	≥333	≥15.7
8	*rac*-**5**	[D$_{14}$]Diglyme	0.10	153	15	350	343 ± 10	16.2 ± 0.5
9	*rac*-**6**	[D$_8$]THF	0.31	150	15.3	343	288 ± 5	13.6 ± 0.2
10	*rac*-**7**	[D$_8$]THF	0.16	162	16.9	377	297	13.9 ± 0.3
11	*rac*-**8**	[D$_8$]THF	0.16	201	16.4	455	325	15.1 ± 0.3

[a] In the presence of 2 equiv. of HMPA. [b] With selective spin-decoupling of the β-methyl group.

the activation parameter for the enantiomerization of the methyl-substituted salt *rac*-**9** be determined by this technique because of a lack of suitable diastereotopic nuclei.

A more detailed comparison of the enantiomerization barriers of the salts and the half-lives of enantiomerization is precluded because of the widely differing coalescence temperatures. The activation parameters $\Delta H^{\ddagger}_{enant}$ and $\Delta S^{\ddagger}_{enant}$ of the salts were not determined by DNMR spectroscopy because of the determination of the racemization dynamics of the salt (*P*)-**6** by polarimetry.[14] The data collected in Table 1 clearly show that there is no chance of obtaining chiral *S*-phenyl-substituted lithium salts of types **I** and **II** for further studies in enantiomerically enriched form even at low temperatures because of their fast racemization. Whereas the *S*-phenyl-substituted salt *rac*-**2** has a half-life $\tau_{1/2}$ of enantiomerization in THF of ca. 1.25×10^{-3} s at 213 K, that of the corresponding *S*-*tert*-butyl-substituted salt *rac*-**6**, calculated under the assumption that $\Delta S^{\ddagger}_{enant} = 0$, is about 16.8 s at 213 K. Thus, an enantioselective synthesis and study of *S*-*tert*-butyl-substituted salts of type **I** should be feasible at low temperatures as far as configurational stability is concerned.

Mechanism of Enantiomerization

The activation parameters for the enantiomerization of the salts *rac*-**1**–**8** were estimated based on the assumption that the process follows first-order kinetics. This raises the question as to the nature of the rate-determining step of the enantiomerization process. The lithium salts *rac*-**1**–**8** exist in THF solution as a mixture of THF-solvated monomeric and dimeric contact ion pairs (CIPs), the Li atom of which is bonded to the O atom(s) (see below). The enantiomerization of *rac*-**1**–**8** has, in principle, to involve (1) a rotation around the C_α–SR^3 bond, (2) an inversion of the C_α atom in the case of a nonplanar coordination geometry, (3) perhaps a conversion of the O–Li CIP carrying, for example, two THF molecules to the CIP with only one THF molecule, or (4) the conversion of the dimeric into the monomeric CIP. The formation of the less solvated CIP could perhaps minimize the steric interaction between the THF-coordinated Li atom and the C_α substituents during C_α–SR^3 bond rotation (see below). The similar barriers for the enantiomerization of *rac*-**1** at different concentrations may be taken as an indication that the establishment of the equilibrium between dimers and monomers is not rate-determining. It is assumed that at least in the case of the salts *rac*-**3**–**8**, which carry the sterically demanding *tert*-butyl group at the S atom, C_α–S bond rotation is the rate-determining step. Polarimetric measurements of the dialkyl-substituted salt (*P*)-**6** at low temperatures showed that its racemization is mainly an enthalpic process with a very small entropic contribution.[3f,3g] Previous studies of the *S*-trifluoromethyl-substituted lithium salts (*P*)-**Ia** and (*M*)-**IIa** and the corresponding potassium and tetrabutylammonium salts in THF and DMSO led to a similar conclusion.[3f,3g] The barriers to enantiomerization for the salts *rac*-**1** and *rac*-**2**, the C_α atoms of which should be planar and pyramidalized, respectively, show furthermore that the inversion of the C_α atom cannot be rate-determining. This is in accordance with theoretical[6b,6c] and chemical evidence[1c,3k,3m,21] that suggests that the inversion barrier of a pyramidalized C_α atom is small. Finally, there seems to be no significant difference in the enantiomerization barriers of the benzylic and non-benzylic α-sulfonyl carbanion as a comparison of the pairs of the salts *rac*-**1**/*rac*-**2** and *rac*-**3**/*rac*-**6** shows.

Aggregation in Solution

The *S*-*tert*-butyl-substituted lithium α-sulfonyl carbanion salts **3**–**10** are promising candidates for the attainment of nonracemic salts of types **I** and **II** and the study of their reactivity. Thus, a determination of their aggregation in THF solution was deemed necessary. Knowledge of the species that prevail in solution should facilitate a rationalization of the enantioselectivity of their reactions with electrophiles. The aggregation of the salts *rac*-**3**–**6** and *rac*-**9** was studied by cryoscopy and low-temperature NMR spectroscopy (see below). Cryoscopic measurements of the salts *rac*-**3**, *rac*-**4**, *rac*-**6**, and *rac*-**9** in THF were successfully performed by the method described by Bauer and Seebach.[22] The cryoscopic constant of THF was determined by measurements with naphthalene and stilbene. As a test, the aggregation of *n*BuLi in THF was determined, which gave good agreement with the literature data ($n = 2.43 \pm 0.07$ at $c = 96.4$ mmol kg^{-1} vs. 2.38 ± 0.13 at $c = 92.9$ mmol kg^{-1}).[22] The cryoscopy measurements were carried out in THF solutions of the salts, which had been prepared with the

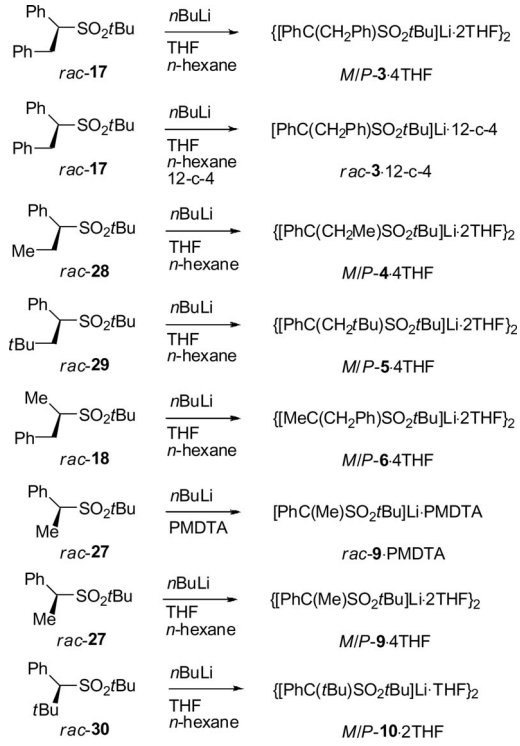

Scheme 2. Synthesis of the salts (*M*/*P*)-**3**·4THF, *rac*-**3**·12-crown-4, (*M*/*P*)-**4**·4THF, (*M*/*P*)-**5**·4THF, (*M*/*P*)-**6**·4THF, *rac*-**9**·PMDTA, (*M*/*P*)-**9**·4THF, and (*M*/*P*)-**10**·2THF.

crystalline salts (*M*/*P*)-**3**·4THF, (*M*/*P*)-**4**·4THF, (*M*/*P*)-**6**·4THF, and (*M*/*P*)-**9**·4THF. The THF content of the salts was determined by NMR spectroscopy. The salts were prepared from the corresponding racemic sulfones *rac*-**17**, *rac*-**28**, *rac*-**18**, and *rac*-**27** as shown in Scheme 2. Several measurements were taken for each salt. After the measurements were completed, the integrity of the salts was checked by deuteriation with CF_3CO_2D and the D content of the corresponding sulfone determined by NMR spectroscopy. Table 2 shows that the salts *rac*-**3**, *rac*-**4**, *rac*-**6**, and *rac*-**9** (entries 1–4) exist in THF at low temperatures as mixtures of monomers and dimers in ratios ranging from 85:15 to 33:67 depending on the substituents on the C_α atom (see below). These results are in accordance with those obtained in previous cryoscopy experiments of lithium salts of chiral and achiral α-sulfonyl carbanions[1c,3f,3g,6k,23] and acidity measurements of sulfones in THF.[5a,5d,5g]

Table 2. Aggregation of the *S*-*tert*-butyl-substituted salts *rac*-**3**, *rac*-**4**, *rac*-**6**, and *rac*-**9** at –108 °C in THF.

Entry	Salt	c [mmol kg^{-1}]	$N \pm \sigma$	Monomer/dimer
1	*rac*-**3**	86.6	1.14 ± 0.15	ca. 85:15
2	*rac*-**4**	54.1	1.36 ± 0.04	ca. 64:36
3	*rac*-**6**	49.9	1.60 ± 0.06	ca. 40:60
4	*rac*-**9**	49.7	1.67 ± 0.18	ca. 33:67

Structures of Lithium α-*tert*-Butylsulfonyl Carbanion Salts in the Crystal

Cryoscopy of the *S*-*tert*-butyl-substituted lithium salts *rac*-**3**, *rac*-**4**, *rac*-**6**, and *rac*-**9** in THF revealed the existence of monomers and dimers in THF solution. Thus, the question arose as to the structures of the monomeric and dimeric salts. Knowledge of the crystal structures of the lithium salts of *S*-*tert*-butylsulfonyl carbanions was required because of the enantioselective synthesis of **3**–**6**, **9**, and **10** and the study of their dynamics and reactivity towards electrophiles.[14] Therefore the crystal structures of the dimeric lithium salts (*M*/*P*)-**3**·4THF, (*M*/*P*)-**4**·4THF, (*M*/*P*)-**5**·4THF, and (*M*/*P*)-**10**·2THF and the monomeric lithium salts *rac*-**3**·12-crown-4 and *rac*-**9**·PMDTA were determined. Although much is known about the structures of the dimers of *S*-aryl-substituted lithium α-sulfonyl carbanion salts in the crystal form,[3] those of *S*-*tert*-butyl-substituted α-sulfonyl carbanion salts were, with one exception, unknown.[3m] Most importantly, however, in general, the structures of the monomers of lithium α-sulfonyl carbanion salts, which are expected to play an important role in reactions with electrophiles, were unknown.[3m]

Dimeric Salts

Single crystals of the dimeric C_α-benzyl-, C_α-ethyl-, and C_α-neopentyl- and *S*-*tert*-butyl-substituted benzylic lithium salts (*M*/*P*)-**3**·4THF, (*M*/*P*)-**4**·4THF, and (*M*/*P*)-**5**·4THF, respectively, were obtained by deprotonation of the corresponding racemic sulfones *rac*-**17**, *rac*-**28**, and *rac*-**29** with *n*BuLi in THF/*n*-hexane and recrystallization from *n*-hexane/THF (cf. Scheme 2). Each salt crystallized with four molecules of THF as a THF-solvated heterochiral dimer (Figures 4, 5, and 6)[24] in a structure similar to that of the *S*-phenyl-substituted salt (*M*/*P*)-**1**·4THF.[3d,3g] The Li atoms are coordinated in a tetrahedral fashion by only four O atoms. The two anions of the dimer are held together by four O–Li bonds, and each anion is coordinated by two Li atoms. Thus, a characteristic eight-membered ring is formed, the O–Li bond lengths of which are between 1.88(1) and 1.900(6) Å (see the Supporting Information). The puckering of the ring of the dimeric salts differs only slightly. The similarity of the rings is reflected by their torsion angles and the deviation of the S and Li atoms from the plane defined by the four O atoms. The anions have a

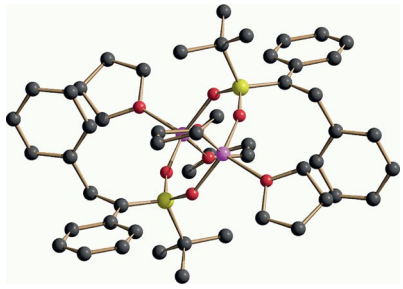

Figure 4. View of the crystal structure of the dimeric benzyl-substituted salt (*M*/*P*)-**3**·4THF with H atoms omitted for clarity. Color code: C, black; S, yellow; O, red; Li, pink.

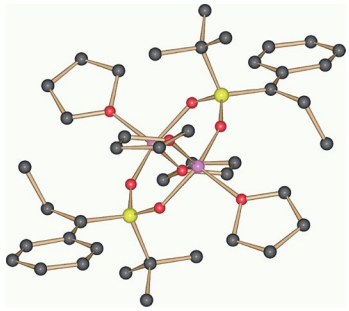

Figure 5. View of the crystal structure of the dimeric ethyl-substituted salt (*M*/*P*)-**4**·4THF with H atoms omitted for clarity. Color code: C, black; S, yellow; O, red; Li, pink.

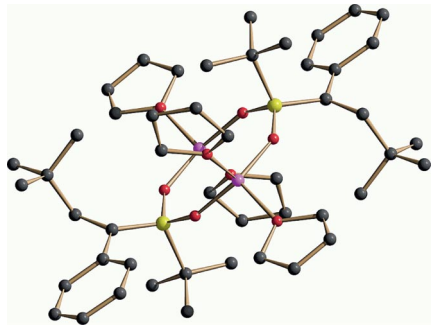

Figure 6. View of the structure of the dimeric neopentyl-substituted salt (*M*/*P*)-**5**·4THF with H atoms omitted for clarity. Color code: C, black; S, yellow; O, red; Li, pink.

typical C_α–S conformation in which the orbital at the C_α atom is *gauche* to both O atoms (see the Supporting Information). They adopt a C_α–CH_2 conformation in which the group in the β position (phenyl, methyl, *tert*-butyl) is *anti* to the *S*-*tert*-butyl group. There are no bonds between the C_α atom and the Li atoms in the dimeric *S*-*tert*-butyl salts, as indicated by C_α–Li nonbonding distances between 4.190(4) and 4.424(7) Å.

Finally, the dimeric C_α,*S*-di-*tert*-butyl-substituted lithium salt (*M*/*P*)-**10**·2THF was synthesized and its crystal structure analyzed. The anion of the salt (*M*/*P*)-**10**·2THF carries the sterically demanding *tert*-butyl group at the C_α atom, which could influence the C_α–S and C_α–Ph conformation (see above). The salt (*M*/*P*)-**10**·2THF was obtained without difficulty in the usual manner by deprotonation of the racemic sulfone *rac*-**30** with *n*BuLi in THF/*n*-hexane solution and recrystallization from *n*-hexane. The salt (*M*/*P*)-**10**·2THF also crystallized as a THF-solvated heterochiral dimer (Figure 7).[24] However, presumably for steric reasons, the Li atoms of (*M*/*P*)-**10**·2THF are each coordinated by only one THF molecule. Thus, the Li atoms achieve a less common tricoordination by O atoms[25] in a slightly nonplanar fashion (Σ∠Li = 354°). Of all the dimeric salts studied, the salt (*M*/*P*)-**10**·2THF has the most puckered eight-membered ring (see the Supporting Information) as revealed by the torsion angles and the deviation of the S atoms from the plane defined by the O atoms. The *S*-*tert*-butyl groups occupy the pseudoequatorial and the *t*Bu(Ph)C fragments the pseudoaxial positions of the chair-like ring.

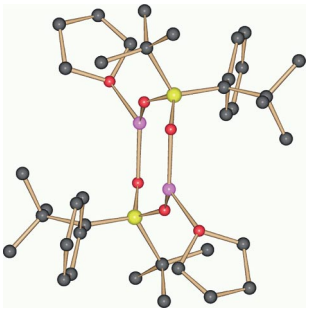

Figure 7. View of the crystal structure of the dimeric *tert*-butyl-substituted salt (*M*/*P*)-**10**·2THF with H atoms omitted for clarity. Color code: C, black; S, yellow; O, red; Li, pink.

An additional structural feature, however, in which the salt (*M*/*P*)-**10**·2THF differs structurally most significantly from the other benzylic salts (*M*/*P*)-**3**·4THF, (*M*/*P*)-**4**·4THF, and (*M*/*P*)-**5**·4THF is the orientation of the α-phenyl ring, which is almost orthogonal to the S–C_α–C_β plane (see the Supporting Information). Consequently, at 1.508(5) Å the C_α–Ph bond in (*M*/*P*)-**10**·2THF is the longest among the benzylic salts described in this paper. There are no C_α–Li bonds as the C_α–Li nonbonding distances of 3.639(8) and 3.688(8) Å show. Because of the pseudoaxial position of the C_α atoms of (*M*/*P*)-**10**·2THF, this salt has the shortest C_α–Li nonbonding distances of all the dimeric salts described. The O–Li bond lengths for the ring are 1.842(7) and 1.885(7) Å, that is, in the normal range. The anion has the typical C_α–S conformation. However, this salt shows a further interesting structural feature. The following parameter seems to indicate a stabilizing interaction between the Li atom and the phenyl ring,[26a] which is not in conjugation with the lone-pair orbital at the C_α atom (see below). First, the nonbonding distance between the coordinatively unsaturated Li atom and the C_o atom of the phenyl ring is, at 2.652(9) Å, smaller than the sum of the van der Waals radii of Li (1.60 Å) and C (1.70 Å); optimization of the model complex C_6H_6·$Li(H_2O)_3^+$ (see the Supporting Information) at the MP2/6-31+G* level resulted in a Li···C distance of 2.447 Å and a binding energy of –13.9 kcal mol^{-1} relative to benzene and $Li(H_2O)_3^+$. Secondly, the phenyl group bends towards the Li atom. Thirdly, the eight-membered ring is strongly puckered. Although these parameters point to a stabilizing C_o···Li interaction, a purely steric origin of the relatively short C_o···Li distance cannot be excluded.[26b]

Monomeric Salts

Having obtained a general picture of the structures of the dimeric lithium *S*-*tert*-butyl salts in the crystal form, it was important to gather information about the structures of the monomeric salts. Because the structure of the dimer (*M*/*P*)-**3**·4THF was known, we chose to synthesize the monomeric salt *rac*-**3**. To attain a monomer of *rac*-**3**, our previous experience of the preparation of the monomeric potassium salt of a α-sulfonyl carbanion[3e] suggested the use of the lithium-ion-specific 12-crown-4 as donor ligand to prevent dimer formation for steric reasons. Single crystals of the C_α-benzyl- and *S*-*tert*-butyl-substituted lithium salt *rac*-**3**·12-crown-4 were obtained by deprotonation of sulfone *rac*-**17** with *n*BuLi in THF/*n*-hexane solution in the presence of 12-crown-4 and crystallization from THF. The X-ray structure analysis of *rac*-**3**·12-crown-4 revealed a monomer with the Li atom coordinated to only one O atom of the anion in addition to the four O atoms of the crown ether molecule (Figure 8).[24] Interestingly, the two known crystal structures of monomeric 18-crown-6-coordinated potassium salts of α-sulfonyl carbanions feature a coordination of the K atom to both sulfonyl O atoms as well as the ether O atoms.[3e,3j] One has to consider, however, that in addition to the different coordination numbers of the Li and K atoms, the O–K bond length of 2.808(3) Å (average value) is much longer than the average O–Li bond length of 2.10(1) Å. Thus, one reason for this striking structural difference between the crown ether coordinated monomeric potassium and lithium salts might be that a monomer of 12-crown-4-coordinated *rac*-**3** in which both sulfonyl O atoms are coordinated to the Li atom is energetically less favorable than *rac*-**3**·12-crown-4 because of van der Waals repulsion between the anion and the crown ether. The diastereomer of *rac*-**3**·12-crown-4 having the relative *P*(*M*),S_S(R_S) configuration crystallized preferentially. Presumably for steric reasons the S, O, and Li atoms are arranged in a nearly linear fashion, as revealed by the Li–O–S angle of 166.4(6)°. The sulfonyl O–Li bond length

[1.864(1) Å] is slightly shorter than the average sulfonyl O–Li bond length in (*M*/*P*)-**3**·4THF [1.983(4) Å]. The average O–Li bond length to the crown ether [2.10(1) Å] is somewhat longer than the average O–Li bond length of the coordinated THF molecules in (*M*/*P*)-**3**·4THF. This feature is, however, in perfect agreement with the Li–O bond lengths in other lithium–crown ether complexes.[25c] The anion of *rac*-**3**·12-crown-4 also has the typical C_α–S conformation (see the Supporting Information). The β-phenyl ring is *anti* to the *tert*-butyl group and there are no C_α–Li bonds as the C_α–Li nonbonding distance of 4.099(13) Å shows.

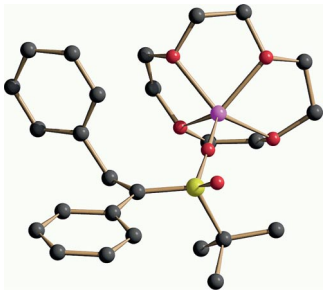

Figure 8. View of the crystal structure of the monomeric benzyl-substituted salt *rac*-**3**·12-crown-4 with H atoms omitted for clarity. Color code: C, black; S, yellow; O, red; Li, pink.

The crystal structure of the salt *rac*-**3**·12-crown-4, which carries a benzyl and phenyl group at the C_α atom, is only the second monomeric acyclic lithium α-sulfonyl carbanion salt known.[3m] Because the monomeric salts are expected to play a crucial role in the reactions of the salts with electrophiles (see below), knowledge of the structure of a further monomeric *S*-*tert*-butylsulfonyl carbanion salt was desirable in order to have a more general picture. The salt *rac*-**9**, which carries a methyl and phenyl group at the C_α atom, was chosen as a model because of the enantioselective synthesis and reactivity study of (*P*)-**9**.[14] Because of our previous success in the synthesis of the monomeric PMDTA-coordinated lithium salt of a bicyclic allylic *S*-*tert*-butylsulfonyl carbanion,[3m] this ligand was also used in this case. Single crystals of the *C*$_\alpha$-methyl- and *S*-*tert*-butyl-substituted lithium salt *rac*-**9**·PMDTA were obtained by deprotonation of the racemic sulfone *rac*-**27** with *n*BuLi in PMDTA solution and recrystallization from PMDTA/THF. X-ray structure analysis of *rac*-**9**·PMDTA revealed a monomer with the Li atom coordinated to only one O atom of the anion in addition to the three N atoms of the triamine (Figure 9).[24] The diastereomer of *rac*-**9**·PMDTA having the relative *M*(*P*),*S*$_S$(*R*$_S$) configuration had preferentially crystallized. The S, O, and Li atoms are not arranged in an almost linear fashion as in *rac*-**3**·12-crown-4, as revealed by the average Li–O–S angle of 138.5(3)°. The sulfonyl O–Li bond length of 1.850(8) Å is slightly shorter than the O–Li bond length of *rac*-**3**·12-crown-4 [1.86(1) Å]. The anion of *rac*-**9**·PMDTA also has the typical C_α–S conformation (see the Supporting Information). There are no C–Li bonds as the C_α–Li nonbonding distance of 3.647(9) Å shows.

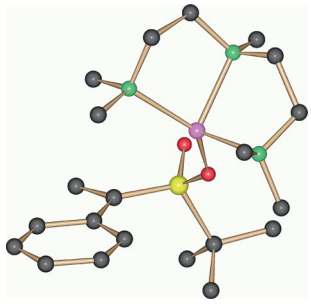

Figure 9. View of the crystal structure of the monomeric methyl-substituted salt *rac*-**9**·PMDTA with H atoms omitted for clarity. Color code: C, black; S, yellow; O, red; N, green; Li, pink.

C$_\alpha$*–S Conformation and C*$_\alpha$ *Configuration of the Dimeric Lithium Salts*

The anions of the dimeric *S*-*tert*-butyllithium salts (*M*/*P*)-**3**·4THF, (*M*/*P*)-**4**·4THF, (*M*/*P*)-**5**·4THF, and (*M*/*P*)-**10**·2THF all have a similar C_α–S conformation irrespective of the second substituent at the C_α atom (Table 3) and the conformation of the eight-membered (Li–O–S–O)$_2$ coordination ring (see the Supporting Information). The lone-pair

Table 3. Torsion angles *α* and *β*,[a] sum of the angles |*α*|+|*β*|, torsion angles S–C_α–C_i–C_o, and S–C_α–CH_2–R,[a] and sum of the bond angles Σ∠C_α of the salts (*M*/*P*)-**3**·4THF, *rac*-**3**·12-crown-4, (*M*/*P*)-**4**·4THF, (*M*/*P*)-**5**·4THF, *rac*-**9**·PMDTA, (*M*/*P*)-**10**·2THF, (*M*/*P*)-**40**·2diglyme, (**41**·diglyme)$_2$, and (**42**·diglyme)$_2$.[b]

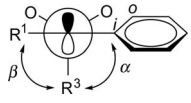

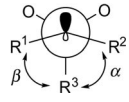

Salt	R^1	R^2	R^3	*α* [°]	*β* [°]	|*α*|+|*β*| [°]	S–C_α–C_i–C_o [°]	S–C_α–CH_2–R [°]	Σ∠C_α [°]
(*M*/*P*)-**3**·4THF	$PhCH_2$	Ph	*t*Bu	83.1	–93.3	176.4	10.5	–108.5	359.9
rac-**3**·12-crown-4	$PhCH_2$	Ph	*t*Bu	88.6(7)	–85.2(5)	173.8	–5.9(8)	–109.5(7)	359.7
(*M*/*P*)-**4**·4THF	$MeCH_2$	Ph	*t*Bu	86.6(7)	–93.0(6)	179.6	6(1)	–107.3(7)	360.0
(*M*/*P*)-**5**·4THF	*t*$BuCH_2$	Ph	*t*Bu	68.7(3)	–94.0(3)	162.7	38.9(5)	–114.3(3)	357.6
rac-**9**·PMDTA	Me	Ph	*t*Bu	–87.7(4)	91.8(4)	179.5	4.6(7)	–	360.0
(*M*/*P*)-**10**·2THF	*t*Bu	Ph	*t*Bu	101.7(3)	–92.7(3)	194.4	77.0(4)	–	358.5
(*M*/*P*)-**40**·2diglyme	Et	Me	Ph	73.8(7)	–73.1(9)	146.9	–	–148.3(6)	351.1
(**41**·diglyme)$_2$	Et	Et	Ph	68.0(2)	–73.6(2)	141.6	–	–148.3(2), 112.9(2)	348.2
(**42**·diglyme)$_2$	–$(CH_2)_5$–		Ph	77.7(5)	–72.2(4)	149.9	–	–158.4(4), 151.1(5)	353.2

[a] Calculated neglecting standard deviations. [b] Charges of the structural formulae have been omitted for clarity.

orbital at the C_α atom is *gauche* to both O atoms, as judged by the torsion angles *α* and *β*. This allows a stabilization of the anions by $n_C–\sigma^*_{SR3}$ hyperconjugation.[6] Because of different van der Waals repulsion within the benzylic anions and the aggregates these torsion angles differ in magnitude. Not surprisingly, the deviation is the strongest for the C_α-*tert*-butyl- and C_α-neopentyl-substituted salts (*M*/*P*)-**10**·2THF and (*M*/*P*)-**5**·4THF, respectively.

Because of the stabilization of the negative charge by conjugation with the phenyl group, the C_α atoms of the anions are almost planar-coordinated, as shown by the sum of their bond angles $\Sigma\angle C_\alpha$. The phenyl rings at the C_α atoms of the benzyl- and ethyl-substituted salts (*M*/*P*)-**3**·4THF and (*M*/*P*)-**4**·4THF, respectively, are nearly coplanar with the S–C_α–C_i plane, as revealed by the torsion angles S–C_α–C_i–C_o. Deviation from coplanarity is such that the conjugative interaction is not significantly hampered. For the neopentyl- and *tert*-butyl-substituted salts (*M*/*P*)-**5**·4THF and (*M*/*P*)-**10**·THF, however, these torsion angles are 38.9(5) and 77.0(4)°. This large deviation from coplanarity most likely results from a steric interaction between the phenyl ring and the *tert*-butyl group. As a consequence, stabilization of the negative charge by the p_π–p_π interaction should be diminished in (*M*/*P*)-**5**·4THF and nearly absent in (*M*/*P*)-**10**·2THF (see below). Therefore the C_α atoms of (*M*/*P*)-**10**·2THF ought to be significantly pyramidalized. However, the resulting steric interaction between the *tert*-butyl groups prevents pyramidalization (see below). Thus, the size of the alkyl substituent at the C_α atom has no significant bearing upon the C_α–S conformation of the anion.

Comparison of the Bonding Parameters of the Salts and Parent Sulfones

A comparison of the structure of the lithium salt (*M*/*P*)-**3**·4THF (Table 4) with that of the parent sulfone *rac*-**17**[14] reveals a considerable shortening of the C_α–S bond by approximately 10% (0.18 and 0.19 Å). The S–O bonds are slightly longer. The shortening of the C_α–S bond and the lengthening of the S–O bond are general phenomena for α-sulfonyl carbanions.[3] The C_α–Ph bond in (*M*/*P*)-**3**·4THF is also shortened significantly in comparison with the corresponding sulfone. There are only minor differences in the C_α–Ph bond length in (*M*/*P*)-**3**·4THF, (*M*/*P*)-**4**·4THF, and (*M*/*P*)-**5**·4THF. Not surprisingly, the C_α-*tert*-butyl-substituted salt (*M*/*P*)-**10**·2THF has the longest C_α–Ph bond, which is, however, shorter than in the corresponding sulfone. Of all the *S*-*tert*-butyl-substituted lithium salts studied, the salt (*M*/*P*)-**10**·2THF has the shortest C_α–S bond and the longest S–O and C_α–Ph bonds. In addition, the lengthening of the S–O bond in (*M*/*P*)-**10**·2THF in comparison with the parent sulfone *rac*-**30** is, although small, the strongest observed for the lithium salt of an α-sulfonyl carbanion. Noticeable changes in bond angles at the S atom of the parent sulfones *rac*-**17** and *rac*-**30** occur upon deprotonation. In the *S*-*tert*-butyl-substituted salts (*M*/*P*)-**3**·4THF and (*M*/*P*)-**10**·2THF the C_α–S–*t*Bu, C_i–C_α–S, and S–C_α–*t*Bu angles are increased and the O–S–O angle is slightly reduced.

Comparison of the Monomeric and Dimeric Salts

The monomeric and dimeric salts are generally expected to have CIP structures (see below) in which the C_α–S conformation and the position of the Li atom are very similar. Indeed, the anions of the monomer *rac*-**3**·12-crown-4 and dimer (*M*/*P*)-**3**·4THF have a very similar conformation. The smaller value of *β* and the larger value of *α* in *rac*-**3**·12-crown-4 seems to be the consequence of van der Waals repulsion between the benzyl group and the neighboring crown ether molecule. The decisive bond lengths and angles in (*M*/*P*)-**3**·4THF and *rac*-**3**·12-crown-4 are almost identical. Thus, the structure of the anion of dimer (*M*/*P*)-**3**·4THF is retained in the monomer *rac*-**3**·12-crown-4. Furthermore it is apparently of no consequence for the structure of the anion whether it is coordinated either to one or two Li atoms. The crystal structures of *rac*-**3**·12-crown-4 and *rac*-**9**·PMDTA can thus serve as appropriate models for the structure of the monomeric lithium salt **I** in THF solution. Although the crystal structure of the dimeric salt (*M*/*P*)-**9**·4THF is not available for comparison, there is little doubt that the structure of the anion in the monomer is not significantly different to that of the dimer. This notion is corroborated by the bonding parameters of *rac*-**9**·PMDTA. It should be emphasized, however, that *rac*-**3**·12-crown-4 and *rac*-**9**·PMDTA are only models for the monomeric O–Li CIPs in THF solution. Crystallization of

Table 4. Selected bond lengths and bond angles for the salts (*M*/*P*)-**3**·4THF, *rac*-**3**·12-crown-4, (*M*/*P*)-**4**·4THF, (*M*/*P*)-**5**·4THF, *rac*-**9**·PMDTA, (*M*/*P*)-**10**·2THF, (*M*/*P*)-**40**·2diglyme, (**41**·diglyme)$_2$, and (**42**·diglyme)$_2$.

	Bond lengths [Å]					Bond angles [°]	
Salt	C_α–S	S–R^3	S–O	C_α–Ph	Li–O	C_α–S–R^3	O–S–O
(*M*/*P*)-**3**·4THF	1.659(2)	1.838(2)	1.457(2), 1.458(2)	1.451(3)	1.878(4), 1.891(4)	113.5(1)	115.1(1)
rac-**3**·12-crown-4	1.68(1)	1.841(8)	1.465(9), 1.46(1)	1.45(1)	1.86(1)	112.2(4)	114.9(6)
(*M*/*P*)-**4**·4THF	1.671(7)	1.830(7)	1.465(5), 1.450(5)	1.43(1)	1.888(12), 1.877(12)	112.3(3)	115.1(3)
(*M*/*P*)-**5**·4THF	1.652(3)	1.842(4)	1.459(3), 1.461(3)	1.467(5)	1.900(6), 1.879(6)	112.9(2)	114.5(1)
rac-**9**·PMDTA	1.675(5)	1.832(5)	1.444(3), 1.466(3)	1.430(6)	1.828(8)	112.9(2)	115.3(2)
	1.667(5)	1.836(5)	1.438(3), 1.466(3)	1.440(6)	1.871(8)	112.6(2)	115.2(2)
(*M*/*P*)-**10**·2THF	1.630(4)	1.847(4)	1.483(2), 1.475(2)	1.508(5)	1.885(7), 1.842(7)	117.0(2)	113.6(2)
(*M*/*P*)-**40**·2diglyme	1.643(7)	1.793(9)	1.450(7), 1.455(6)	–	1.898(11), 1.940(18)	113.1(4)	115.9(3)
(**41**·diglyme)$_2$	1.636(2)	1.802(2)	1.458(2), 1.466(1)	–	1.894(4), 1.943(4)	111.5(1)	116.5(1)
(**42**·diglyme)$_2$	1.641(4)	1.780(5)	1.459(4), 1.461(4)	–	1.914(11), 1.912(8)	112.4(2)	117.1(2)

the monomer of a lithium α-sulfonyl carbanion salt that is coordinated only by THF molecules has yet to be accomplished.

Configuration of the Anionic C Atom of the C_α-Dialkyl-Substituted Salts

Crystal analysis of the dimeric *S*-*tert*-butyl-substituted benzylic salts (*M*/*P*)-**3**·4THF, (*M*/*P*)-**4**·4THF, and (*M*/*P*)-**5**·4THF had revealed structures with a planar anionic C atom, a feature that can now be regarded as a general one for benzylic lithium α-sulfonyl carbanion salts. In contrast, the question of the coordination geometry of the C_α atom of the lithium salts of α,α-dialkyl-substituted α-sulfonyl carbanions remained largely unanswered. Although X-ray crystal structure analysis of the *S*-phenyl-substituted lithium salt **35** (dimeric O–Li CIP; $\Sigma\angle C_\alpha$ = 346.5°),[3d] the corresponding salt **36** [solvent-separated ion pair (SIP); 351.7°],[3h] and, to a lesser extent, the bicyclic allylic salts *rac*-**37** (dimeric O–Li CIP; $\Sigma\angle C_\alpha$ = 349.8°) and *rac*-**38** (dimeric O–Li CIP; $\Sigma\angle C_\alpha$ = 355.2°)[3k] revealed strongly pyramidalized C_α atoms, that of the bicyclic allylic *S*-*tert*-butyl-substituted salt *rac*-**39** (monomeric O–Li CIP; $\Sigma\angle C_\alpha$ = 359.7°) is planar (Figure 10).[3m] Ab initio calculations on the counterion-free carbanions **37**(–Li) and **38**(–Li) also showed their anionic C atoms to be pyramidalized.[3k] Because of this seemingly contradictory evidence and the perhaps nonrepresentative structures of the bicyclic salts (allylic conjugation), it was desirable to obtain further information about the coordination geometry of the dialkyl-substituted C_α atom of the *S*-phenyl- and especially *S*-*tert*-butylsulfonyl carbanions. First, the *S*-phenyl-substituted salts (*M*/*P*)-**40**·2diglyme, (**41**·diglyme)$_2$, and (**42**·diglyme)$_2$ were prepared and their crystal structures determined in order to acquire a general picture of the coordination geometry of the C_α atom of dialkyl-substituted α-phenylsulfonyl carbanions. These salts were chosen because of our previous determination of the structure of **35** and the corresponding C_α-phenyl- and -methyl-substituted salt.[3d] Sulfones *rac*-**46**,[27a] **47**,[27b] and **48**[27c] (Scheme 3) were synthesized from the corresponding bromides via the corresponding sulfides by standard procedures (see the Supporting Information). Single crystals of the salts (*M*/*P*)-**40**·2diglyme, (**41**·diglyme)$_2$, and (**42**·diglyme)$_2$ were obtained by deprotonation of the corresponding sulfones with *n*BuLi in diglyme and recrystallization of the salts from diglyme.

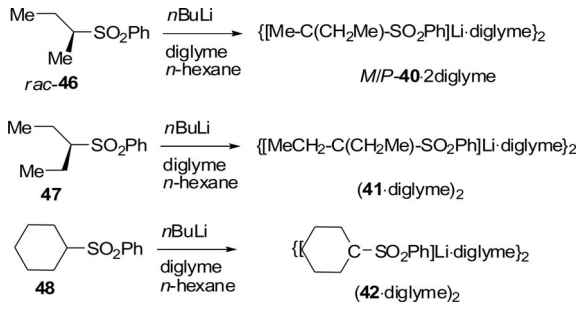

Scheme 3. Synthesis of the salts (*M*/*P*)-**40**·2diglyme, (**41**·diglyme)$_2$, and (**42**·diglyme)$_2$.

Each salt crystallized together with two molecules of diglyme as the diglyme-solvated dimer[3d] (Figures 11, 12, and 13).[24] The Li atoms are coordinated by five O atoms. The two anions of the dimer are held together by four O–Li bonds, each anion carrying two Li atoms. Thereby the dimer has the characteristic eight-membered ring (see the Supporting Information), the O–Li bond lengths of which are between 1.894(4) and 1.943(4) Å. Whereas the coordination ring of (*M*/*P*)-**40**·2diglyme and (**41**·diglyme)$_2$ shows only a small deviation from planarity, that of (**42**·diglyme)$_2$ is strongly puckered. The anions of (*M*/*P*)-**40**·2diglyme, (**41**·diglyme)$_2$, and (**42**·diglyme)$_2$ adopt the typical C_α–S conformation (see the Supporting Information) and their C_α–S bond lengths (cf. Table 4) are also in the typical region. However, the C_α atoms of (*M*/*P*)-**40**·2diglyme, (**41**·diglyme)$_2$, and (**42**·diglyme)$_2$ are strongly

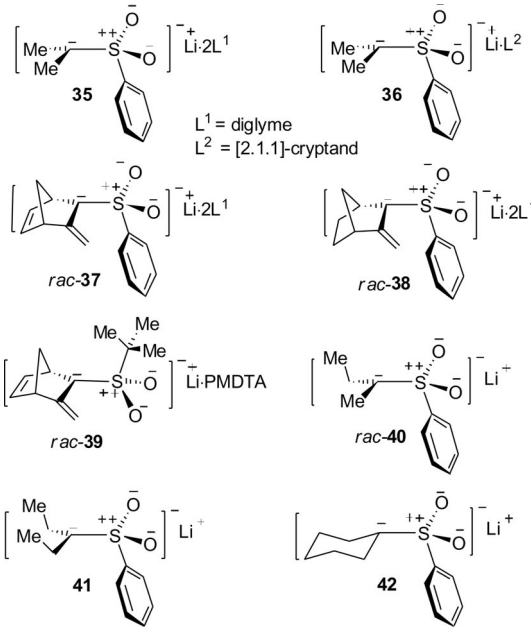

Figure 10. α,α-Disubstituted non-benzylic lithium α-sulfonyl carbanion salts.

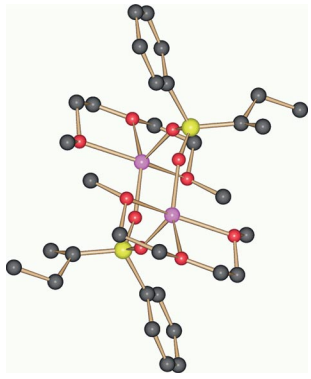

Figure 11. View of the crystal structure of the dimeric salt (*M*/*P*)-**40**·2diglyme with H atoms omitted for clarity. Color code: C, black; S, yellow; O, red; Li, pink.

pyramidalized in the direction of the O atoms, as revealed by the dihedral angles α and β and the sum of the bond angles around the C_α atom (cf. Table 3). The C_α atom of the α,α-dimethyl-substituted salt **35** shows a similar degree of pyramidalization with dihedral angles of α = 72.9° and β = –66.4° and a sum of bond angles of 346.5°.[3d,3h] Because of these results and those obtained previously, it can now be safely stated that the C_α atoms of dialkyl-substituted *S*-phenylsulfonyl carbanions and perhaps also *S*-arylsulfonyl carbanions are generally pyramidalized (half-way between sp^2 and sp^3).

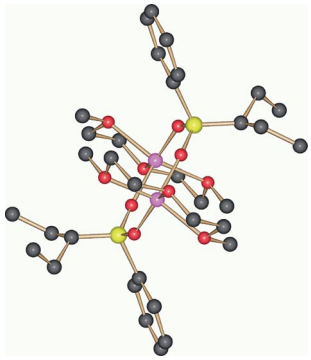

Figure 12. View of the crystal structure of the dimeric salt (**41**·diglyme)$_2$ with H atoms omitted for clarity. Color code: C, black; S, yellow; O, red; Li, pink.

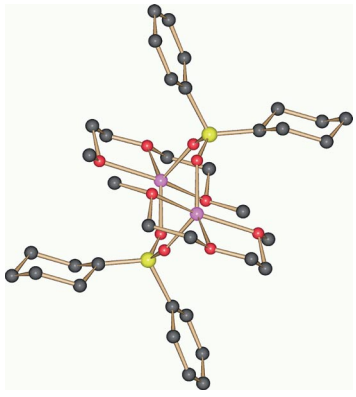

Figure 13. View of the crystal structure of the dimeric salt (**42**·diglyme)$_2$ with H atoms omitted for clarity. Color code: C, black; S, yellow; O, red; Li, pink.

Ab Initio Calculations of C_α-Dialkyl-Substituted Counterion-Free Carbanions

Left open was the question of the coordination geometry of the C_α atom of the dialkyl-substituted *S*-*tert*-butylsulfonyl carbanion. Unfortunately, we could not obtain suitable single crystals of the *S*-*tert*-butyl-substituted salt *rac*-**6**. Therefore calculations on the counterion-free carbanions **43**, **44**, and **45**, which carry a methyl, trifluoromethyl, and *tert*-butyl group at the S atom, respectively, were carried out to see whether the steric size of the S substituent [E_s (Me) = –1.24, E_s (CF_3) = –2.4, E_s (CMe_3) = –2.78][11] has a bearing on the coordination geometry of the anionic C atom.

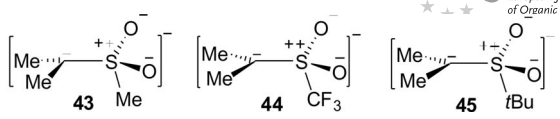

Ab initio geometry optimizations at the MP2/6-31+G* level of theory were performed for the carbanions **43**, **44**, and **45** (Figure 14). Calculation and diagonalization of the force constant matrices of the obtained stationary points showed that they were local minima. The molecular energies were at minima for structures in which the sums of the bond angles at the anionic carbon atom are 344.6° for the *S*-methyl carbanion **43**, 354.1° for the *S*-trifluoromethyl carbanion **44**, and 356.1° for the *S*-*tert*-butyl carbanion **45** (Table 5). The corresponding C_α–S bond lengths correlate with the energy of interaction between the lone pair at the C_α atom ($n_{C\alpha}$) and the antibonding orbital of the S–CR_3 (R = H, F, Me) bond (σ^*_{S-CR3}; see $\Delta E_{n\rightarrow\sigma^*}$, footnote d, Table 10) in that a more negative value of $\Delta E_{n\rightarrow\sigma^*}$ corresponds to a shorter C_α–S bond. Consequently the length of the S–CR_3 bond increases in the same direction. Delocalization of the anionic lone pair into the σ^*_{S-CR3} orbital is also reflected by a decrease in the charge on the CMe_2 group. According to the NBO calculation there is no such lone pair at the C_α atom of carbanion **45** but a S–C π bond instead. However, almost 90% of this π bond is located at the C_α atom so that it can be considered a lone pair. Thus, comparison of the *S*-*tert*-butyl carbanion **45** with the *S*-methyl carbanion **43** shows the C_α atom of the former is planar and the C_α–S bond is shorter. A similar situation exists in the case of the *S*-trifluoromethyl carbanion **44**. However, carbanion **44** is a special case because of the strong effect exerted by the fluorine atoms upon the structure and stabilization.[3f,3g,6h,6j]

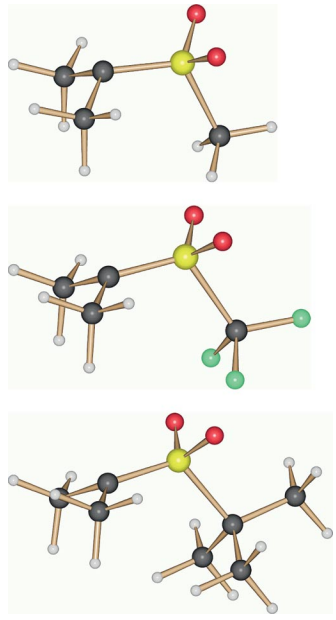

Figure 14. Structure of the *S*-methylsulfonyl carbanion **43** (top), *S*-trifluoromethylsulfonyl carbanion **44** (middle), and *S*-*tert*-butylsulfonyl carbanion **45** (bottom) obtained at the MP2/6-31+G* level of theory. Color code: C, black; S, yellow; O, red; F, green; H, grey.

Table 5. Selected bond angles and lengths, energies, and charges for the carbanions **43**, **44**, and **45**.

Parameter	**43**	**44**	**45**
$\Sigma\angle C_\alpha$ [°]	344.6	354.1	356.1
C_α–S [Å]	1.674	1.640	1.660
S–CR_3 [Å]	1.835	1.904	1.887
$q(C_\alpha Me_2)$ [e]	–0.87	–0.75	–0.83
σ^*_{S-CR3} [kcal mol^{-1}]	–35.1	–65.9	–43.8

In summary, there is much experimental and theoretical evidence showing that dialkyl-substituted α-sulfonyl carbanions generally have a strongly pyramidalized C_α atom except for when the S atom bears a bulky substituent, in which case the C_α atom is planar. The planarization of the C_α atom of the dialkyl-substituted α-sulfonyl carbanion causes an energy increase, which is outweighed by the decrease in the steric interaction between all substituents and the increase in negative hyperconjugation. The experimental and theoretical data point to a small intrinsic energy difference between pyramidalized and planar dialkyl-substituted α-sulfonyl carbanions.[3h,6b,6c]

Accessibility of the Anionic C Atom of the Monomeric and Dimeric Salts for Electrophiles

What can be predicted about the reactivity of the monomeric and dimeric lithium α-*tert*-butylsulfonyl carbanion salts towards electrophiles? An inspection of the space-filling models of the dimeric salts in the crystal form shows that the C_α atoms are completely shielded by THF molecules, as highlighted by the space-filling model of the salt (*M*/*P*)-**3**·4THF (Figure 15). Thus, the reactions of (*M*/*P*)-**3**·4THF with electrophiles at the anionic C atom should be very slow if not impossible. Therefore for a reaction of the dimeric salt with an electrophile to occur at least one THF molecule must dissociate with the formation of the corresponding tricoordinated dimer. The C_α atom of the tricoordinated salt is less shielded, as hinted by in the space-filling model of (*M*/*P*)-**3**·3THF (Figure 16), which was generated as a model from (*M*/*P*)-**3**·4THF by omitting one of the THF molecules. However, the monomeric lithium salt is expected to have a higher reactivity than the dimeric salt if only the shielding of the C_α atom is considered. The space-filling model of *rac*-**3**·12-crown-4 (Figure 17), which may be considered as a model for the THF-coordinated monomer (see below), shows that the C_α atom is less shielded than that in (*M*/*P*)-**3**·3THF. An inspection of the space-filling models of the salts (*M*/*P*)-**3**·3THF, (*M*/*P*)-**3**·4THF, and *rac*-**3**·12-crown-4 furthermore shows a strong steric shielding of one side of the anionic C_α atom by the *S*-*tert*-butyl group. Thus, reactions of *S*-*tert*-butyl-substituted α-sulfonyl carbanions with electrophiles at the C_α atom should take place nearly exclusively *syn* to the O atoms and *anti* to the *tert*-butyl group.

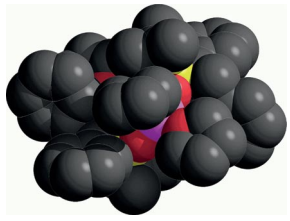

Figure 15. Space filling model of the crystal structure of the dimeric tetracoordinated salt (*M*/*P*)-**3**·4THF with H atoms omitted for clarity. Color code: C, black; S, yellow; O, red; Li, pink.

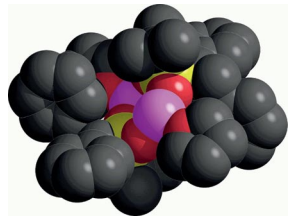

Figure 16. Space filling model of the crystal structure of the dimeric tricoordinated salt (*M*/*P*)-**3**·4THF with H atoms and one THF molecule omitted. Color code: C, black; S, yellow; O, red; Li, pink.

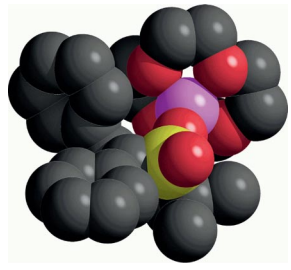

Figure 17. Space filling model of the crystal structure of the monomeric salt *rac*-**3**·12-crown-4 with H atoms omitted for clarity. Color code: C, black; S, yellow; O, red; Li, pink.

Structures of Lithium α-*tert*-Butylsulfonyl Carbanion Salts in Solution

The Anionic C Atom − Coordination Geometry and Negative Charge

Cryoscopy of the methyl-, ethyl-, benzyl-, and dialkyl-substituted salts *rac*-**9**, *rac*-**4**, *rac*-**3**, and *rac*-**6**, respectively, in THF revealed monomeric and dimeric CIPs, and X-ray analysis of *rac*-**9**·PMDTA, (*M*/*P*)-**4**·4THF, and *rac*-**3**·12-crown-4 provided models for their structures. Therefore the structures of the salts *rac*-**9**, *rac*-**4**, and *rac*-**3** in [D_8]THF and [D_6]benzene solution were investigated by NMR spectroscopy. The salts *rac*-**5** and *rac*-**10** were also included in this study. Although the crystalline THF-solvated dimeric salts dissolved in [D_8]THF solution form dimer/monomer mixtures, they are expected to retain their dimeric structure in [D_6]benzene solution because of the low polarity of the solvent. The ^{13}C NMR spectra of the salts *rac*-**9**, *rac*-**4**, *rac*-**3**, *rac*-**5**, *rac*-**10**, and *rac*-**6** (cf. Figure 2) each showed, in comparison with those of the corresponding sulfones, the expected upfield shift[3k,3m,4a,4b,4e,4g,5g,5k] of the signal of the anionic C_α atom (Table 6). Interestingly, although the upfield shifts are similar in magnitude for the methyl-, benzyl-, ethyl-, and neopentyl-substituted benzylic salts *rac*-**9**, *rac*-**4**, *rac*-**3**, and *rac*-**5**, respectively, that of the *tert*-butyl-substi-

Table 6. ^{13}C NMR chemical shifts of the C_α atoms of the salts *rac*-**9**, *rac*-**4**, *rac*-**3**, *rac*-**5**, and *rac*-**10** and the corresponding sulfones *rac*-**27**, *rac*-**28**, *rac*-**17**, *rac*-**29**, *rac*-**18**, and *rac*-**30**.

Chemical shift	Salt *rac*-**9**	Sulfone *rac*-**27**	Salt *rac*-**4**	Sulfone *rac*-**28**	Salt *rac*-**3**	Sulfone *rac*-**17**	Salt *rac*-**5**	Sulfone *rac*-**29**	Salt *rac*-**6**	Sulfone *rac*-**18**	Salt *rac*-**10**	Sulfone *rac*-**30**
δ [ppm]	53.1[a]	59.9[b]	60.8[a]	66.6[b]	57.8	62.3	58.4[a]	63.2[b]	37.9[a]	55.3[b]	57.8[a]	71.8[b]
$\Delta\delta$ [ppm][c]	–6.8		–5.8		–4.5		–4.8		–17.4		–14.0	
δ [ppm]	52.2[d,e]	–	59.5[d]	66.6[d]	56.7[d]	–	54.7[d]	63.1[d]	–	–	58.0[d]	71.8[d]
$\Delta\delta$ [ppm][c]	–		–7.1		–		–8.4		–		–13.8	

[a] In [D_8]THF at room temperature. [b] In $CDCl_3$ at room temperature. [c] $\Delta\delta = \delta$ (salt) – δ (sulfone). [d] The crystalline THF-solvated dimeric salt was dissolved in [D_6]benzene at room temperature. [e] In the presence of 2 equiv. of TMEDA.

tuted benzylic salt *rac*-**10** is larger and that of the non-benzylic salt *rac*-**6** is larger still. These high-field shifts can be mainly ascribed to the following factors. First, the accumulation of negative charge at the C_α atom causes a high-field shift, the magnitude of which depends on the electron demands of the sulfonyl group, secondly, the interaction of the negative charge with the phenyl group (see below) causes a downfield shift, and thirdly, the change in the coordination geometry of the C_α atom from sp^3 to sp^2 or sp^{3-x} results in a downfield shift of the signal. The sulfonyl group stabilizes the negative charge mainly by electrostatic and hyperconjugative interactions.[6] Therefore much of the negative charge at the C_α atom is available for interaction with the phenyl group. Although the C_α atom of the salt *rac*-**10** is nearly planar, its ^{13}C NMR signal experiences a significantly larger high-field shift than those of the other C_α-phenyl-substituted salts. This seems to be the result of a higher negative charge at the C_α atom of *rac*-**10** in comparison with *rac*-**9**, *rac*-**4**, *rac*-**3**, and *rac*-**5**. Because of the C_α–Ph conformation of *rac*-**10**, an optimal co-alignment of the lone-pair orbital and the orbitals of the phenyl ring is not possible (see below) and benzylic conjugation is strongly reduced (see below). The salt *rac*-**6**, which carries two alkyl groups at the C_α atom, shows the largest upfield shift. Although the C_α atom of this *S*-*tert*-butyl-substituted salt is expected to be planar, a charge-reducing interaction with the phenyl ring, as in *rac*-**9**, *rac*-**4**, *rac*-**3**, and *rac*-**5**, is not available. It is interesting to note that for the non-benzylic *S*-phenyl-substituted salts (*M*/*P*)-**40**·2diglyme, (**41**·diglyme)$_2$, and (**42**·diglyme)$_2$, the C_α atoms of which are significantly pyramidalized, the changes in the chemical shifts of the C_α atoms on going from the sulfone to the salt are $\Delta\delta$ = –14.0, –12.7, and –11.0, respectively. These values are similar in magnitude to those of *rac*-**6** and *rac*-**10**.

Benzylic Conjugation and C_α–Ph Conformation

Because of the mode of stabilization of the negative charge of the α-sulfonyl carbanion, much of the negative charge resides on the anionic C_α atom, which can interact with the phenyl group. This interaction is described in one model as conjugation between the lone-pair orbital at the C_α atom and the orbitals of the phenyl ring. The conjugation leads to charge transfer to the phenyl ring and thus to a higher electron density at the C_o and C_p atoms. Therefore the changes in the chemical shifts of H_p and C_p [$\Delta\delta(H_p)$, $\Delta\delta(C_p)$] on going from the corresponding sulfone to the salts *rac*-**9**, *rac*-**4**, *rac*-**3**, *rac*-**5**, and *rac*-**10** act as probes for the interaction between the negative charge at the C_α atom and the phenyl ring.[4e] Table 7 shows that the signals of H_p and C_p of *rac*-**9**, *rac*-**4**, *rac*-**3**, and *rac*-**5** experience a strong high-field shift relative to the corresponding sulfones. With regard to the magnitude of this effect, sulfonyl-substituted benzylic carbanions behave quite differently, for example, from nitro-substituted benzylic carbanions.[4e] The nitro group stabilizes the negative charge mainly by π conjugation, which leaves less negative charge at the C_α atom and thus less charge is transferred to the $C_{p(o)}$ atom than in the case of the sulfonyl group. As a result, the nitro-substituted C_α atom of the benzyl carbanion experiences a much larger low-field shift and the C_p atom a much smaller high-field shift.[4e]

Interestingly, although the C_p atoms of the methyl-, ethyl- and benzyl-substituted salts *rac*-**9**, *rac*-**4**, and *rac*-**3**, respectively, experience a high-field shift of similar magnitude, that of the neopentyl-substituted salt *rac*-**5** shows a smaller high-field shift, and that of the *tert*-butyl-substituted salt *rac*-**10** even smaller. The conjugative interaction between the anionic C_α atom and the phenyl group also

Table 7. Chemical shifts of H_o and H_p in the ^1H NMR spectra and of C_o and C_p in the ^{13}C NMR spectra of the salts *rac*-**9**, *rac*-**4**, *rac*-**3**, *rac*-**5**, and *rac*-**10** and the corresponding sulfones *rac*-**27**, *rac*-**28**, *rac*-**17**, *rac*-**29**, and *rac*-**30** in [D_8]THF.

Chemical shift	Salt *rac*-**9**	Sulfone *rac*-**27**	Salt *rac*-**4**	Sulfone *rac*-**28**	Salt *rac*-**3**	Sulfone *rac*-**17**	Salt *rac*-**5**	Sulfone *rac*-**29**	Salt *rac*-**10**	Sulfone *rac*-**30**
$\delta(H_o)$ [ppm][a]	7.09	7.50	7.13	7.48	7.05	7.35	7.38	7.53	7.39	7.55
$\Delta\delta(H_o)$ [ppm][a,b]	–0.41		–0.35		–0.30		–0.15		–0.16	
$\delta(H_p)$ [ppm][a]	6.18	7.35	6.19	7.36	6.15	7.27	6.22	7.34	6.82	7.34
$\Delta\delta(H_p)$ [ppm][a,b]	–1.17		–1.17		–1.12		–1.12		–0.52	
$\delta(C_o)$ [ppm][a]	119.2	128.9	120.2	129.5	120.1	–[c]	123.1	130.1	138.5	131.1
$\Delta\delta(C_o)$ [ppm][a,b]	–9.6		–9.3		–		–7.0		+7.4	
$\delta(C_p)$ [ppm][a]	113.7	128.7	114.0	128.7	114.0	128.7	115.3	128.6	123.3	128.1
$\Delta\delta(C_p)$ [ppm][a,b]	–15.0		–14.7		–14.7		–13.4		–4.8	

[a] Sulfone in $CDCl_3$ at room temperature. [b] $\Delta\delta = \delta$(salt) – δ(sulfone). [c] Signal could not be assigned.

depends on the proper co-alignment of the p orbital of the C_α atom and the orbitals of the phenyl group. In a first approximation, the quality of this alignment can be judged by the dihedral angles S–C_α–C_i–C_o of the salts *rac*-**9**, *rac*-**4**, *rac*-**3**, *rac*-**5**, and *rac*-**10** in the crystal form (Figure 18). Although the dihedral angles of the salts *rac*-**9**·PMDTA, (*M*/*P*)-**4**·4THF, (*M*/*P*)-**3**·4THF, and *rac*-**3**·12-crown-4 are small and similar in magnitude (5–10°; cf. Table 3), that of (*M*/*P*)-**5**·4THF is large (37°) and that of (*M*/*P*)-**10**·2THF even larger (77°) (see the Supporting Information). Interestingly, the magnitude of the high-field shifts of C_p and C_o for *rac*-**9**, *rac*-**4**, *rac*-**3**, *rac*-**5**, and *rac*-**10** show a rough correlation with the deviation of the lone-pair orbital from coplanarity with the p orbital of the phenyl ring, as judged by the dihedral angles S–C_α–C_i–C_o of the corresponding salts in the crystal form (Figure 18a–c).

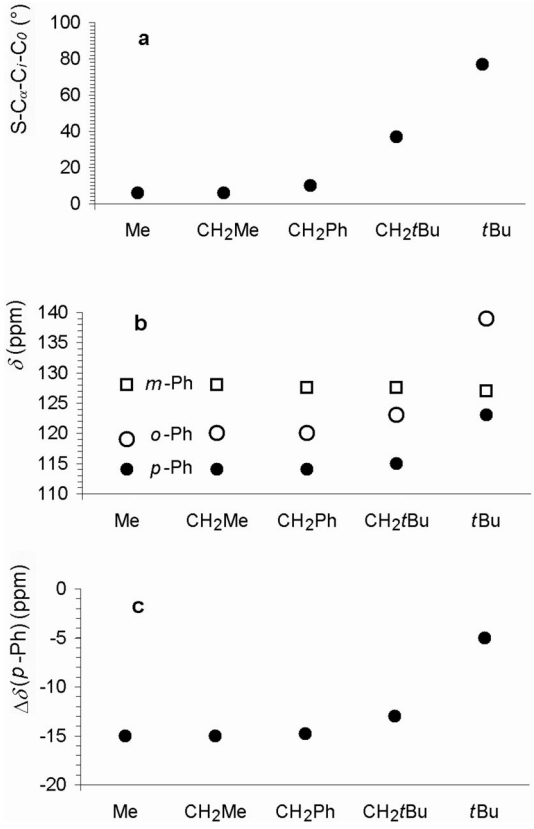

Figure 18. (a) Dihedral angles S–C_α–C_i–C_o of the salts *rac*-**9**·PMDTA (Me), (*M*/*P*)-**4**·4THF (Et), (*M*/*P*)-**3**·4THF (CH_2Ph), (*M*/*P*)-**5**·4THF (CH_2tBu), and (*M*/*P*)-**10**·2THF (*t*Bu) in the crystal form. (b) Chemical shifts of C_m (□), C_o (○), and C_p (●) of the salts *rac*-**9**, *rac*-**4**, *rac*-**3**, *rac*-**5**, and *rac*-**10** in [D_8]THF at room temperature. (c) Chemical shift differences for C_p in the salts *rac*-**9**, *rac*-**4**, *rac*-**3**, *rac*-**5**, and *rac*-**10** ([D_8]THF, room temperature) and the corresponding sulfones *rac*-**27**, *rac*-**28**, *rac*-**17**, *rac*-**29**, and *rac*-**30** ($CDCl_3$, room temperature).

Benzylic Rotation

Temperature-dependent ^{1}H and ^{13}C NMR spectroscopy of the methyl-, ethyl-, and neopentyl-substituted salts *rac*-**9**, *rac*-**4**, and *rac*-**5**, respectively, in [D_8]THF and [D_{14}]diglyme showed reversible coalescence phenomena of the H_o, H_m, C_o, and C_m signals, which indicates a hindered rotation around the C_α–C_i bond. The topomerization of these nuclei has to involve a rotation around the C_α–C_i bond. This provided a means to study the benzylic rotation by DNMR spectroscopy. Information about the C_α–C_i rotational barrier of benzylic carbanions carrying an additional carbanion-stabilizing group at the C_α atom is scarce. The barriers for the sulfonyl-substituted carbanion [$CF_3SO_2C_6H_4C(H)SO_2CF_3$)]$^-$ [$\Delta G^\ddagger_{rot}$ (256 K) = 11.5 kcal mol^{-1}, DMSO][4f] and cyano-substituted carbanion [PhC(H)CN]Li [$\Delta G^\ddagger_{rot}$ (213 K) = 10.7 kcal mol^{-1}, THF][28] have previously been reported. The activation free energies for the rotation of the phenyl ring of *rac*-**9**, *rac*-**4**, and *rac*-**5** at the coalescence temperature were estimated[20] based on the assumption that the topomerization follows first-order kinetics. Although barriers of $\Delta G^\ddagger_{rot}$ = 9.6–9.9 and 9.7 kcal mol^{-1} were estimated for the methyl- and ethyl-substituted salts *rac*-**9** and *rac*-**4**, respectively, the barrier for the neopentyl-substituted salt *rac*-**5** was significantly higher at $\Delta G^\ddagger_{rot}$ = 11.0–11.2 kcal mol^{-1} at 223 K (Table 8). Although a direct comparison of the barriers for *rac*-**4**, *rac*-**5**, and *rac*-**9** is precluded because of the different coalescence temperatures, the higher barrier for *rac*-**5** is perhaps due to the steric hindrance posed by the *tert*-butyl group. For comparison, the barrier for the *S*-phenyl-substituted salt *rac*-**1** towards C_α–C_i rotation in the presence of 2 equiv. of HMPA was also determined. ^{1}H DNMR spectroscopy showed a reversible coalescence phenomenon of the H_m signals, the analysis of which gave an activation free energy of $\Delta G^\ddagger_{rot}$ = 9.5 kcal mol^{-1} at the coalescence temperature of 196 K, which is in good agreement with those of *rac*-**9** and *rac*-**4**.

A particularly interesting case is the C_α-*tert*-butyl-substituted benzylic salt *rac*-**10**, which has an unusual C_α–C_i con-

Table 8. Estimated activation free energies $\Delta G^\ddagger_{rot}$ (T_c) for the rotation of C_α–Ph in the salts *rac*-**9**, *rac*-**4**, *rac*-**5**, and *rac*-**1**·2HMPA by ^{1}H and ^{13}C DNMR spectroscopic analysis (500 and 125 MHz).

Parameter	*rac*-**9**[a]			*rac*-**4**[b,c]	*rac*-**5**[a]			*rac*-**1**·2HMPA[a]
	H_o	C_o	C_m	H_o	H_o	C_o	C_m	H_m
$\Delta\nu$ [Hz]	700	356	154	700	460	276	65	47
T_c [K]	228 ± 5	218 ± 10	208 ± 10	223 ± 10	253 ± 5	243 ± 10	228 ± 10	196 ± 10
k_{rot} [s]	1555	791	342	1555	1022	613	144	104
$\Delta G^\ddagger_{rot}$ (T_c) [kcal mol^{-1}]	9.9 ± 0.2	9.7 ± 0.5	9.6 ± 0.5	9.7 ± 0.5	11.2 ± 0.3	11.0 ± 0.5	11.0 ± 0.5	9.5 ± 0.3

[a] In [D_8]THF. [b] In [D_{14}]diglyme. [c] Upon cooling a solution of *rac*-**4** in [D_8]THF to – 40 °C the same changes in the H_o signal were observed as in [D_{14}]diglyme.

formation. Determination of its enantiomerization barrier by DNMR spectroscopy was not possible because of the nonobservance of different chemical shifts for the diastereotopic nuclei at the *ortho* and *meta* positions of the phenyl group. The variable-temperature ^{1}H and ^{13}C NMR spectra of *rac*-**10** in [D$_8$]THF showed no coalescence phenomena due to hindered C_α–C_i rotation at low temperatures. The ^{1}H NMR spectrum at –100 °C displayed only minor line-broadening for the signal of H_o, whereas the doubling of the signal of H_p is due to the presence of several CIPs (see below). Furthermore, the number of signals of C_o and C_m did not exceed those of C_p and C_i. The lack of doubling of the signals of H_o, H_m, C_m, and C_o of the salt *rac*-**10** in equal intensity at –100 °C can be rationalized as follows. First, the signals of H_o, H_m, C_m, and C_o are incidentally isochronous under the conditions of measurement. This is not very likely given the structure of *rac*-**10** (see above and below). In strong contrast to the salts *rac*-**9**, *rac*-**4**, *rac*-**3**, and *rac*-**5**, the salt *rac*-**10** adopts in the crystal form and most probably also in solution a C_α–Ph conformation in which the phenyl ring is almost orthogonal to the $C_{t\mathrm{Bu}}$–C_α–S plane (cf. Figure 7). Thus, one H_o is *syn* to the Li-coordinated O atom, whereas the other one is *syn* to the *S*-*tert*-butyl group. The same holds true for the H_m, C_o, and C_m atoms. The different chemical environments of the nuclei should be manifested in different chemical shifts. Secondly, the barrier towards C_α–C_i rotation could be much lower than that of *rac*-**9**, *rac*-**4**, and *rac*-**5**. Although the ground states of the salts *rac*-**9**, *rac*-**4**, and *rac*-**5** are stabilized through the conjugation of the lone-pair orbital at the C_α atom with the phenyl ring, it is the transition state of the C_α–C_i rotation of the salt *rac*-**10** that will be stabilized by benzylic conjugation. Thus, the NMR spectra of *rac*-**10** at –100 °C could still be a reflection of a fast exchange regime. It is more than questionable, however, whether this energy-lowering effect of the transition state is sufficient to overcome the destabilization by the severe interaction of H_o with the C_α-*tert*-butyl group. Even in the ground state of *rac*-**10** there is a significant interaction between the C_α-*tert*-butyl and phenyl groups, as indicated by the rather small C_i–C_α–S angle of 115.2°. The corresponding angles for the salts *rac*-**3**·12-crown-4, (*M*/*P*)-**4**·4THF, and (*M*/*P*)-**5**·4THF are 124.6, 124.5, and 119.9°, respectively, and are, thus, significantly larger. Thirdly, and most importantly, because of the C_α–Ph conformation of *rac*-**10**, topomerization of the H_o, H_m, C_m, and C_o atoms of the phenyl ring can also occur by rotation around the C_α–S bond. Thus, the absence of any dynamic phenomenon in the temperature-dependent NMR spectra of *rac*-**10** could imply that at –100 °C the topomerization of the nuclei is still in the fast exchange regime because of the low enantiomerization barrier of the salt. Because the phenyl ring is fixed in a position almost orthogonal to the $C_{t\mathrm{Bu}}$–C_α–S plane, C_α–S rotation can take place whereby the *tert*-butyl group attached to the S atom can get past the face of the phenyl ring but not the *tert*-butyl group. A phenyl group in such a position is smaller sterically than a methyl group, as shown by E_s values of –1.01 and –1.24, respectively.[11]

Low-Temperature NMR Spectroscopy in [D$_8$]THF – Monomer–Dimer Equilibria

The possible structures of the monomers of the salts *rac*-**3**–**6**, *rac*-**9**, and *rac*-**10** in THF solution are the O–Li CIPs **III**–**V** and the O,C–Li CIPs **VI** and **VII** (Figure 19). Monomer **III** features a coordination of the Li atom to both O atoms. The Li atoms of the diastereomeric monomers **IV** and **V**, which have a stereogenic S atom, are only coordinated to one of the O atoms in the anions. Structures **IV** and **V** resemble those found for the monomers *rac*-**3**·12-crown-4 and *rac*-**9**·PMDTA in the crystal form. Monomers **VI** and **VII** exhibit a coordination of the Li atom to both the O atom and the anionic C_α atom. In addition to the monomers, four dimers of salts *rac*-**3**–**6**, *rac*-**9**, and *rac*-**10** are conceivable, the achiral dimers *anti*-(*P*/*M*)-**VIII** (C_i) and *syn*-(*P*/*M*)-**IX** (C_s) and the chiral dimers *anti*-(*P*/*P*)-**X** (C_2) and *syn*-(*P*/*P*)-**XI** (C_2).[29] In the crystal form, the dimers adopt a structure of the type *anti*-(*P*/*M*)-**VIII**. The results of the ^{6}Li{^{1}H} NOE experiments on *rac*-**3**, *rac*-**5**, *rac*-**6**, and *rac*-**10** in [D$_8$]THF are more in favor with the Li atom being positioned at the O atom of the carbanion, as in structures **III**–**V** and **VIII**–**XI**, than at the O and C_α atom, as in **VI** and **VII**. However, because the ^{6}Li{^{1}H} NOE experiments were conducted at room temperature, only information concerning the averaged structures of the various monomers and dimers was obtained (see the Supporting Information). Therefore NMR experiments on the benzylic salts *rac*-**4**, *rac*-**5**, *rac*-**9**, and *rac*-**10** at low temperatures were performed to seek more information about the monomers and dimers

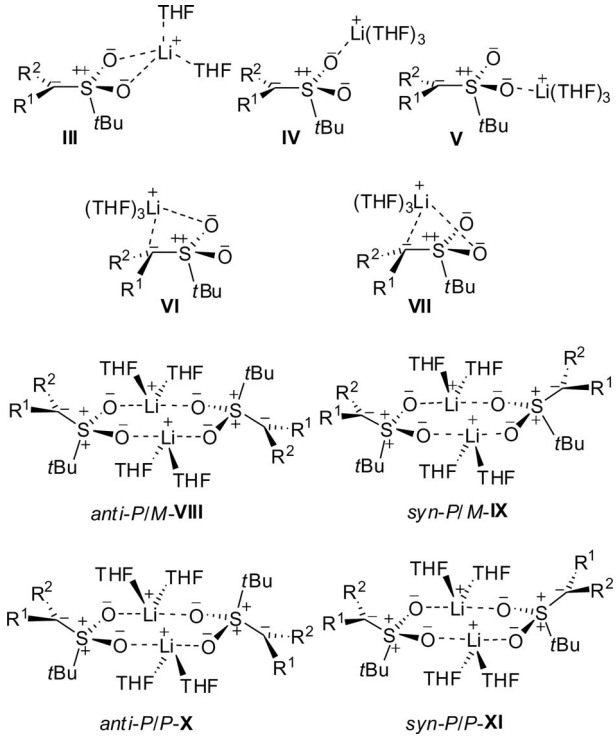

Figure 19. Possible structures of the monomers and dimers of lithium α-*tert*-butylsulfonyl carbanion salts (priority: $R^1 > R^2$).

and to find a correlation with the results of the cryoscopy experiments.

The ^1H and ^{13}C NMR spectra of the methyl-, ethyl-, and neopentyl-substituted salts *rac*-**9**, *rac*-**4**, and *rac*-**5**, respectively, showed at low temperatures, in addition to the coalescence phenomena originating from a reduction of the frequency of the C_α–S and C_α–C_i bond rotations, further line-broadenings and reversible coalescence phenomena. This caused the appearance of further signals in addition to those originating from a slowing of the bond rotation. Finally, the spectra of *rac*-**9**, *rac*-**4**, *rac*-**5**, and *rac*-**10** at –100 °C revealed the presence of two to five different equilibrium species in various ratios (Table 9). In several cases, the sample of the salt used for the low-temperature NMR studies also contained some of the corresponding sulfone. However, the NMR spectra of the mixtures at the various temperatures and ratios gave no indication of complex formation between the salt and the corresponding sulfone.

Table 9. Number of species of the salts *rac*-**4**–**6**, *rac*-**9**, and *rac*-**10** present at –100 °C in [D_8]THF according to ^1H, ^{13}C, and ^6Li NMR spectroscopy.

	Species (Ratio)		
Salt	^1H NMR (500 MHz)	^{13}C NMR (125 MHz)	^6Li NMR (75 MHz)
rac-**9**	3[a] (75:15:10)	4 (45:30:15:10)	–[b]
rac-**4**	2[c] (85:15)	2 (85:15)	–[b]
rac-**5**	3 (55:40:5)	2 (60:40)	2 (60:40)
rac-**10**	≥2[d,e] (–)	5 (50:20:10:10:10)	3 (70:20:10)
rac-**6**	2[e] (60:40)	–[b]	–[b]

[a] Four C_α-methyl signals were observed in a ratio of 45:30:15:10. [b] Not investigated. [c] At –80 °C in [D_{14}]diglyme. [d] Because of the large line width, the number of signals and their intensity could not be determined with certainty. [e] At –60 °C.

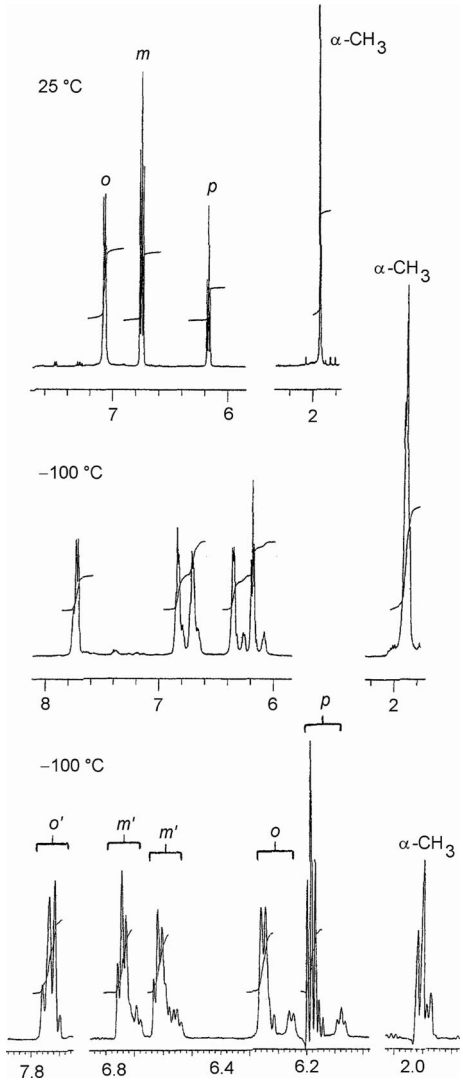

Figure 20. ^1H NMR (500 MHz) spectra (in part) of the salt *rac*-**9** in [D_8]THF at ca. 25 °C and –100 °C.

The ^1H NMR spectrum of the α-methyl-substituted salt *rac*-**9** in [D_8]THF at –100 °C exhibited a three-fold splitting of the signals of H_o, $H_{o'}$, H_p, H_m, and $H_{m'}$. In addition, a four-fold splitting of the signal of the C_α-methyl group was observed. This splitting points to the presence of four species in a ratio of 45:30:15:10 (Figure 20). The ^{13}C NMR spectrum exhibited two signals for C_i, three signals for C_o and $C_{o'}$, four signals for C_p, four signals for *S*-*t*Bu, and four signals for C_α, which indicates the presence of four species in a ratio of approximately 45:30:15:10 (Figure 21). Cryoscopy of *rac*-**9** in THF at –100 °C had shown a dimer-to-monomer ratio of approximately 70:30.

The ^1H NMR spectrum of the C_α-ethyl-substituted salt *rac*-**4** in [D_{14}]diglyme at –80 °C showed, according to the doubling of the signals of H_o, $H_{o'}$, and H_p, the presence of two species in a ratio of 85:15. Similarly, a doubling of the ^{13}C NMR signals of C_i, C_o, $C_{o'}$, C_p, and C_α also revealed the presence of two species in approximately the same ratio. The differences in the shifts of the ^1H and ^{13}C NMR signals for the two species are only small.

The ^1H NMR spectrum of the α-neopentyl-substituted salt *rac*-**5** in [D_8]THF at –100 °C featured a three-fold splitting of the signals of H_o, H_p, $H_{o'}$, and the methylene group and thus indicates the presence of three species in a ratio of approximately 55:40:5 (Figure 22). The ^{13}C NMR spectrum exhibited two complete and very similar signal sets in accord with the presence of two species in a ratio of 60:40 (Figure 23).

The ^1H NMR spectrum of the C_α-*tert*-butyl-substituted salt *rac*-**10** in [D_8]THF at –100 °C showed a doubling of the signals for the *tert*-butyl groups and thus the presence of at least two species. The ^{13}C NMR spectrum, however, exhibited four signals for C_i, five signals for C_o, three signals for C_p, two signals for the *S*-*tert*-butyl group, three signals for C_α, and three signals for the C_α-*tert*-butyl group. This splitting points to the presence of five species in a ratio of 50:20:10:10:10.

The ^1H NMR spectrum of the C_α-dialkyl-substituted salt *rac*-**6** in [D_8]THF at –60 °C showed, according to a doubling of the signals of the methyl and methylene groups, the

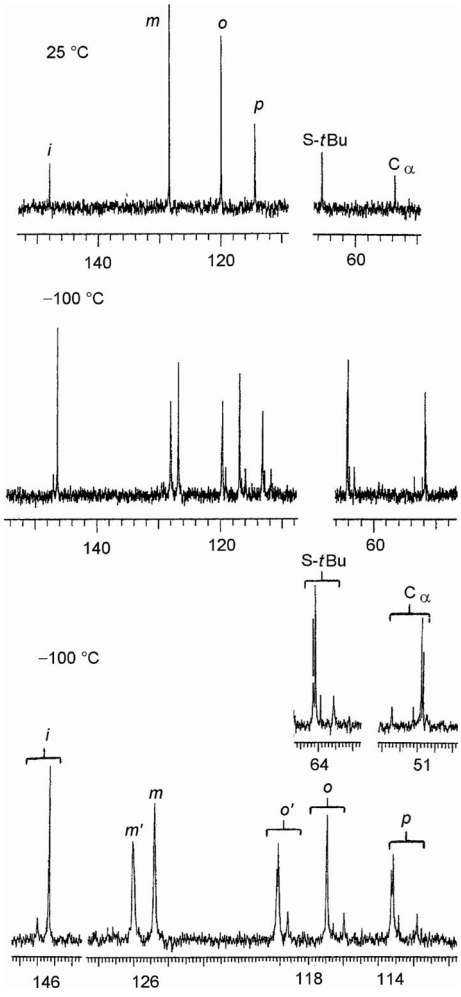

Figure 21. ^{13}C NMR (125 MHz) spectra (in part) of the salt *rac*-**9** in [D_8]THF at ca. 25 °C and –100 °C.

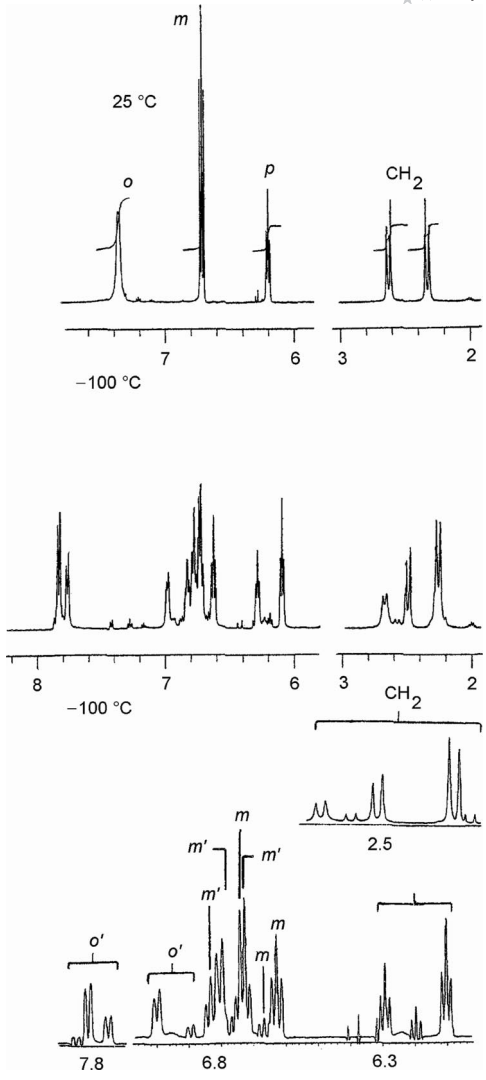

Figure 22. ^{1}H NMR (500 MHz) spectra (in part) of the salt *rac*-**5** in [D_8]THF at ca. 25 °C and –100 °C (the expanded spectrum was obtained with resolution enhancement).

presence of two species in a ratio of 60:40. Cryoscopy of *rac*-**6** in THF at –100 °C had shown the existence of dimers and monomers in a ratio of approximately of 60:40.

The low-temperature ^{1}H and ^{13}C NMR experiments on the salts *rac*-**9**, *rac*-**4**, *rac*-**5**, and *rac*-**10** were complemented by ^{6}Li NMR experiments on the salts *rac*-**5** and *rac*-**10** in [D_8]THF at –100 °C. Although the low-temperature spectrum of the C_α-neopentyl-substituted salt *rac*-**5** exhibited two signals in a ratio of 60:40, that of the C_α-*tert*-butyl-substituted salt *rac*-**10** showed three signals in a ratio of 70:20:10.

The ^{1}H and ^{13}C NMR spectra of the racemic salts *rac*-**9**, *rac*-**4**, *rac*-**5**, and *rac*-**10** in [D_8]THF at –100 °C showed the existence of up to five different species. The chemical shifts of the various species are very similar. Low-temperature ^{7}Li, ^{1}H, and ^{13}C NMR studies of other lithium α-sulfonyl carbanion salts have also indicated the existence of several species in [D_8]THF and THF/Et_2O at very low temperatures.[3m,30] It is thus proposed that the monomers of the salts *rac*-**9**, *rac*-**4**, *rac*-**5**, and *rac*-**10** adopt the structures of the O–Li CIPs **III**–**V** and the dimers the structures of the CIPs **VIII**–**XI**. This would be in accordance with (1) the cryoscopic aggregation numbers of *rac*-**4**, *rac*-**9**, and *rac*-**5**, (2) the ^{6}Li{^{1}H} NOE experiments on *rac*-**3** and *rac*-**5** in [D_8]THF (see the Supporting Information), and (3) the low-temperature NMR investigation, which revealed up to five different species of the salts. However, it should be emphasized that cryoscopy only gives aggregation numbers that are an average over all monomers and possible aggregates. In addition, the ^{6}Li{^{1}H} NOE experiments only provided averaged information because they were performed at room temperature (see the Supporting Information) at which a fast equilibration of all species takes place. Nevertheless, the crystal structures of (*M*/*P*)-**3**·4THF, (*M*/*P*)-**4**·4THF, (*M*/*P*)-**5**·4THF, (*M*/*P*)-**10**·2THF, *rac*-**3**·12-crown-4, and *rac*-**9**·PMDTA can serve as models for the structures of the dimers and monomers in THF solution. Although all available evidence points to CIP structures of the type **III**–**V** for the monomers in THF, which exhibit only O–Li and no C–Li bonds, the existence of C,O–Li CIPs of the type **VI** and

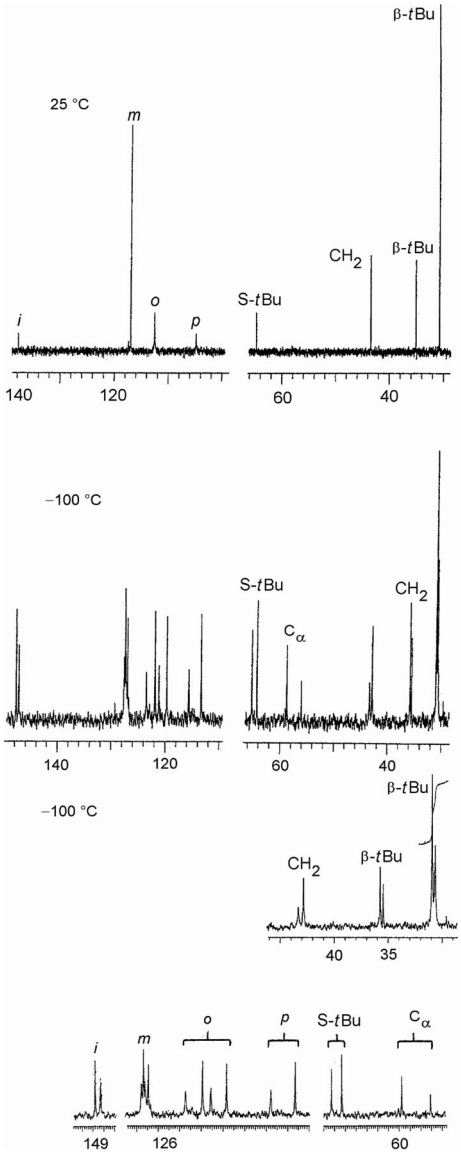

Figure 23. ^{13}C NMR (125 MHz) spectra (in part) of the salt *rac*-**5** in [D_8]THF at ca. 25 °C and –100 °C.

VII cannot be excluded. The ^{13}C NMR spectra showed for all the species present a singlet for the anionic C_α atom and thus no splitting due to C–Li coupling. Low-temperature ^{13}C NMR studies of the lithium salts of bicyclic α-sulfonyl carbanions also failed to reveal $J(^{13}C,^{6}Li)$ coupling.[3m] However, C,O–Li CIPs of the type **VI** and **VII** may be present in only small amounts and escape detection. Alternatively, they could be amongst the up to five species detected by NMR spectroscopy at –100 °C and undergo a fast C–Li exchange even at –100 °C, which would prevent the detection of C–Li coupling in the ^{13}C and ^{6}Li NMR spectra. All attempts to detect a species of the type **VI** or **VII**, either as a monomer or dimer, exhibiting a C–Li bond in solution have thus far failed. Only in the case of an α,α-dilithiosulfone could the existence of a C–Li bond in THF solution be demonstrated by NMR spectroscopy.[31] Ab initio calculations on the monomeric salts **49**·2THF[6k] and **50**·2Et_2O[3q] gave the two structures **51** and **52** (Figure 24). Whereas the Li atom of **52** is coordinated by one O atom and the C_α atom, that of **51** is coordinated by both O atoms. Interestingly, both structures have the typical C_α–S conformation in which the lone-pair orbital at the C_α atom bisects or nearly bisects the O–S–O angle. Although the allylic CIPs **51a** and **52a** (S = THF) have the same energy, the alkyl O,C–Li CIP **52b** is 2.5 kcal mol^{-1} more stable than the O–Li CIP **51b** (S = OEt_2). There is, however, an important structural difference between the salts studied in this work and the salts **49** and **50**. Although the C_α atoms of **49** and **50** carry only one substituent, those of the lithium *tert*-butylsulfonyl carbanion salts bear either an alkyl and a phenyl group or two alkyl groups. This could perhaps make, in the case of the C_α-disubstituted carbanions, the C,O–Li CIPs of the type **VI** and **VII** (cf. Figure 22) energetically less favorable than O–Li CIPs of the type **III**–**V** because of steric interactions between the THF-coordinated Li atom and the substituents R^1 and R^2. Recently, the crystal structure of **50**·THF, the Li atom of which carries only one THF molecule, has been determined.[3q] This salt is a polymer in the crystal form that features a C–Li bond and two O–Li bonds but contains no four-membered C_α–Li–O–S ring like **52b**. The C_α atom of **50**·THF is pyramidalized and the salt has a C_α–S conformation in which the C–Li bond almost bisects the O–S–O angle. The coordination of the Li atom to the C_α atom and thus the formation of a C–Li bond in the crystal is most likely the result of a lack of solvating THF molecules for the Li atom. In summary, all available data on salts *rac*-**1**–**10** point to the existence of monomeric and dimeric O–Li CIPs of the type **III**–**V** and **VIII**–**XI** in THF that are in fast equilibrium.

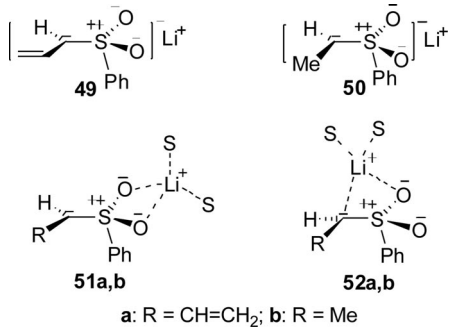

Figure 24. Calculated structures **51** and **52** of the salts **49** and **50**.[3q,6k]

Low-Temperature NMR Spectroscopy in the Presence of HMPA − the CIP/SIP Equilibrium

Finally, low-temperature ^{7}Li and ^{31}P NMR spectroscopic experiments on the methyl-substituted salt *rac*-**9** were conducted in [D_8]THF in the presence of HMPA. It was of interest to see whether this strongly Li-coordinating molecule would lead to the formation of SIPs.[4d,32] DNMR spectroscopy of the benzylic *S*-phenyl salt *rac*-**1** in [D_8]THF

in the presence and absence of HMPA has revealed a higher free energy of activation for the enantiomerization in the former case. The *S*-*tert*-butyl salt *rac*-**9** was studied instead of *rac*-**1** in more detail because of a higher configurational stability. The ^{7}Li NMR spectrum of the salt *rac*-**9**, which in THF at –108 °C is an equilibrium mixture of four different monomers and dimers, in [D$_8$]THF/*n*-hexane (20:1) at –115 °C in the presence of 2 equiv. of HMPA showed a quintet (J = 7.6 Hz) at $\delta \approx -0.70$ ppm and a broad signal centered at $\delta \approx -0.30$ ppm in a ratio of approximately 50:50 (external reference, LiBr in H_2O). Although the latter signal could not be assigned, it appeared to be a combination of two signals, a doublet and a quartet. Warming the solution of *rac*-**9** to –60 °C resulted in the disappearance of the splitting of the signals and the appearance of two singlets, which finally collapsed at room temperature to one singlet. The ^{31}P NMR spectrum of *rac*-**9** in [D$_8$]THF/*n*-hexane (20:1) at –115 °C in the presence of 2 equiv. of HMPA exhibited a singlet at $\delta \approx 23.1$ ppm, presumably free HMPA, and a broader singlet at $\delta \approx 23.7$ ppm (external reference, H_3PO_4 in H_2O) in a ratio of 45:55. Unfortunately, a splitting of the latter signal due to ^{31}P,^{7}Li-coupling could not be resolved. The two signals in the ^{31}P NMR spectrum merged at –60 °C into one singlet. Nearly the same ^{7}Li and ^{31}P NMR spectra of *rac*-**9** in [D$_8$]THF at –115 °C were recorded in the presence of 5 equiv. of HMPA, except that the apparent doublet/quartet-to-quintet signal ratio in the ^{7}Li spectrum changed to a ratio of 30:70 in favor of the quintet. In the ^{31}P NMR spectrum the ratio of the two singlets increased to 35:65. The quintet in the ^{7}Li NMR spectrum arises from a Li ion to which four HMPA molecules are coordinated. This is in accordance with the magnitude of the $^{2}J(^{31}P,^{7}Li)$ coupling of 7.6 Hz.[30] Thus, this signal was assigned to the SIP *rac*-**9**·4HMPA (Figure 25). This result shows that *rac*-**9** forms a SIP in the presence of HMPA. The apparent doublet [$^{2}J(^{31}P,^{7}Li)$ = 12.1 Hz] in the low-temperature ^{7}Li spectrum could be caused by the monomeric CIPs *rac*-**9**·THF·HMPA and *rac*-**9**·HMPA·THF or their dimers, the Li atoms of which carry one HMPA molecule. The apparent quartet indicates the presence of the SIP *rac*-**9**·3HMPA, which has three HMPA molecules. The signals of the HMPA-coordinated monomers and dimers were, however, not resolved. Reich and co-workers previously studied the behavior of the *S*-phenyl-substituted salts *rac*-**50**, [HC(H)-SO_2Ph]Li and [MeC(Ph)SO_2Ph]Li towards HMPA in [D$_8$]-THF/Et$_2$O at –110 to –135 °C by ^{7}Li and ^{31}P NMR spectroscopy.[4d,30] It was found that the monomeric and dimeric CIPs are converted upon the addition of HMPA into the corresponding CIPs bearing one HMPA molecule. The further addition of HMPA then transforms these CIPs into SIPs bearing three HMPA molecules and finally into SIPs bearing four HMPA molecules. The CIPs with two HMPA molecules are not stable but disproportionate into the CIP with one HMPA and the SIP with three HMPA molecules.

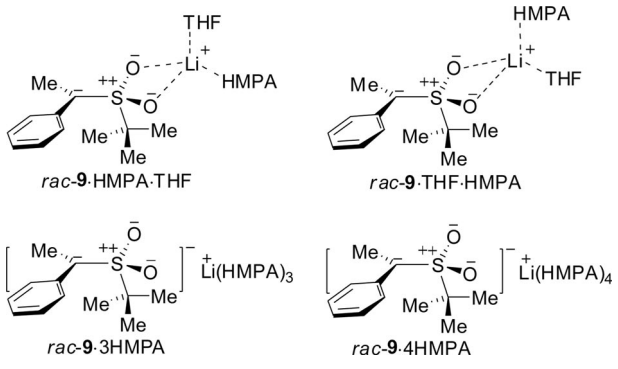

Figure 25. Structures of the HMPA-coordinated SIPs and CIPs of the salt *rac*-**9**.

Ab initio Calculations on a Counterion-Free *S*-*tert*-Butyl Carbanion − Electronic Structure and Roational Barrier

Having obtained experimentally information about the structure of the salt *rac*-**9** in the crystal form and in solution, ab initio calculations on its counterion-free carbanion **9**(–Li) were undertaken. The rate-determining step of the racemization of (*M*)-**9** is the C_α–S bond rotation, which can occur in a clockwise and counter-clockwise fashion. Because of the two different substituents at the C_α atom, there are two different barriers and only the lowest barrier is accessible by kinetic experiments. Theoretical calculations on **9**(–Li) were expected to give not only information about both barriers but also about the electronic structure of the anion. In particular, information as to the magnitude of the benzylic conjugation was sought, which has already been probed by NMR spectroscopy (see above). Previous ab initio calculations on counterion-free α-sulfonyl carbanions dealt only with non-benzylic derivatives.[6b,6c,6j] Ab initio calculations at different levels of theory employing the Gaussian 03 suite of quantum-chemical routines[33] were carried out to elucidate the binding near the anionic C atom. To determine the preferred relative orientation of the substituents we performed a complete rotation about the C_α–S bond starting from a structure fully optimized at the HF/6-31+G* level with an equilibrium dihedral angle Θ(O–S–C_α–C_{Me}) of 15.4°. In these calculations the C_α atom was forced into the plane defined by its nearest neighbors (S, C_{Me}, and C_i). Moreover, the phenyl group was constrained to planarity but allowed to rotate freely about the C_α–C_i bond. The dihedral angle Θ was changed in steps of 10° and by freezing this angle at the corresponding value we optimized the remaining structural parameters at the HF/6-31+G* level under the constraints described above. The resulting potential curve is shown in Figure 26 (dotted).

To obtain more reliable relative energies we then performed single-point calculations employing the larger 6-311++G** basis set, including the correlation energy by means of the second-order Møller–Plesset perturbation theory (MP2).[34] The potential curve obtained in this way is also shown in Figure 26 (solid line). The curve calculated upon including the correlation energy in single-point calculations is quite similar to that obtained at the HF/6-31+G* level. Both curves have two minima, **9A**(–Li) and **9B**(–Li), and two maxima, **9C**(–Li) and **9D**(–Li). The structures of

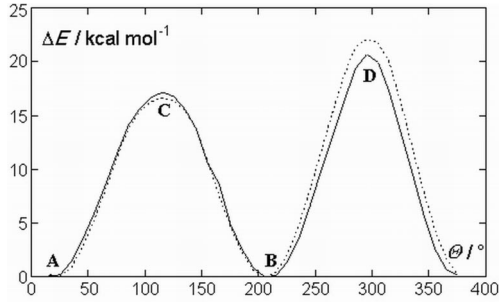

Figure 26. Energies (kcal mol^{-1}) of **9**(–Li) relative to the most stable conformer as a function of the dihedral angle Θ(O1–S–C_α–C_{Me})- (dotted: HF/6-31+G*//HF/6-31+G*; solid: MP2/6-311++G**// HF/6-31+G*).

the four conformations viewed along the C_α–S axis are shown in Figure 27. At the MP2/6-311++G**//HF/6-31+G* level, the energetically most favorable conformer **9A**(–Li) was found at Θ = 15.4° (ΔE_{HF} = 0.25 kcal mol^{-1}). The other minimum, **9B**(–Li) (ΔE_{MP2} = 0.14 kcal mol^{-1}), occurs at 205.4° (ΔE_{HF} = 0.00 kcal mol^{-1}). At both levels of theory the energetically least favorable conformation, **9D**(–Li), was found at Θ = 295.4° corresponding to an energy of ΔE_{MP2} = 20.82 kcal mol^{-1} (ΔE_{HF} = 22.10 kcal mol^{-1}) relative to **9A**(–Li). An energetically somewhat lower maximum, **9C**(–Li) (ΔE_{MP2} = 17.30 kcal mol^{-1}), occurs at Θ = 115.4° (ΔE_{HF} = 16.64 kcal mol^{-1}; Table 10).

Striking structural differences between the minima and maxima were found. First, the orientation of the phenyl ring relative to the plane of the C_α atom as defined by the dihedral angle Φ = C_{Me}–C_α–C_i–C_o as a function of the dihedral angle Θ is shown in Figure 28. The dotted curve is the potential curve obtained at the MP2/6-311++G**//HF/6-31+G* level of theory. Note that the dihedral angles Φ in **9A**(–Li), **9B**(–Li), **9C**(–Li), and **9D**(–Li) are less than 10° and therefore the phenyl ring and the plane defined by the nearest neighbors of the C_α atom are more or less coplanar. The largest deviation from the value of 0°, ideal for a conjugative interaction between the anionic C_α atom and the phenyl group, occurs for the minima **9A**(–Li) (9.5°) and **9B**(–Li) (–5.8°), whereas smaller values were found for the maxima **9C**(–Li) (0.3°) and **9D**(–Li) (–4.8°). Consequently the phenyl groups of the minimum structures carry a less negative (natural) charge [**9A**(–Li), **9B**(–Li): –0.25*e*] than those of the maxima [**9C**(–Li): –0.27*e*; **9D**(–Li): –0.36*e*; for the special case of **9D**(–Li): see below]. Moreover, on

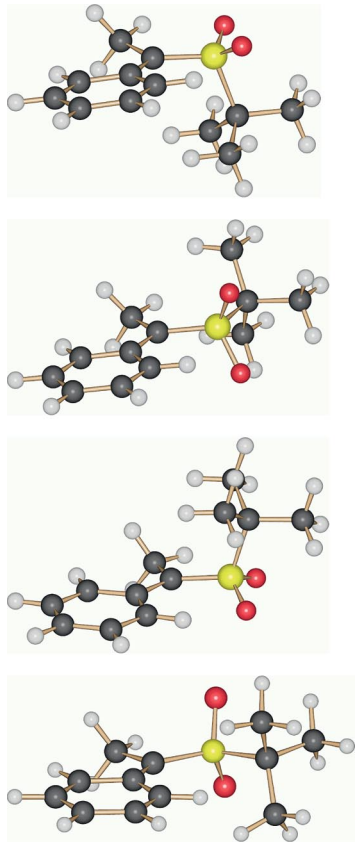

Figure 27. Structures of the conformations **9A**(–Li) (top), **9C**(–Li) (middle), **9B**(–Li) (lower middle), and **9D**(–Li) (bottom) obtained at the HF/6-31+G* level employing the constraints described in the text. Color code: C, black; S, yellow; O, red; H, grey.

average, the C–C bonds of the phenyl ring are slightly longer for the maxima [**9C**(–Li): 1.399 Å; **9D**(–Li): 1.401 Å] than for the minima [**9A**(–Li): 1.398 Å; **9B**(–Li): 1.398 Å]. Secondly, on average, the S–C_α bonds are 0.034 Å longer in the maxima than in the minima. The lengths of these bonds will be discussed below in the description of the interactions of the bonding and antibonding MOs within the framework of the NBO method.[35] Figure 28 reveals interesting changes in the C_α–C_i and C_α–S conformations on going from the minimum **9B**(–Li) via the maximum **9D**(–Li) to the minimum **9A**(–Li), which involves a higher C_α–S rotational barrier. Upon rotation around the C_α–S bond of **9B**(–Li), a simultaneous rotation around the C_α–C_i bond occurs up to a maximum value of Θ = –30°, which corre-

Table 10. Energies, angles, bond lengths, charges (q) and occupation numbers (n) for **9A**(–Li), **9B**(–Li), **9C**(–Li), and **9D**(–Li).

9(–Li)	ΔE_{HF}[a] [kcal mol^{-1}]	Θ[b] [°]	ΔE_{MP2}[c] [kcal mol^{-1}]	C_α–S [Å]	C_α–C_i [Å]	q (C_α) [e]	n_n (C_α)	$\Delta E_{n(C\alpha)\rightarrow Ry^*}$[d] [kcal mol^{-1}]	$\Delta E_{n(C\alpha)\rightarrow BD^*}$[d] [kcal mol^{-1}]	$n_{\sigma S-C\alpha}$	$n_{\sigma^* S-C\alpha}$
A	0.25	15.4	0.00	1.693	1.441	–0.6784	1.5881	–18.67	–166.74	1.9785	0.1024
B	0.00	205.4	0.14	1.693	1.441	–0.6771	1.5872	–18.97	–167.97	1.9784	0.1020
C	16.64	115.4	17.30	1.717	1.432	–0.6389	1.5871	–15.02	–174.34	1.9773	0.1038
D	22.10	295.4	20.82	1.736	1.416	–0.5933		–8.94[e]	–50.10[e]	1.9763	0.1068

[a] Relative to the most stable conformer. [b] Dihedral angle C_{Me}–C_α–S–O. [c] For the HF/6-31+G*-optimized geometry relative to the most stable conformer. [d] $\Delta E_{n\rightarrow\sigma^*} = -q_n\langle n|F|\sigma^*\rangle^2/(\varepsilon_{\sigma^*} - \varepsilon_n)$, in which F is the Fock operator of the molecule and q_n the occupation number of the lone pair. ε_{σ^*} and ε_n are the NBO orbital energies of the σ* and the nonbonding orbital n, respectively. [e] Interaction of $\pi_{C\alpha\text{-}Ci}$ with Ry* and BD*.

sponds to the conformation **9E**(–Li) (Figure 29). Further C_α–S rotation sees a simultaneous rotation around the C_α–C_i bond in the opposite direction with the attainment of conformation **9D**(–Li) in which the phenyl ring adopts a conformation optimal for benzylic conjugation (Θ = 300° and Φ = 0°) and the *tert*-butyl group and phenyl ring are synperiplanar. Upon further rotation around the C_α–S bond of **9D**(–Li) again simultaneous rotation around the C_α–C_i bond occurs up to a maximum value of Φ = 30° with the attainment of conformation **9F**(–Li). Further C_α–S rotation sees a simultaneous rotation around the C_α–C_i bond in the opposite direction with the attainment of conformer **9A**(–Li). The C_α–S and C_α–C_i rotations are most likely accompanied by simultaneous rotation around the S–*t*Bu bond.

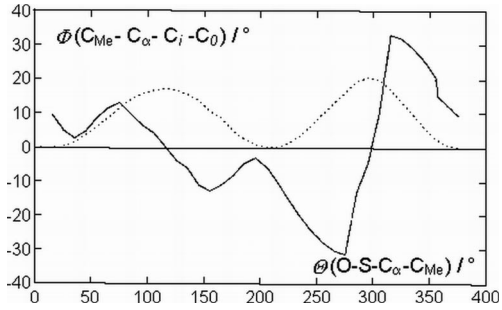

Figure 28. The dihedral angle Φ = C_{Me}–C_α–C_i–C_o of **9**(–Li) as a function of Θ = O1–S–C_α–C_{Me} [°] (solid).

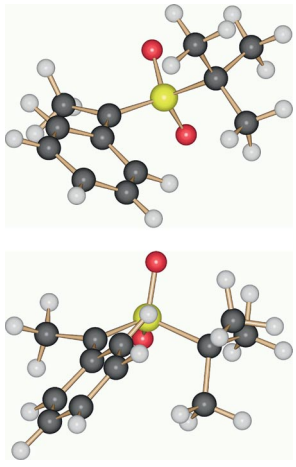

Figure 29. Structures of conformations **9E**(–Li) (Θ = –30°) (top) and **9F**(–Li) (Θ = 30°) (bottom) obtained at the HF/6-31+G* level employing the constraints described in the text. Color code: C, black; S, yellow; O, red; H, grey.

To gain a deeper insight into the electronic structures of **9A**(–Li), **9B**(–Li), **9C**(–Li), and **9D**(–Li) we analyzed the corresponding molecular wavefunctions using the NBO method (version 3.1, as implemented in Gaussian 03)[34] at the MP2/6-311++G**//HF/6-31+G* level. The NBO analyses gave a single σ bond without an additional π component between the C_α and C_i atoms of **9A**(–Li), **9B**(–Li), and **9C**(–Li). The C_α atoms in these conformations carry a lone pair of essentially pure p character. In contrast to **9A**(–Li), **9B**(–Li), and **9C**(–Li), there is no such lone pair at C_α in the case of **9D**(–Li) but an additional π bond to the C_i atom. This π bond, however, is largely located at C_α (74.4%). Note that at 1.416 Å this conformer also has the shortest C_α–C_i bond and that the C_α atom of **9D**(–Li) also carries the least (natural) negative charge of all four structures. In all four cases the S atom is bonded to C_α by a σ bond between two hybrid orbitals (approximately sp^3) with coefficients of about equal size at both atoms. According to the NBO analyses there is no additional π bond. The S–O bonds are σ bonds between an sp^3 hybrid at sulfur and an $sp^{2.3}$ orbital at oxygen with no additional π bond. Each O atom carries three lone pairs one of which has about 70% s and 30% p character, whereas the other two are essentially pure p orbitals. The potential curve obtained at the correlated level (MP2/6-311++G**//HF/6-31+G*) was also subjected to a Fourier analysis employing a five-term Fourier series [Equation (1)].[36,37]

$$V(\Theta) = 0.5V_1(1 - \cos\Theta) + 0.5V_2\,(1 - \cos 2\Theta) + 0.5V_3(1 - \cos 3\Theta) + V_4\sin\Theta + V_5\sin 2\Theta \quad (1)$$

The resulting V_i parameters are collected in Table 11. The potential curve is dominated by a strongly positive V_2 (17.6 kcal mol^{-1}), which results in minima at Θ = 0 and 180° and maxima at 90 and 270°. The large and positive V_2 might indicate a stabilizing interaction between the lone pair at C_α and the σ* orbital of the S–$C_{t\mathrm{Bu}}$ bond (negative hyperconjugation).[6] Indeed, the NBO analyses indicate significant interactions between these orbitals in **9A**(–Li) (–24.6 kcal mol^{-1}) and **9B**(–Li) (–24.8 kcal mol^{-1}), whereas interactions of the lone pair of **9C**(–Li) or the C_α–S π orbital in the case of **9D**(–Li) with the S–$C_{t\mathrm{Bu}}$ σ* orbital are negligible. However, the different degrees of n→σ* interaction in **9A**(–Li) and **9B**(–Li) on the one hand and in **9C**(–Li) on the other is not reflected by the S–$C_{t\mathrm{Bu}}$ bond lengths in **9A**(–Li), **9B**(–Li), and **9C**(–Li), which are comparable [**9A**(–Li): 1.846 Å; **9B**(–Li): 1.844 Å; **9C**(–Li): 1.846 Å], nor by the occupation numbers of $n(C_\alpha)$ which are also similar for all three conformers (see Table 11). Moreover, the total energies of the interactions between the lone pair at C_α and the weakly occupied antibonding (BD*) and Rydberg-like orbitals (Ry*) are comparable (–185 to –189 kcal mol^{-1}) for structures **9A**(–Li), **9B**(–Li), and **9C**(–Li), and even slightly more stabilizing for the maximum **9C**(–Li) (–189 kcal mol^{-1}) than for the minima **9A**(–Li) (–185 kcal mol^{-1}) and **9B**(–Li) (–187 kcal mol^{-1}). At –8.9 and –50.1 kcal mol^{-1} the interactions of the C_α–C_i π bond, mostly located at C_α, of **9D**(–Li) with the Ry* and BD* orbitals are much weaker. The σ* orbital of the C_α–S bond interacts more strongly with the occupied NBOs in the maxima, which results in higher/lower occupation numbers of the $\sigma^*_{C\alpha-S}/\sigma_{C\alpha-S}$ bonds and therefore larger C_α–S bond lengths in these conformers. It therefore appears that the shapes of the curves shown in Figure 26 are not determined by different degrees of negative hyperconjugation in the four structures but rather by repulsive interactions between the substituents. Thus, in the maxima, the *tert*-butyl group on the one hand and the methyl or phenyl group on

the other are in a synperiplanar orientation in which repulsion between the groups should be strong. Moreover, this repulsive interaction should be stronger between the phenyl substituent and the *tert*-butyl group in **9D**(–Li) than between the methyl and the *tert*-butyl group in **9C**(–Li). Consequently, conformation **9D**(–Li), in which the phenyl substituent and the *tert*-butyl group are oriented synperiplanar, is higher in energy than the maximum **9C**(–Li), in which we have such a relative orientation of the methyl and *tert*-butyl groups. Such an interpretation of the potential curve does not contradict the large and positive V_2 term because this quantity merely describes the angular dependence of the energy and does not imply any stabilizing or destabilizing mechanism in the minima and maxima.

Table 11. Potential constants obtained from a fit of the five-term Fourier series to the potential curve of **9**(–Li) calculated at the MP2/6-311++G**//HF/6-31+G* level.

V_i [kcal mol^{-1}]				
V_1	V_2	V_3	V_4	V_5
–0.3	17.6	1.3	–0.1	–3.0

Conclusions

Because of their relatively high enantiomerization barriers, lithium α-*tert*-butylsulfonyl carbanion salts bearing two substituents at the C_α atom should have at low temperatures a configurational stability sufficient for enantioselective synthesis and a study of the racemization dynamics and reactivity. The rate-determining step of the enantiomerization of the lithium α-*tert*-butylsulfonyl carbanion salts is the C_α–S bond rotation and not C_α atom inversion or dimer-to-monomer conversion. Ab initio calculations on the counterion-free benzylic α-sulfonyl carbanion [MeC(Ph)SO_2tBu]$^-$ gave two different C_α–S rotational barriers, which are mainly determined by steric interaction in the transition state. Lithium *S*-*tert*-butylsulfonyl carbanion salts form in THF monomeric and dimeric O–Li CIPs. X-ray crystal structure analysis of a number of monomeric and dimeric salts of type [$R^1C(R^2)SO_2t$Bu]Li ($R^1 \neq R^2$) gave a general picture of their structures, which can serve as a solid basis for the structures of the monomers and dimers in solution. The monomeric and dimeric *S*-*tert*-butyl-substituted O–Li CIPs are devoid of a C_α–Li bond. They feature a planar C_α atom in the case of a phenyl substituent and exhibit, because of the C_α–S conformation, a stereogenic axis. There is a high degree of similarity in the structures of the lithium salts of α-sulfonyl carbanions irrespective of the substituents at the S and C_α atoms. An exception is the configuration of the anionic C atom. Crystal structure analysis and ab initio calculations show that dialkyl-substituted α-phenyl- and α-methylsulfonyl carbanions have a strongly pyramidalized anionic C atom. Ab initio calculations on counterion-free dimethyl-substituted α-sulfonyl carbanions revealed a change in the coordination geometry of the C_α atom from pyramidalized to planar on going from the *S*-Me- to the *S*-CF_3- and *S*-*t*Bu-substituted carbanions. The planarization the C_α atom with increasing steric size of the S substituent seems to be a result of a minimization of the steric interaction between the S and C_α substituents in combination with a small intrinsic energy difference between the planar and pyramidal coordination geometry. Because of shielding of the anionic C atom by the *S*-*tert*-butyl group, the lithium α-*tert*-butylsulfonyl carbanion salts are expected to react with electrophiles with high stereoselectivity. The addition of HMPA to the CIP causes the formation of SIPs, a feature that is perhaps of importance in the case of insufficient reactivity of nonracemic CIPs at low temperatures. The crystal structures of the lithium salts of the benzylic α-*tert*-butylsulfonyl carbanions revealed an increasing deviation of the coplanarity of the phenyl ring with the C_i–C_α–S plane with increasing steric size of the substituent at the C_α atom. This feature results in a gradual decrease in benzylic conjugation, as shown by the NMR spectroscopic data of the salts in solution. Ab initio calculations on [MeC(Ph)-SO_2tBu]$^-$ in combination with a NBO analysis showed that the C_α atom carries a lone pair of pure p character. There is neither a π bond between the C_α and C_i atoms nor between the C_α and S atoms. The lack of a π bond, however, does not preclude an interaction between the lone pair and the phenyl group leading to charge transfer, as revealed by NMR spectroscopy.

Experimental Section

General: All manipulations with the lithium α-sulfonyl carbanion salts were performed in oven-dried glassware under dry argon or nitrogen using Schlenk and syringe techniques unless otherwise stated. Solvents were purified and dried prior to use by distillation from an appropriate drying agent under argon. [D_6]Benzene, [D_{14}]-diglyme, and diglyme were distilled from potassium benzophenone ketyl. *n*-Hexane and *n*-pentane were distilled from sodium benzophenone ketyl and tetrahydrofuran (THF) was distilled from potassium benzophenone ketyl. N^1,N^1,N^2,N^2-Tetramethylethane-1,2-diamine (TMEDA), dimethylformamide (DMF), 12-crown-4 (12-crown-4), hexamethylphosphoric triamide (HMPA), and N^1-[2-(dimethylamino)ethyl]-N^1,N^2,N^2-trimethylethane-1,2-diamine (PMDTA) were distilled from calcium hydride. Diethyl ether was distilled from sodium benzophenone ketyl. The starting materials were obtained from commercial sources and used without further purification unless otherwise stated. A solution of *n*-butyllithium (*n*BuLi) in *n*-hexane was purchased from Chemmetall and standardized by titration with diphenylacetic acid.[38] ^{6}Li-Labeled *n*-propyllithium (*n*Pr^{6}Li) in *n*-pentane was prepared from 1-chloropropane and ^{6}Li and standardized by titration with diphenylacetic acid. *n*Bu^{6}Li in *n*-hexane was prepared from 1-chlorobutane and ^{6}Li[39] and standardized by titration with diphenylacetic acid. Analytical thin-layer chromatography (TLC) was performed on E. Merck precoated TLC plates (silica gel 60 F_{254}, layer thickness 0.2 mm). Column chromatography was performed with Merck silica gel 60 (70–230 mesh). Temperatures were measured with a Lauda TP10 digital thermometer and a Pt-82 thermosensor. Melting points were determined using a Büchi SMP-20 apparatus and are uncorrected. ^{1}H, ^{13}C, ^{6}Li, and ^{31}P NMR spectra were recorded with Bruker AM 400, Bruker, WM 300, Bruker WM 250, Varian Unity 500, Varian Inova 400, Varian VXR 300, and Varian Gemini

300 instruments. ^{1}H NMR chemical shifts of measurements in $CDCl_3$, are reported in ppm relative to Me_4Si (δ = 0.00 ppm) as the internal standard. ^{1}H NMR chemical shifts of measurements in [D_6]benzene, [D_8]THF, and [D_{14}]diglyme are reported in ppm relative to [D_5]benzene (δ = 7.12 ppm), [D_7]THF (δ = 3.56 ppm), and [D_{13}]diglyme (δ = 3.22 ppm), respectively, as the internal standards. Splitting patterns are designated as follows: s singlet, d doublet, dd double doublet, t triplet, q quartet, quint quintet, sext sextet, sept septet, m multiplet, br. broad, ps pseudo in the case that the apparent multiplicity is a result of the overlap of several multiplets or additional couplings are not resolved because of line-broadening; sh., shoulder; unsym., unsymmetrical; hn, hidden; app., apparent. ^{13}C NMR chemical shifts of measurements in $CDCl_3$ are reported in ppm relative to Me_4Si (δ = 0.00 ppm) as the internal standard. ^{13}C NMR chemical shifts of measurements in [D_6]benzene, [D_8]THF, and [D_{14}]diglyme are reported in ppm relative to [D_5]benzene (δ = 128.0 ppm), [D_7]THF (δ = 25.5 ppm), and [D_{13}]diglyme (δ = 57.9 ppm), respectively, as the internal standard. Peaks in the ^{13}C NMR spectra are denoted as "u" for carbons with zero of two attached protons and as "d" for carbons with one or three attached protons, as determined from the attached proton test (APT) pulse sequence. The following abbreviations are used to designate the peaks: br. broad, vbr. very broad, t triplet. ^{6}Li NMR chemical shifts are reported in ppm relative to LiBr in water (δ = 0.00 ppm) as the external standard. ^{31}P NMR chemical shifts are reported in ppm relative to H_3PO_4 in water (δ = 0.00 ppm) as the external standard. Low-resolution mass spectra were recorded with a Varian MAT 212 mass spectrometer. Only peaks of $m/z \geq 80$ and an intensity of ≥5%, except decisive ones, are listed. IR spectra were recorded with Perkin–Elmer FT 1760 S and 1760 instruments. Only peaks of $\tilde{\nu} \geq 800$ cm^{-1} are listed. The following abbreviations are used to designate the peaks: vs very strong, s strong, m medium, w weak. Elemental analyses were performed by the Institute of Organic Chemistry Microanalytical Laboratory.

The cryoscopy experiments of the lithium α-sulfonyl carbanion salts were carried out by the method described by Bauer and Seebach.[40] The cryoscopy apparatus consisted of a cryoscopy flask with an outside joint, which allowed its insertion into a Schlenk-type conical glass jacket. The outer jacket-flask, which served as a thermo-insulating device, was evacuated. The whole apparatus was placed in a Dewar flask, which had an alumina bottom and was filled with liquid nitrogen. A Schlenk-type steep-breasted flask was used as the cryoscopy flask, which contained a Teflon-coated magnetic stirring bar in a vertical alignment. A magnet (adhering force 470 N) connected to an IKA mixer RW20 served as a stirrer. The steep-breasted flask was closed with a rubber septum, which was fitted with a thermoelement reaching to 5 mm above the bottom of the flask. Temperatures were measured with a Kelvimat type 4321 (Burster Präzisionsmeßtechnik, Gernsbach, Germany) precision digital thermometer, which had an accuracy of measurement of 10 mK and a reproducibility of ±2 mK. A Pt-100 thermocouple of type 42943 (Burster Präzisionsmeßtechnik, Gernsbach, Germany) was used as the thermoelement, which was suitable for measurements in the range –200 to +500 °C. According to the specifications it had for temperatures of approximately –100 °C a deviation from the actual value of $\Delta T \leq 200$ mK. An additional maximal distortion of the real temperature of 2 mK was produced by the necessary measurement current of 1 mA. The measurement data were transferred via an RS232C interface to a computer and processed. Every three seconds a measurement with a resolution of 1 mK was recorded. The cryoscopy measurements of the salt solutions in THF were performed by introducing the solution into the cryoscopy flask to the gauge mark (approximately 60 mL) through a cannula under argon. The solutions were kept under a slight argon pressure and then the thermometer was inserted into the septum. The insulating jacket was evacuated with a high-vacuum pump and the vacuum was maintained throughout the measurements. Then the apparatus was placed in the Dewar flask, which was subsequently filled with liquid nitrogen. During the measurements the solutions were stirred. The cooling rate was 5 K min^{-1} at the beginning, which declined to 1 K min^{-1} at the freezing point. In each cryoscopy experiment at least seven freeze/thaw cycles of the solution of the salt were performed, whereby care was taken that during freezing no salt deposited.

Crystallographic Structure Determination and Refinement: Different techniques were employed to mount crystals for X-ray structure determination. Crystals of (*M*/*P*)-**40**·2diglyme, (**41**·diglyme)$_2$, and (**42**·digylme)$_2$ were transferred into a glass capillary, which was then sealed. Irregular crystals of *rac*-**3**·12-crown-4 were cut and a rod-like specimen was transferred into a glass capillary with a diameter of 0.5 mm, which was sealed under nitrogen. Crystals of (*M*/*P*)-**3**·4THF were transferred into a glass capillary with a diameter of 0.5 mm, which was then sealed under argon. In the cases of (*M*/*P*)-**4**·4THF, (*M*/*P*)-**5**·4THF, *rac*-**9**·PMDETA, and (*M*/*P*)-**10**·2THF, the crystals were transferred directly under a stream of nitrogen from the flask to the top of a glass fiber tipped with a droplet of highly viscous silicon grease. In these cases, data were collected under a stream of cooled nitrogen. The structure of (*M*/*P*)-**3**·4THF was solved by direct methods (SHELXL-86) and refined with SHELX-76.[41] The structures of *rac*-**3**·12-crown-4, (*M*/*P*)-**4**·4THF, (*M*/*P*)-**5**·4THF, *rac*-**9**·PMDETA, (*M*/*P*)-**10**·2THF, (*M*/*P*)-**40**·2diglyme, (**41**·diglyme)$_2$, and (**42**·digylme)$_2$ were solved by direct methods as implemented in the Xtal 3.2 package of crystallographic routines: GENSIN[42] was employed to generate structure invariant relationships and GENTAN[43] for the general tangent phasing procedure. The final refinements were performed using Xtal 3.7.[44] Crystallographic data are summarized in the Supporting Information

General Procedure for the Preparation of Solutions of Salts *rac*-1–8 for DNMR Spectroscopy (GP1): A Schlenk flask equipped with a Teflon-coated magnetic stirring bar and a septum, which had been dried with a heat gun in vacuo and filled with argon, was charged with *n*PrLi (0.12–0.22 mL of 0.89 M in *n*-hexane, 0.1–0.2 mmol). The solvent was removed in vacuo and the remaining oil was dried for 5 min at 133 Pa. After cooling the flask to –90 °C, it was filled with argon and [D_8]THF (0.4 mL) was added. In a separate Schlenk flask, which had been dried with a heat gun in vacuo and filled with argon, the sulfone (0.1–0.2 mmol) and [D_8]THF (0.5 mL) were successively added under argon. Then the solution of the sulfone was added at –90 °C with a syringe to the solution of *n*PrLi in [D_8]THF. After stirring the mixture for 5 min, it was warmed to room temperature and concentrated in vacuo to a volume of 0.6 mL. Then the solution was transferred under argon with a syringe to an NMR tube (from the bottom), which had been dried with a heat gun under vacuum and filled with argon. The NMR tube contained a ground joint carrying a three-way Teflon stopcock. The NMR tube with the solution of the salt was cooled to –90 °C, evacuated twice for 5 s, filled with argon, evacuated a third time, and then sealed with an acetylene/oxygen microburner.

{[PhCH$_2$C(Ph)SO$_2$*t*Bu]Li·2THF}$_2$ [(*M*/*P*)-3·4THF]: *n*BuLi (0.20 mL of 1.59 M in *n*-hexane) was added dropwise to a solution of sulfone *rac*-**35** (100 mg, 0.33 mmol) in THF (0.8 mL) at –90 °C. The solution was stirred for 20 min at this temperature and then warmed to room temperature over 15 min. After the addition of *n*-hexane (1 mL), the solution was concentrated at room temperature

in vacuo to a volume of 1 mL and kept for 2 d at 2 °C. The crystals formed were freed from the mother liquor with a syringe, washed with *n*-hexane, and dried at room temperature in vacuo at 133 Pa for 2 min. the salt (*M*/*P*)-**3**·4THF (130 mg, 90%) was obtained as pale-yellow crystals. ^{1}H NMR (250 MHz, [D$_8$]THF): δ = 1.31 (s, 9 H, *t*Bu), 3.98 (s, *J* = 49 Hz, 2 H, CH$_2$), 6.16 (m, 1 H, *p*-α-Ph), 6.69 (m, 2 H, *m*-α-Ph), 6.94 (m, 1 H, *p*-β-Ph), 7.00–7.12 (m, 4 H, *o*-α-Ph, *m*-β-Ph), 7.32 (m, 2 H, *o*-β-Ph) ppm. ^{13}C NMR (100 MHz, [D$_8$]-THF): δ = 26.0 (*t*Bu-CH$_3$, d), 58.0 (C$_\alpha$, u), 64.6 (CH$_2$, u), 114.2 (*p*-α-Ph, d), 120.3 (*o*-α-Ph, d), 125.1 (*p*-β-Ph, d), 127.4 (*m*-α-Ph, d), 128.0 (*m*-β-Ph, d), 129.2 (*o*-β-Ph, d), 145.8 (*i*-Ph, u), 146.1 (*i*-Ph, u) ppm. Single crystals of (*M*/*P*)-**3**·**4**THF were obtained by dissolving the above crystals in *n*-hexane/THF (1:1; 1 mL) until only a few crystals remained by warming the suspension to 50 °C. The solution was cooled over 5 h to room temperature, whereupon crystals were formed. The mother liquor was removed with a syringe and the crystals were washed with *n*-hexane (4 × 1 mL) and dried at room temperature for 1 min at 133 Pa.

[PhCH$_2$C(Ph)SO$_2$*t*Bu]Li·12-crown-4 (*rac*-3·12-crown-4): *n*BuLi (0.66 mL of 1.5 N in *n*-hexane) was added to a solution of sulfone *rac*-**35** (300 mg, 0.99 mmol) and freshly distilled 12-crown-4 (262 mg, 1.49 mmol) in THF (10 mL) at –78 °C. After the addition a microcrystalline solid was formed, which did not dissolve even at room temperature. The suspension was concentrated in vacuo to a volume of 3 mL. The mother liquor was removed with the aid of a syringe. The crystals were washed with *n*-hexane and dried in vacuo. The salt *rac*-**3**·12-crown-4 (366 mg, 75%) was isolated as pale-yellow crystals. Single crystals were obtained by the addition of THF (20 mL) to the above crystals to give a clear solution, which was kept at –15 °C for 2 d. The irregular colorless crystals that were formed were freed from the mother liquor by the aid of a syringe and dried in a stream of argon at room temperature. ^{1}H NMR ([D$_8$]THF, 500 MHz): δ = 1.28 (s, 9 H, *t*Bu), 3.58 (s, 16 H, 12-crown-4), 3.70–4.08 (br. s, 2 H, CH$_2$), 6.12 (tt, 1 H, *p*-α-Ph), 6.65 (tm, 2 H, *m*-α-Ph), 6.92 (tm, 1 H, *p*-β-Ph), 7.02–7.06, 7.16–7.24, 7.30–7.34 (m, 6 H, Ph) ppm. ^{13}C NMR ([D$_8$]THF, 125 MHz): δ = 26.9 (*t*Bu-CH$_3$, d), 39.0 (CH$_2$, u), 65.2 (*t*Bu-C, u), 72.6 (12-crown-4, u), 114.7 (d), 121.0 (d), 125.9 (d) (*p*-β-Ph, *m*-β-Ph, *o*-α-Ph), 128.3 (d), 128.8 (d), 130.1 (d) (*p*-β-Ph, *m*-β-Ph, *o*-β-Ph), 147.0 (u), 147.3 (u) (*i*-Ph, u) ppm. The signal of C$_\alpha$ could not be detected.

{[MeCH$_2$C(Ph)SO$_2$*t*Bu]Li·2THF}$_2$ [(*M*/*P*)-4·4THF]: *n*BuLi (14.5 mL, 22 mmol of 1.52 M in *n*-hexane) was added dropwise over 15 min to a suspension of sulfone *rac*-**28** (4.83 g, 20 mmol) in THF (40 mL) at –75 °C. After stirring the mixture for 20 min at –75 °C, *n*-hexane (80 mL) was added and the yellow-orange solution was warmed to room temperature. The solution was concentrated in vacuo to a volume of 40 mL and *n*-hexane (100 mL) was added. After 2 d at 2 °C the mother liquor was removed with the aid of a syringe and the crystals were washed with *n*-hexane (3 × 15 mL). The salt (*M*/*P*)-**4**·4THF was obtained as colorless crystals. For the preparation of single crystals, THF (1 mL) and *n*-hexane (25 mL) were added to the crystalline salt (*M*/*P*)-**4**·4THF obtained above and the suspension was slowly heated to 50 °C. The clear solution formed was slowly cooled to room temperature and kept for 1 d at 2 °C. The microcrystalline material formed was dissolved by the addition of THF (1 mL) and heating the suspension to 50 °C. The solution was slowly cooled to room temperature and kept for 3 d at 2 °C. After repeating this procedure twice and extending the crystallization time in the last run to 1 week, (*M*/*P*)-**4**·4THF was obtained as bundles of needles or rods up to 0.5 mm in diameter and 4 mm in length. The mother liquor was removed with the aid of a syringe and the crystals (3.08 g, 39%) were washed with *n*-hexane (4 × 5 mL). ^{1}H NMR (500 MHz, [D$_6$]benzene): δ = 1.40 (t, *J* = 7.0 Hz, 3 H, CH$_3$), 1.42 (s, 9 H, S-*t*Bu), 1.44 (m, 8 H, β-THF), 2.91 (br. q, *J* = 7.0 Hz, 2 H, CH$_2$), 3.70 (m, 8 H, α-THF), 6.80 (m, 1 H, *p*-Ph), 7.30 (m, 2 H, *m*-Ph), 7.61 (m, 2 H, *o*-Ph) ppm. ^{13}C NMR (125 MHz, [D$_6$]benzene): δ = 16.0 (CH$_3$, d), 24.4 (CH$_2$, u), 25.5 (β-THF, u), 25.7 (S-*t*Bu-CH$_3$, d), 59.5 (C$_\alpha$, u), 64.0 (S-*t*Bu-C, u), 68.1 (α-THF, d), 115.0 (*p*-Ph, d), 120.2 (*o*-Ph, d), 145.0 ppm (*i*-Ph, u) (the signal of *m*-Ph was hidden below the signal of [D$_5$H]-benzene at δ = 128.0 ppm).

{[*t*BuCH$_2$C(Ph)SO$_2$*t*Bu]Li·2THF}$_2$ [(*M*/*P*)-5·4THF]: *n*BuLi (7.5 mL, 11.3 mmol of 1.5 M in *n*-hexane) was added dropwise over 10 min to a suspension of sulfone *rac*-**29** (2.82 g, 10 mmol) in THF (20 mL) at –66 °C. A clear yellow solution was formed from which, after stirring for 1 h at –75 °C, the salt (*M*/*P*)-**5**·4THF partially crystallized. After the addition of *n*-hexane (40 mL) the mixture was warmed to room temperature, whereupon the solid dissolved. The clear solution was concentrated in vacuo to a volume of 20 mL, whereupon a partial crystallization took place. After the addition of *n*-hexane (40 mL) the suspension was heated slowly to 60 °C, whereupon the solid dissolved completely. The heating device was removed and the solution was kept for 1 d at room temperature. Crystallization of (*M*/*P*)-**5**·4THF as colorless crystals up to 1 mm in length started after several hours. The pale-yellow mother liquor was removed by the aid of a syringe and the crystals were washed with *n*-hexane (4 × 10 mL) and dried at room temperature in vacuo for 10 min. The salt (*M*/*P*)-**5**·4THF (2.35 g, 54%) was obtained as pale-yellow crystals. ^{1}H NMR (500 MHz, [D$_6$]benzene): δ = 1.17 (s, 9 H, β-*t*Bu), 1.32 (s, 9 H, S-*t*Bu), 1.45 (m, 8 H, β-THF), 2.57 (unsym. br. s, 1 H, CH$_2$), 3.14 (unsym. br. s, 1 H, CH$_2$), 3.79 (m, 8 H, α-THF), 6.90 (app. t, 1 H, *p*-Ph), 7.29 (m, 2 H, *m*-Ph), 7.87 (app. br. d, 2 H, *o*-Ph) ppm. ^{13}C NMR (125 MHz, [D$_6$]benzene): δ = 25.5 (β-THF, u), 26.1 (S-*t*Bu, d), 30.5 (β-*t*Bu, d), 35.0 (β-*t*Bu, d), 43.5 (CH$_2$), 54.7 (C$_\alpha$, u), 64.9 (S-*t*Bu-C, u), 68.2 (α-THF, d), 117.4 (*p*-Ph, d), 124.1 (*o*-Ph, d), 127.6 (*m*-Ph, d), 146.4 (*i*-Ph, u) ppm. For the preparation of single crystals, (*M*/*P*)-**5**·4THF was dissolved in *n*-hexane/THF (6:1; 35 mL) by slowly warming the suspension in an oil bath to 60 °C. The heat supply to the oil bath was removed, and the pale-yellow solution was allowed to cool slowly to room temperature. After 24 h some only slightly distorted octahedral crystals of 1 mm in diameter had been formed. The mother liquor was removed by a syringe and heated to 60 °C to dissolve any crystalline material that had formed. The resulting solution was cooled slowly to room temperature, upon which crystallization started again. Once again the mother liquor was removed and warmed to dissolve any crystals that had formed. Cooling the solution slowly to room temperature gave faint yellow octahedral crystals of up to 5 mm in length.

{[*t*BuC(Ph)SO$_2$*t*Bu]Li·THF}$_2$ [(*M*/*P*)-10·2THF]: *n*BuLi (7.0 mL, 11.3 mmol of 1.62 M in *n*-hexane) was added dropwise to a suspension of sulfone *rac*-**30** (2.73 g, 10.2 mmol) in THF (20 mL) at –69 °C whilst stirring (the mixture remained a suspension because of the salt that deposited). After stirring the suspension for 2.5 h at –74 °C, *n*-hexane (40 mL) was added and the suspension was warmed to room temperature, whereupon the solid dissolved completely at –30 °C. The pale-yellow solution was concentrated in vacuo at room temperature to a volume of 10 mL. After the addition of *n*-hexane (60 mL), a suspension formed, which was heated in an oil bath to 65 °C upon which a clear solution was obtained. The heat supply to the oil bath was removed, and the solution was allowed to cool to room temperature. After 4 h colorless crystals up to 3 mm in diameter had formed. The mother liquor was removed with a syringe and the crystals were washed with *n*-hexane (3 × 10 mL) and dried in vacuo for 10 min. The salt (*M*/*P*)-**10**·2THF (1.63 g, 49%) was obtained as pale-yellow crystals. ^{1}H

NMR (500 MHz, [D$_6$]benzene): δ = 1.27 (m, 4 H, β-THF), 1.55 (s, 9 H, S-*t*Bu), 1.58 (s, 9 H, α-*t*Bu), 3.31 (m, 4 H, α-THF), 7.09 (app. t, 1 H, *p*-Ph), 7.31 (m, 2 H, *m*-Ph), 7.81 (app. br. d, 2 H, *o*-Ph) ppm. ^{13}C NMR (125 MHz, [D$_6$]benzene): δ = 25.2 (β-THF, u), 27.0 S-*t*Bu-CH$_3$, d), 34.6 (α-*t*Bu-CH$_3$, d), 34.7 (α-*t*Bu-CH$_3$, d), 58.0 (C$_\alpha$, u), 61.9 (S-*t*Bu-C, u), 67.9 (α-THF, u), 124.9 (*p*-Ph, d), 127.5 (*m*-Ph, d), 138.8 (*o*-Ph, d), 145.4 (*i*-Ph) ppm. For the preparation of suitable single crystals, THF (1 mL) and *n*-hexane (30 mL) were added to the crystals and the suspension slowly warmed to 65 °C, whereupon a clear solution was formed. Upon cooling the solution to room temperature, pale-yellow, strongly distorted octahedral crystals were formed. The mother liquor was removed with a syringe and the crystals were washed with *n*-hexane (3 × 10 mL) and dried.

[MeC(Ph)SO$_2$*t*Bu]Li·PMDTA (*rac*-10·PMDTA): *n*BuLi (0.64 mL of 1.60 M in *n*-hexane, 1.03 mmol) was added dropwise to a suspension of sulfone *rac*-**27** (226 mg, 1 mmol) in PMDTA (2 mL) under argon at –70 °C. After stirring the suspension at –70 °C for 20 min, the cooling bath was removed and the mixture was warmed to room temperature. Upon the addition of THF (0.68 mL) the milky mixture turned to a yellow solution within 10 min. The solution was kept at 2 °C for 4 d whereupon colorless platelet-like crystals of *rac*-**10**·PMDTA were formed. The mother liquor was removed with a syringe and the crystals were dried in a stream or argon.

{[MeCH$_2$C(Me)SO$_2$Ph]Li·diglyme}$_2$ [(*M*/*P*)-40·2diglyme]: *n*BuLi (2.6 mL of 1.5 M in *n*-hexane, 3.97 mmol) was added dropwise to a solution of sulfone *rac*-**46** (767 mg, 3.87 mmol) in diglyme (4.9 mL) at 0 °C. The solution turned yellow-orange and a yellow solid deposited. *n*-Hexane and *n*-butane were removed by concentration of the mixture in vacuo at room temperature for 1 min. The yellow suspension was slowly warmed to 30 °C, whereupon a yellow-orange solution was obtained. Upon cooling the solution to room temperature yellow rod-like crystals were formed. Removal of the mother liquor and washing the crystals with cold diethyl ether gave the salt (*M*/*P*)-**40**·2diglyme (1.14 g, 87%) as yellow needle-like crystals. ^{1}H NMR (300 MHz, [D$_8$]THF): δ = 0.84 (t, *J* = 7.4 Hz, 3 H, CH$_3$), 1.54 (s, 3 H, CH$_3$), 1.96 (q, *J* = 7.4 Hz, 2 H, CH$_2$), 3.27 (s, OMe, diglyme), 3.43 (m, diglyme), 3.53 (m, diglyme), 7.04 (m, 1 H, *p*-Ph), 7.15 (m, 2 H, *m*-Ph), 7.51 (m, 2 H, *o*-Ph) ppm. ^{13}C NMR (75 MHz, [D$_8$]THF): δ = 15.6 (CH$_3$, d), 16.1 (CH$_3$, d), 26.9 (CH$_2$, u), 47.5 (C$_\alpha$, u), 59.1 (OMe, diglyme, d), 71.6 (OCH$_2$, diglyme, u), 73.1 (OCH$_2$, diglyme, u), 125.3 (*m*-Ph, d), 127.1 (*p*-Ph, d), 128.3 (*o*-Ph, d), 132.5 (*i*-Ph, u) ppm.

{[MeCH$_2$C(CH$_2$Me)SO$_2$Ph]Li·diglyme}$_2$ (41·diglyme)$_2$: *n*BuLi (12.23 mL of 1.5 M in *n*-hexane, 18.35 mmol) was added dropwise to a solution of sulfone **47** (3.90 g, 18.35 mmol) in diglyme (22.5 m) at 0 °C. The solution turned yellow and a yellow solid deposited. *n*-Hexane and *n*-butane were removed by concentration of the mixture in vacuo at room temperature for 1 min. The yellow suspension was slowly warmed to 80 °C, whereupon a yellow-orange solution was obtained. Upon cooling the solution to room temperature yellow rod-like crystals were formed. Removal of the mother liquor and washing the crystals with cold diethyl ether gave the salt (**41**·diglyme)$_2$ (5.06 g, 78%) as yellow needle-like crystals. ^{1}H NMR (300 MHz, C$_6$D$_6$): δ = 1.23 (t, *J* = 7.15 Hz, 6 H, CH$_3$), 2.26 (q, *J* = 7.32 Hz, 4 H, CH$_2$), 3.17 (s, OMe, diglyme), 3.27 (m, diglyme), 3.35 (m, diglyme), 7.01 (m, 1 H, *p*-Ph), 7.17 (m, 2 H, *o*-Ph), 7.93 (m, 2 H, *m*-Ph) ppm. ^{13}C NMR (75 MHz, C$_6$D$_6$): δ = 15.4 (CH$_3$, d), 22.9 (CH$_2$, u), 54.3 (C$_\alpha$, u), 58.7 (OMe, diglyme, u), 70.1 (OCH$_2$, u), 71.4 (OCH$_2$, u), 125.0 (*m*-Ph, d), 127.1 (*p*-Ph, d), 128.1 (*o*-Ph, d), 153.7 (*i*-Ph, u) ppm.

{[(CH$_2$)$_5$CSO$_2$Ph]Li·diglyme}$_2$ (42·diglyme)$_2$: *n*BuLi (2.84 mL of 1.38 M in *n*-hexane, 3.92 mmol) was added dropwise to a solution of sulfone **48** (800 mg, 3.57 mmol) in diglyme (4.5 mL) at 0 °C. The solution turned orange and an orange solid deposited. *n*-Hexane and *n*-butane were removed by a concentration of the mixture in vacuo at room temperature for 1 min. The orange suspension was slowly warmed to 100 °C (oil bath) whereupon an orange solution was obtained. Upon cooling the solution in the oil bath to room temperature orange rod-like crystal were formed. Removal of the mother liquor and washing the crystals with cold diethyl ether gave the salt (**42**·diglyme)$_2$ (950 mg, 82%) as orange rod-like crystals. ^{1}H NMR (300 MHz, [D$_8$]THF): δ = 1.28–1.35 (m, 6 H, CH$_2$), 1.89–1.93 (m, 4 H, CH$_2$), 3.28 (s, 6 H, OMe, diglyme), 3.45 (m, 4 H, diglyme), 3.53 (m, 4 H, diglyme), 7.06 (m, 1 H, *p*-Ph), 7.18 (m, 2 H, *m*-Ph), 7.50 (m, 2 H, *o*-Ph) ppm. ^{13}C NMR (75 MHz, [D$_8$]THF): δ = 28.5 (CH$_2$, u), 28.6 (CH$_2$, u), 30.0 (CH$_2$, u), 52.5 (C$_\alpha$, d), 58.8 (OMe, diglyme, d), 71.3 (OCH$_2$, u), 72.8 (OCH$_2$, u), 124.9 (*m*-Ph, u), 126.9 (*p*-Ph, u), 128.1 (*o*-Ph, u), 150.6 (*i*-Ph, u) ppm.

Cryoscopy of [PhCH$_2$C(Ph)SO$_2$*t*Bu]Li (*rac*-3) in THF: *n*BuLi (10.4 mL of 1.52 M in *n*-hexane, 15.8 mmol) was added to a suspension of sulfone *rac*-**35** (4.54 g, 15 mmol) in THF (30 mL) under argon at –90 °C. Then *n*-hexane (30 mL) was added dropwise, whereupon a white solid deposited. Subsequently the suspension was heated at 60 °C until a clear solution was formed. The solution was slowly cooled to room temperature and kept at 4 °C for 4 d, whereupon colorless crystals were formed. The mother liquor was removed with a syringe. Washing of the crystals with *n*-hexane and drying in vacuo for 15 min gave the salt (*M*/*P*)-**3**·4THF. ^{1}H NMR (300 MHz, [D$_8$]THF): δ = 1.26 (s, 9 H, *t*Bu), 3.83 (br. s, 2 H, CH$_2$), 6.12 (t, *J* = 7.1 Hz, 1 H, *p*-α-Ph), 6.64 (dd, *J* = 8.5, *J* = 7.1 Hz, 2 H, *m*-α-Ph), 6.90 (t, *J* = 7.1 Hz, 1 H, *p*-β-Ph), 7.01–7.04 (m, 4 H, *o*-α-Ph, *m*-β-Ph) ppm. The ^{1}H NMR spectrum of (*M*/*P*)-**3**·4THF showed it to contain four molecules of THF (δ = 1.73, 3.58 ppm) and the presence of 4% of sulfone *rac*-**35**. ^{13}C NMR (75 MHz, [D$_8$]THF): δ = 26.2 (*t*Bu-CH$_3$, d), 58.2 (C$_\alpha$, u), 64.8 (CH$_2$, u), 114.4 (*p*-α-Ph, d), 120.5 (*o*-α-Ph, d), 125.3 (*p*-β-Ph, d), 127.6 (d), 128.2 (d), 129.4 (d) (*m*-α-Ph, *o*-β-Ph, *m*-β-Ph), 146.1 (u), 146.3 (u) (*i*-α-Ph, *i*-β-Ph) ppm. Three independent experiments with a solution of *rac*-**3** in THF (70 mL) of different concentrations were performed. Experiment 1: c = 86.6 mmol kg^{-1}; experiment 2: c = 44.2 mmol kg^{-1}; experiment 3: c = 41.0 mmol kg^{-1}. The solution was transferred through a cannula to the cryoscopy flask up to the graduation. Then the insulating jacket was evacuated and the apparatus was cooled with liquid nitrogen. Several cooling curves were recorded in each experiment. Determination of the melting points in experiments 2 and 3 proved not to be possible because of the occurrence of a two-phase undercooling. Several cooling curves were recorded in experiment 1. Analysis of the curves gave the melting points listed in Table 12. After the experiment had finished, the solution of *rac*-**3** in THF was treated at –80 °C with [D]TFA (12.5 mL of 2 M [D]TFA in THF, 25 mmol). Work-up and ^{1}H NMR spectroscopy of the crude material revealed the presence of *rac*-D-**35** and 4% of sulfone *rac*-**35**.

Table 12. Cryoscopy of the salt *rac*-**3** in THF under conditions of experiment 1 (c = 86.6 mmol kg^{-1}).

Measurement	T [K]
a	164.417
b	164.435
c	165.427
Mean value	164.426

The experiments were performed with the cryoscopy set-up of T_{THF} = 164.566 ± 0.003 K and E_K = 1.85 K mol^{-1} kg. Calculation of the aggregation number (n): Experiment 1: $\Delta\bar{T} = T_{THF} - \bar{T}_{exp}$ = 164.566 K – 164.426 K = 0.140 K, $\bar{c}_{exp} = \Delta\bar{T}/E_K$ = 75.7 mmol kg^{-1}, $\bar{n} = c_{nom}/\bar{c}_{exp}$ = 1.14 ± 0.15.

DNMR Spectroscopy of [PhCH$_2$C(Ph)SO$_2$*t*Bu]Li (*rac*-3): According to **GP1**, a solution of sulfone *rac*-**35** (51 mg, 0.17 mmol) in [D$_8$]-THF (6 mL) was treated with *n*PrLi (0.20 mL of 0.90 M in *n*-hexane, 0.18 mmol). The thus obtained solution of *rac*-**3** was sealed in an NMR tube. ^{1}H NMR (250 MHz, [D$_8$]THF, room temperature): δ = 1.31 (s, 9 H, *t*Bu-CH$_3$), 1.73 (m, β-THF), 3.58 (m, α-THF), 3.89 (s, ω = 49 Hz, 2 H, CH$_2$), 6.16 (m, 1 H, *p*-α-Ph), 6.69 (m, 2 H, *m*-α-Ph), 6.94 (m, 1 H, *p*-β-Ph), 7.00–7.12 (m, 4 H, *o*-α-Ph), 7.32 (m, 2 H, *o*-β-Ph) ppm. ^{13}C NMR (100 MHz, [D$_8$]THF, room temperature): δ = 25.3 (quint, β-THF, u), 26.0 (*t*Bu-CH$_3$, d), 58.0 (C$_\alpha$, u), 64.6 (CH$_2$, u), 67.4 (quint, α-THF, u), 114.2 (*p*-α-Ph, d), 120.3 (*o*-α-Ph, d), 125.1 (*p*-β-Ph, d), 127.4 (*m*-α-Ph, d), 128.0 (*m*-β-Ph, d), 129.2 (*o*-β-Ph, d), 145.8 (*i*-Ph, u), 146.1 (*i*-Ph, u) ppm. ^{1}H NMR (250 MHz, [D$_8$]THF, 17 °C, in part): δ = 3.88 (s, ω = 67 Hz, 2 H, CH$_2$) ppm. ^{1}H NMR (250 MHz, [D$_8$]THF, –40 °C, in part): δ = 3.70 (d, J = 17.9 Hz, 1 H, CH$_2$), 4.03 (d, J = 17.9 Hz, 1 H, CH$_2$) ppm. J_{AB} = 17.9 ± 0.2 Hz, $\Delta\nu$ = 86 ± 5 Hz, T_c = 283 ± 5 K. K (T_c) = $\pi(\Delta\nu^2 + 6J_{AB}^2)^{1/2}/\sqrt{2}$, k_{283} = 214 ± 10 s^{-1}; $\Delta G^{\ddagger}$ (T_c) = 4.57T[10.32 – log(k/T_c)], $\Delta G^{\ddagger}_{283}$ = 13.5 ± 0.2 kcal mol^{-1}.

NMR Spectroscopy of [MeC(Ph)SO$_2$*t*Bu]Li (*rac*-9) at Low Temperatures: According to **GP1**, a solution of sulfone *rac*-**27** (22.7 mg, 0.10 mmol) in [D$_8$]THF (1 mL) was treated at –78 °C with *n*Pr^{6}Li (1.48 mL of 0.088 M in *n*-pentane, 0.130 mmol). After stirring the mixture at –78 °C for 10 min, it was concentrated in vacuo and the residue dried in vacuo. The salt (*M*/*P*)-**9**·2THF was dissolved in [D$_8$]THF (0.5 mL) and the solution was sealed in an NMR tube. ^{1}H NMR (300 MHz, [D$_8$]THF): δ = 1.25 (s, 9 H, S-*t*Bu), 1.95 (s, 3 H, α-CH$_3$), 6.18 (ps.-t, 1 H, *p*-Ph), 6.77 (ps.-t, 2 H, *m*-Ph), 7.09 (ps.-d, 2 H, *o*-Ph) ppm. ^{13}C NMR (75 MHz, [D$_8$]THF): δ = 18.6 (α-CH$_3$, d), 26.1 (S-*t*Bu-CH$_3$ d), 53.0 (C$_\alpha$, u), 64.8 (S-*t*Bu-C, u), 113.7 (*p*-Ph, d), 119.2 (*o*-Ph, u), 127.7 (*m*-Ph, d), 147.3 (*i*-Ph, u) ppm. Tables 13, 14, and 15 list the ^{1}H and ^{13}C NMR spectroscopic data at low temperatures.

Table 13. ^{1}H NMR spectroscopy (500 MHz) of the salt *rac*-**9** in [D$_8$]THF at various temperatures.

T [°C]	*o*-Ph: δ [ppm] (signal), species	*m*-Ph: δ [ppm] (signal), species	*p*-Ph: δ [ppm] (signal), species	α-CH$_3$: δ [ppm] (signal), species	S-*t*Bu: δ [ppm] (signal)
ca. 22	7.09 (ps.-d)	6.77 (ps.-t)	6.18 (ps.-t)	1.95 (s)	1.25 (s)
–40	7.07 (br.)	6.77 (br. ps.-t)	6.18 (br. s)	1.93 (s)	1.24 (s)
–50	7.8–6.2 (br.)[a]	6.77 (br. s)	6.18 (br. s)	1.93 (br. s)	1.24 (br. s)
–70	7.73 (br. s), 6.34 (br.)	6.77 (br. s)	6.18 (br. t), 6.15 (br. t)	1.92 (br., sh), 1.91 (br.)	1.24 (br. s)
	6.28 (br.)	6.67 (br., sh)	6.09 (br. s)	1.90 (br., sh)	
–80	7.73 (br.), 6.36 (br.)	6.82 (br.), 6.72 (br.)	6.19 (br.), 6.16 (br.)	1.92 (br. s), 1.91 (br. s)	1.25 (br. s)
	6.27 (br.)		6.08 (br. s)	1.89 (br., sh)	
–100	7.75 (d, *o*′), **9**–**3**[b]	6.84 (m, *m*′), **9**–**1/2**	6.18 (t), **9**–**1/2**	1.92 (s), **9**–**2**	1.24 (s)
	7.73 (d, *o*′), **9**–**1/2**	6.82 (m, *m*′), **9**–**4**	6.16 (t), **9**–**4**	1.90 (s), **9**–**1**	
	7.70 (d, *o*′), **9**–**4**	6.79 (t, *m*′), **9**–**3**	6.08 (t), **9**–**3**	1.89 (s), **9**–**4**	
	6.35 (d, *o*), **9**–**1/2**	6.72 (m, *m*), **9**–**1/2**		1.87 (s), **9**–**3**	
	6.32 (d, *o*), **9**–**4**	6.68 (t, *m*), **9**–**4**			
	6.25 (d, *o*), **9**–**3**	6.65 (t, *m*), **9**–**3**			

[a] Coalescence range with very broad singlets at δ = 7.71 and 6.32 ppm. [b] The ratio of the species **9**–**1/2**, **9**–**3**, and **9**–**4** at –100 °C was 75:15:10 according to the intensity of the *o*-Ph signals. The ratio of the species **9**–**1**, **9**–**2**, **9**–**3**, and **9**–**4** at –100 °C was 45:30:15:10 according to the intensity of the β-CH$_3$ signals.

Table 14. ^{13}C NMR spectroscopy (125 MHz) (aromatic region) of the salt *rac*-**9** in [D$_8$]THF at various temperatures.

T [°C]	*i*-Ph: δ [ppm] (signal), species	*m*-Ph: δ [ppm] (signal), species	*o*-Ph: δ [ppm] (signal), species	*p*-Ph: δ [ppm] (signal), species
ca. 22[a]	147.3	127.7	119.2	113.7
–50	147.0 (br.)	127.8 (br.)	119.1 (br. s)	113.8 (br.)
–80	147.5 (br.), 146.8	128.4 (br.), 127.2 (br.)	120.2 (br.), 117.5 (br.), 116.5	113.8, 113.7, 112.4 (br. d)
–100	147.5, **9**–**3**; 146.8, **9**–**1/2**	128.5, **9**–**2**; 127.3, **9**–**1**	120.2 (*o*′), **9**–**2**; 120.2 (*o*′), **9**–**1**; 119.6 (*o*′), **9**–**3**; 117.4 (*o*), **9**–**1/2**; 116.4 (*o*), **9**–**3**	113.7, **9**–**2**; 113.6, **9**–**1** 113.3, **9**–**4**; 112.2, **9**–**3**

[a] 75 MHz NMR spectrum.

Table 15. ^{13}C NMR spectroscopy (125 MHz) (aliphatic region) of the salt *rac*-**9** in [D$_8$]THF at various temperatures.

T [°C]	S-*t*Bu-C: δ [ppm] (signal), species	C$_\alpha$: δ [ppm] (signal)	S-*t*Bu-CH$_3$: δ [ppm]	CH$_3$: δ [ppm] (signal), species
ca. 22[a]	64.8	53.0	26.1	18.6
–50	64.7 (br.)	52.3 (br.)	25.8	18.8 (br.)
–80	64.7, 64.7, 63.7 (br.)	52.3, 52.2	25.7	18.9, 18.7
–100	64.7, **9**–**2**[b]; 64.6, **9**–**1**; 64.3, **9**–**4**; 63.5, **9**–**3**	53.9, **9**–**3**; 52.7, **9**–**4**; 52.3, **9**–**1**; 52.2, **9**–**2**	25.5	19.0, **9**–**1**; 18.8, **9**–**2**

[a] 75 MHz NMR spectrum. [b] The ratio of the species **9**–**1**, **9**–**2**, **9**–**3**, and **9**–**4** at –100 °C was 45:30:15:10.

Supporting Information (see also the footnote on the first page of this article): General experimental procedures, experimental procedures and characterization data for *rac*-**17**, *rac*-**18**, *rac*-**23**–**34**, **46**, **47**, **59**, **60**, *rac*-**62**, **64**, and **66**; synthetic scheme for *rac*-**31**–**34** and *rac*-**45**–**47**; general cryoscopy data; cryoscopy data for *rac*-**4**, *rac*-**6**, and *rac*-**9**; DNMR spectroscopic data for *rac*-**1**, *rac*-**2**, *rac*-**6**–**8**; NMR spectroscopic data for *rac*-**5**, *rac*-**4**, *rac*-**9** and *rac*-**10** at low temperatures; chemical shifts of H_o, H_p, C_o, and C_p of the salts *rac*-**3**, *rac*-**4**, *rac*-**9**, and *rac*-**10** and sulfones *rac*-**17**, *rac*-**27**–**30**; NOE data for *rac*-**3**, *rac*-**4**, *rac*-**6**, *rac*-**9**, and *rac*-**10**; ^{7}Li and ^{31}P NMR data for *rac*-**9** in the presence of HMPA at low temperatures; torsion angles and deviation of the S and Li atoms from the O_4 plane for the eight-membered ring of the salts in the crystal form; figures showing the structures of the salts in the crystal form; discussion of the NOE data of the salts; views of the structures of complex $C_6H_6{\cdot}Li(H_2O)_3^+$; crystal data and experimental details of the structure determination of the salts.

Acknowledgments

This research was supported by the Deutsche Forschungsgemeinschaft (DFG), the Volkswagen Foundation, and Fonds der Chemischen Industrie. We thank Professor Dr. H. Fritz and Dr. D. Hunkler for NMR measurements, Professor Dr. W. Bauer for cryoscopy measurements and valuable experimental advice, Dr. E. Keller for a version of SCHAKAL, and C. Vermeeren and D. Wolters for the preparation of the graphics. We are grateful to Professor Dr. H. J. Reich for his assistance in the analysis of the NMR spectra of the salt *rac*-**9** in the presence of HMPA and for information concerning his unpublished results of a NMR spectroscopic study on the behaviour of lithium *S*-phenylsulfonyl carbanion salts towards HMPA.

[1] For reviews, see: a) A. Simon (Ed.), *The Total Synthesis of Natural Products*, Wiley, New York, **1973**–**1992**, vol. 1–9; b) S. Oae, Y. Uchida, in: *The Chemistry of Sulphones and Sulphoxides* (Eds.: S. Patai, Z. J. M. Rappoport, C. Stirling), Wiley, New York, **1988**, pp. 583–664; c) G. Boche, *Angew. Chem.* **1989**, *101*, 286–306; *Angew. Chem. Int. Ed. Engl.* **1989**, *28*, 277–297; d) N. S. Simpkins, *Sulphones in Organic Synthesis*, Pergamon Press, Oxford, **1993**; e) C. Nájera, J. M. Sansano, *Rec. Res. Develop. Org. Chem.* **1998**, *2*, 637–683; f) A. R. Katritzky, M. Piffl, H. Lang, E. Anders, *Chem. Rev.* **1999**, *99*, 665–722; g) A. Batsu, S. Thayumanavan, *Angew. Chem.* **2002**, *114*, 740–763; *Angew. Chem. Int. Ed.* **2002**, *41*, 716–738; h) P. R. Blackmore, *J. Chem. Soc. Perkin Trans. 1* **2002**, 2563–2585; i) T. Toru, S. Nakamura, *Top. Organomet. Chem.* **2003**, *5*, 177–216; j) H.-J. Gais, in: *Organosulfur Chemistry in Asymmetric Synthesis* (Eds.: T. Toru, C. Bolm), Wiley-VCH, Weinheim, **2008**, pp. 375–398.

[2] For recent applications, see: a) A. P. Dishington, R. E. Douthwaite, A. Mortlock, A. B. Muccioli, N. C. Simpkins, *J. Chem. Soc. Perkin Trans. 1* **1997**, 323–337; b) L. F. Basil, A. I. Meyers, A. Hassner, *Tetrahedron* **2002**, *58*, 207–213; c) A. Hassner, D. Usak, R. Kumareswaran, O. Friedman, *Eur. J. Org. Chem.* **2004**, 2421–2426; d) T. Satoh, A. Kondo, J. Musashi, *Tetrahedron* **2004**, *60*, 5453–5460; e) A. Orita, F. Ye, G. Babu, T. Ikemoto, J. Otera, *Can. J. Chem.* **2005**, *83*, 716–727; f) S. Ciblat, J. Kim, C. A. Stewart, J. Wang, P. Forgione, D. Clyne, L. A. Paquette, *Org. Lett.* **2007**, *9*, 719–722; g) J. J. Caldwell, D. Craig, *Angew. Chem.* **2007**, *119* 2685–2688; *Angew. Chem. Int. Ed.* **2007**, *46*, 2631–2634; h) Y.-F. Chang, C.-Y. Liu, C.-E. Guo, Y.-C. Wang, J.-M. Fang, W. Y. Cheng, *J. Org. Chem.* **2008**, *73*, 7197–7203.

[3] a) G. Boche, M. Marsch, K. Harms, G. M. Sheldrick, *Angew. Chem.* **1985**, *97*, 577–578; *Angew. Chem. Int. Ed. Engl.* **1985**, *24*, 573–574; b) H.-J. Gais, H. J. Lindner, J. Vollhardt, *Angew. Chem.* **1985**, *97*, 865; *Angew. Chem. Int. Ed. Engl.* **1985**, *24*, 859–860; c) H.-J. Gais, J. Vollhardt, H. J. Lindner, *Angew. Chem.* **1986**, *98*, 916–917; *Angew. Chem. Int. Ed. Engl.* **1986**, *25*, 939–941; d) H.-J. Gais, J. Vollhardt, G. Hellmann, H. Paulus, H. J. Lindner, *Tetrahedron Lett.* **1988**, *29*, 1259–1262; e) H.-J. Gais, J. Vollhardt, K. Krüger, *Angew. Chem.* **1988**, *100*, 1108–1110; *Angew. Chem. Int. Ed. Engl.* **1988**, *27*, 1092–1094; f) H.-J. Gais, G. Hellmann, H. Günther, F. Lopez, H. J. Lindner, S. Braun, *Angew. Chem.* **1989**, *101*, 1061–1064; *Angew. Chem. Int. Ed. Engl.* **1989**, *28*, 1025–1028; g) H.-J. Gais, G. Hellmann, H. J. Lindner, *Angew. Chem.* **1990**, *102*, 96–99; *Angew. Chem. Int. Ed. Engl.* **1990**, *29*, 100–103; h) H.-J. Gais, J. Müller, J. Vollhardt, H. J. Lindner, *J. Am. Chem. Soc.* **1991**, *113*, 4002–4003; i) H.-J. Gais, G. Hellmann, *J. Am. Chem. Soc.* **1992**, *114*, 4439–4440; j) P. G. Cozzi, C. Floriani, A. Chiesi-Villa, C. Rizzoli, *Organometallics* **1995**, *14*, 1756–1760; k) H.-J. Gais, M. van Gumpel, G. Raabe, M. Müller, S. Braun, H. J. Lindner, S. Rohs, J. Runsink, *Eur. J. Org. Chem.* **1999**, 1627–1651; l) M. T. Reetz, S. Hütte, R. Goddard, *Eur. J. Org. Chem.* **1999**, 2475–2478; m) H. J. Gais, M. van Gumpel, M. Schleusner, G. Raabe, J. Runsink, C. Vermeeren, *Eur. J. Org. Chem.* **2001**, 4275–4303; n) K. W. Henderson, A. R. Kennedy, D. J. MacDougall, D. Shanks, *Organometallics* **2002**, *21*, 606–616; o) K. W. Henderson, A. R. Kennedy, D. J. MacDougall, *Inorg. Chem.* **2003**, *42*, 2736–2741; p) D. J. MacDougall, A. R. Kennedy, B. C. Noll, K. W. Henderson, *Dalton Trans.* **2005**, 2084–2091; q) M. Linnert, C. Bruhn, C. Wagner, D. J. Steinborn, *Organomet. Chem.* **2006**, *35*, 2358–2367; r) M. Linnert, C. Wagner, K. Merzweiler, D. J. Steinborn, *Z. Anorg. Allg. Chem.* **2008**, *634*, 43–48.

[4] a) R. Lett, G. Chassaing, A. Marquet, *J. Organomet. Chem.* **1976**, *111*, C17–C20; b) G. Chassaing, A. Parquet, *Tetrahedron* **1978**, *34*, 1399–1404; c) G. Chassaing, A. Marquet, J. Corset, F. Froment, in: *Comprehensive Carbanion Chemistry* (Eds.: E. Buncel, T. Durst), Elsevier, New York, **1980**, pp. 125–185; d) H. J. Reich, J. P. Borst, *J. Am. Chem. Soc.* **1991**, *113*, 1835–1837; e) S. Bradamante, G. A. Pagani, *Adv. Carb. Chem.* **1996**, *2*, 189–263, and references cited therein; f) M. Gromova, C. G. Béguin, R. Goumont, N. Faucher, M. Tordeux, F. Terrier, *Magn. Reson. Chem.* **2000**, *38*, 655–661; g) R. Goumont, E. Kizilian, E. Buncel, F. Terrier, *Org. Biomol. Chem.* **2003**, *1*, 1741–1748.

[5] a) M. J. Kaufmann, S. Bronert, D. A. Bors, A. Streitwieser, *J. Am. Chem. Soc.* **1987**, *109*, 602–603; b) F. G. Bordwell, *Acc. Chem. Res.* **1988**, *21*, 456–463; c) S. Wodzinski, J. W. Bunting, *J. Am. Chem. Soc.* **1994**, *116*, 6910–6915; d) A. Streitwieser, G. Peng Wang, D. A. Bors, *Tetrahedron* **1997**, *53*, 10103–10112; e) A. Streitwieser, G. W. Schriver, *Heteroat. Chem.* **1997**, *8*, 533–537; f) F. Terrier, E. Kizilian, R. Goumont, N. Faucher, C. Wakselman, *J. Am. Chem. Soc.* **1998**, *120*, 9496–9503; g) C. F. Bernasconi, K. W. Kittredge, *J. Org. Chem.* **1998**, *63*, 1944–1953; h) R. Tanikaga, T. Nishikawa, N. Tomita, *Bull. Chem. Soc. Jpn.* **1999**, *72*, 1057–1062; i) J. F. King, R. Rathore, Z. Guo, M. Li, N. C. Payne, *J. Am. Chem. Soc.* **2000**, *122*, 10308–10324; j) A. Facchetti, Y.-J. Kim, A. Streitwieser, *J. Org. Chem.* **2000**, *65*, 4195–4197; k) J. F. King, M. Li, A. Z. Cheng, V. Dave, N. C. Payne, *Can. J. Chem.* **2003**, *81*, 638–646; l) F. Terrier, E. Magnier, E. Kizilian, C. Wakselman, E. Buncel, *J. Am. Chem. Soc.* **2005**, *127*, 5563–5571; m) S. T. A. Berger, A. R. Ofial, H. Mayr, *J. Am. Chem. Soc.* **2007**, *129*, 9753–9761; n) F. Seeliger, H. Mayr, *Org. Biomol. Chem.* **2008**, *6*, 3052–3058; o) I. Binkowska, J. Jarczewski, *J. Mol. Struct.* **2008**, *875*, 86–90.

[6] a) S. Wolfe, *Stud. Org. Chem.* **1985**, *19*, 133–191; b) D. A. Bors, A. Streitwieser, *J. Am. Chem. Soc.* **1986**, *108*, 1397–1404; c) R. Koch, E. Anders, *J. Org. Chem.* **1994**, *59*, 4529–4534; d) P. Speers, K. E. Laidig, A. Streitwieser, *J. Am. Chem. Soc.* **1994**, *116*, 9257–9261; e) K. B. Wiberg, H. Castejon, *J. Am. Chem. Soc.* **1994**, *116*, 10489–10497; f) T. Hoz, H. Basch, in: *Sup-*

plement S: The chemistry of sulphur-containing functional groups (Eds.: S. Patai, Z. Rappoport), Wiley, New York, **1993**, pp. 1–100; g) G. Boche, J. W. Lohrenz, J. Cioslowski, W. Koch, in: *Supplement S: The chemistry of sulphur-containing functional groups* (Eds.: S. Patai, Z. Rappoport), Wiley, New York, **1993**, pp. 339–362; h) G. Raabe, H.-J. Gais, J. Fleischhauer, *Phosphorus Sulfur Silicon Relat. Elem.* **1994**, *95–96*, 345–346; i) D. Benrabah, R. Arnaud, J.-Y. Sanchez, *Electrochim. Acta* **1995**, *40*, 2437–2443; j) G. Raabe, H.-J. Gais, J. Fleischhauer, *J. Am. Chem. Soc.* **1996**, *118*, 4622–4630; k) M. Piffl, J. Weston, W. Guenther, E. Anders, *J. Org. Chem.* **2000**, *65*, 5942–5950; l) E. D. Glending, A. L. Shrout, *J. Phys. Chem. A* **2005**, *109*, 4966–4972; m) P. Merino, V. Mannucci, T. Tejero, *Tetrahedron* **2005**, *61*, 3335–3347; n) E. Cadoni, M. Arca, S. De Montis, C. Fattuoni, E. Perra, M. Cabiddu, G. M. Usai, S. Cabbidu, *Tetrahedron* **2007**, *63*, 11122–11134; o) A. M. Belostotskii, A. Albeck, A. Hassner, *Eur. J. Org. Chem.* **2007**, 4837–4844; p) Y. Fu, K. Shen, L. Liu, Q.-X. Guo, *J. Am. Chem. Soc.* **2007**, *129*, 13510–13519; q) E. Denehy, J. M. White, S. J. Williams, *Inorg. Chem.* **2007**, *46*, 8871–8886; r) S. Nakamura, N. Hirata, R. Yamada, T. Kita, N. Shibata, T. Toru, *Chem. Eur. J.* **2008**, *14*, 5519–5527.

[7] a) J. E. Taylor, F. H. Verhoek, *J. Am. Chem. Soc.* **1959**, *81*, 4537–4540; b) D. J. Cram, W. D. Nielsen, B. Rickborn, *J. Am. Chem. Soc.* **1960**, *82*, 6415–6416; c) E. J. Corey, E. T. Kaiser, *J. Am. Chem. Soc.* **1961**, *83*, 490–491; d) D. J. Cram, D. A. Scott, W. D. Nielsen, *J. Am. Chem. Soc.* **1961**, *83*, 3696–3707; e) D. J. Cram, R. D. Partos, S. H. Pine, H. Jäger, *J. Am. Chem. Soc.* **1962**, *84*, 1742–1743; f) E. J. Corey, H. König, T. H. Lowry, *Tetrahedron Lett.* **1962**, *12*, 515–520; g) H. L. Goering, D. L. Towns, B. Dittmar, *J. Org. Chem.* **1962**, *27*, 736–739; h) D. J. Cram, A. S. Wingrove, *J. Am. Chem. Soc.* **1963**, *85*, 1100–1107; i) E. J. Corey, T. H. Lowry, *Tetrahedron Lett.* **1965**, *13*, 803–809; j) E. J. Corey, T. H. Lowry, *Tetrahedron Lett.* **1965**, *13*, 793–801; k) D. J. Cram, *Fundamentals of Carbanion Chemistry*, Academic Press, New York, **1965**; l) S. Wolfe, A. Rauk, I. G. Scizmadia, *J. Am. Chem. Soc.* **1969**, *91*, 1567–1569.

[8] a) N. S. Simpkins, *Chem. Ind.* **1988**, 387–389; b) P. J. Cox, N. S. Simpkins, *Tetrahedron: Asymmetry* **1991**, *2*, 1–26.

[9] T. Akiyama, M. Shimizu, T. Mukaiyama, *Chem. Lett.* **1984**, 611–614.

[10] S. Nakamura, N. Hirata, T. Kita, R. Yamada, D. Nakane, N. Shibata, T. Toru, *Angew. Chem.* **2007**, *119*, 7792–7794; *Angew. Chem. Int. Ed.* **2007**, *46*, 7648–7650.

[11] a) S. H. Unger, C. Hansch, *Prog. Phys. Org. Chem.* **1976**, *12*, 91–118; b) R. Gallo, C. Roussel, U. Berg, *Adv. Heterocycl. Chem.* **1988**, *43*, 173–299; c) C. H. Suresh, N. Koga, *J. Am. Chem. Soc.* **2002**, *124*, 1790–1797.

[12] For the reactivity of *S*-trifluoromethylsulfonyl carbanions, see: a) J. B. Hendrickson, D. D. Sternbach, K. W. Bair, *Acc. Chem. Res.* **1977**, *10*, 306–312; b) A. Mahadevan, P. L. Fuchs, *Tetrahedron Lett.* **1994**, *35*, 6025–6028.

[13] For previous short communications, see ref.[3g,3i]

[14] R. Scholz, G. Hellmann, S. Rohs, D. Özdemir, G. Raabe, C. Vermeeren, H.-J. Gais, *Eur. J. Org. Chem.* **2010**, 4588–4616, following contribution.

[15] a) H. Rheinboldt, F. Mott, E. Motzkus, *J. Prakt. Chem.* **1932**, *134*, 257–281; b) T. Mukaiyama, T. Masui, T. Izawa, *Chem. Lett.* **1976**, *11*, 1177–1180; c) F. G. Bordwell, B. M. Pitt, *J. Am. Chem. Soc.* **1955**, *77*, 572–577; d) K. Ivin, B. D. Flockhart, R. C. Pink, B. D. Sharma, *J. Chem. Soc., Chem. Commun.* **1971**, *7*, 339–340.

[16] a) M. Labrouillère, C. Le Roux, H. Gaspard-Iloughmane, J. Dubac, *Synlett* **1994**, 723–724; b) S. Winstein, B. K. Morse, *J. Am. Chem. Soc.* **1952**, *74*, 1133–1139.

[17] a) J.-F. Bielmann, H. D'Orchymont, J.-L. Schmitt, *J. Am. Chem. Soc.* **1979**, *101*, 3283–3288; b) M. Dagonneau, *Compt. Rend. Sci., Ser. C* **1973**, *276*, 1683–1685.

[18] K. Nishihata, M. Nishio, *Tetrahedron Lett.* **1977**, *18*, 1041–1044.

[19] a) H. Hellmann, D. Eberle, *Justus Liebigs Ann. Chem.* **1963**, *662*, 188–201; b) L. Benati, P. C. Montevecchi, P. Spagnolo, *Tetrahedron* **1993**, *49*, 5365–6376.

[20] a) R. J. Kurland, M. B. Rubin, W. B. Wise, *J. Chem. Phys.* **1964**, *40*, 2426–2427; b) G. Binsch, *Top. Stereochem.* **1968**, *3*, 97–192.

[21] R. Tanikaga, T. Nishikawa, N. Tomita, *Bull. Chem. Soc. Jpn.* **1999**, *72*, 1057–1062.

[22] W. Bauer, D. Seebach, *Helv. Chim. Acta* **1984**, *67*, 1972–1988.

[23] a) F. Haller, Diploma Thesis, University Marburg, **1990**; b) G. Boche, personal communication, **1997**.

[24] CCDC-768752 [for (*M*/*P*)-**3**·4THF], -768755 [for (*M*/*P*)-**4**·4THF], -768756 [for (*M*/*P*)-**5**·4THF], -768753 for [(*M*/*P*)-**10**·2THF], -768757 (for *rac*-**3**·12-crown-4), -768758 (for *rac*-**9**·PMDTA), -768754 [for (*M*/*P*)-**40**·2diglyme], -768750 [for (**41**·diglyme)$_2$], and -768751 [for (**42**·diglyme)$_2$] contain the supplementary crystallographic data for this paper. These data can be obtained free of charge from The Cambridge Crystallographic Data Centre via www.ccdc.ac.uk/data_request/cif.

[25] a) W. N. Setzer, P. v. R. Schleyer, *Adv. Organomet. Chem.* **1985**, *24*, 353–451; b) U. Olsher, R. M. Izatt, J. S. Bradshaw, N. K. Dalley, *Chem. Rev.* **1991**, *91*, 137–164; c) P. P. Power, *Acc. Chem. Res.* **1988**, *21*, 147–153.

[26] a) D. Barr, W. Clegg, R. W. Mulvey, R. Snaith, D. S. Wright, *J. Chem. Soc., Chem. Commun.* **1987**, 716–718; b) U. Pieper, D. Stalke, *Organometallics* **1993**, *12*, 1201–1206.

[27] a) A. C. Cope, D. E. Morrison, L. Field, *J. Am. Chem. Soc.* **1950**, *72*, 59–67; b) M. Julia, H. Lauron, J. N. Verpeaux, Y. Jeannin, C. Bois, *J. Organomet. Chem.* **1988**, *358*, C11–C16; c) J. I. Cunneen, *J. Am. Chem. Soc.* **1947**, *69*, 36–40.

[28] Z. Strzalko, J. Seyden-Penne, L. Wartski, J. Corset, M. Castella-Ventura, F. Froment, *J. Org. Chem.* **1998**, *63*, 3287–3294.

[29] All the structures of the O–Li CIPs are depicted with planar C_α atoms. However, salts with a pyramidalized C_α atom adopt similar CIP structures.

[30] a) H. J. Reich, J. Borst, M. Bevan, unpublished results; b) H. J. Reich, personal communication, **2009**.

[31] H.-J. Gais, J. Vollhardt, H. Günther, D. Moskau, H. J. Lindner, S. Braun, *J. Am. Chem. Soc.* **1988**, *110*, 978–980.

[32] a) H. J. Reich, J. P. Borst, R. R. Dykstra, D. P. Green, *J. Am. Chem. Soc.* **1993**, *115*, 8728–8741; b) W. H. Sikorski, H. J. Reich, *J. Am. Chem. Soc.* **2001**, *123*, 6527–6535.

[33] M. J. Frisch, G. W. Trucks, H. B. Schlegel, G. E. Scuseria, M. A. Robb, J. R. Cheeseman, J. A. Montgomery Jr., T. Vreven, K. N. Kudin, J. C. Burant, J. M. Millam, S. S. Iyengar, J. Tomasi, V. Barone, B. Mennucci, M. Cossi, G. Scalmani, N. Rega, G. A. Petersson, H. Nakatsuji, M. Hada, M. Ehara, K. Toyota, R. Fukuda, J. Hasegawa, M. Ishida, T. Nakajima, Y. Honda, O. Kitao, H. Nakai, M. Klene, X. Li, J. E. Knox, H. P. Hratchian, J. B. Cross, C. Adamo, J. Jaramillo, R. Gomperts, R. E. Stratmann, O. Yazyev, A. J. Austin, R. Cammi, C. Pomelli, J. W. Ochterski, P. Y. Ayala, K. Morokuma, G. A. Voth, P. Salvador, J. J. Dannenberg, V. G. Zakrzewski, S. Dapprich, A. D. Daniels, M. C. Strain, O. Farkas, D. K. Malick, A. D. Rabuck, K. Raghavachari, J. B. Foresman, J. V. Ortiz, Q. Cui, A. G. Baboul, S. Clifford, J. Cioslowski, B. B. Stefanov, G. Liu, A. Liashenko, P. Piskorz, I. Komaromi, R. L. Martin, D. J. Fox, T. Keith, M. A. Al Laham, C. Y. Peng, A. Nanayakkara, M. Challacombe, P. M. Gill, B. Johnson, W. Chen, M. W. Wong, C. Gonzalez, J. A. Pople, *Gaussian 03*, *Revision B.04*, Gaussian, Inc., Wallingford, CT, **2004**.

[34] C. Møller, S. Plesset, *Phys. Rev.* **1934**, *46*, 618–622.

[35] F. Weinhold, C. Landis, *Valency and Bonding. A Natural Bond Orbital Donor-Acceptor Perspective*, Cambridge University Press, Cambridge, **2005**.

[36] L. Radom, W. J. Hehre, J. A. Pople, *J. Am. Chem. Soc.* **1972**, *94*, 2371–2381.

[37] More recently the physical basis of this analysis has been challenged, see: U. Salzner, P. v. R. Schleyer, *J. Org. Chem.* **1994**, *59*, 2138–2155.

[38] W. G. Kofron, L. M. Baclawski, *J. Org. Chem.* **1976**, *41*, 1879–1880.
[39] D. Seebach, R. Hässig, J. Gabriel, *Helv. Chim. Acta* **1983**, *66*, 308–337.
[40] W. Bauer, D. Seebach, *Helv. Chim. Acta* **1984**, *67*, 1972–1988.
[41] G. M. Sheldrick, *Acta Crystallogr., Sect. A* **2008**, *64*, 112–122.
[42] V. Subramanian, S. R. Hall, *GENSIN*, *Xtal 3.2 System* (Eds.: S. R. Hall, H. D. Flack, J. M. Stewart), University of Western Australia, **1992**.
[43] S. R. Hall, *GENTAN*, *Xtal 3.2 System* (Eds.: S. R. Hall, H. D. Flack, J. M. Stewart), University of Western Australia, **1992**.
[44] S. R. Hall, D. J. du Bonlay, R. Olthof-Hazekamp, *Xtal 3.7 System*, University of Western Australia, **2000**.

Received: March 26, 2010
Published Online: July 14, 2010

